Characterization of the Complexin Membrane Interactions

Qian Liang
Hanzhong, China

Master of Science in Chemistry, Texas A&M University-Commerce, 2015

A Dissertation presented to the Faculty of the University of Virginia in Candidacy for the Degree of Doctor of Philosophy

Department of Chemistry

University of Virginia
June, 2021

ABSTRACT

In neuronal exocytosis, neurotransmitters are released via membrane fusion between synaptic vesicle and presynaptic plasma membrane. Assembly of the soluble *N*-ethylmaleimide-sensitive factor attachment protein receptors (SNAREs) drive this membrane fusion in a millisecond within the Ca^{2+} trigger. While SNAREs constitutively catalyze relatively slow membrane fusion processes involved in intracellular vesicle trafficking, the ultrafast synaptic vesicle fusion process is accomplished through multiple protein-protein and protein-lipid interactions. Among the most extensively investigated interactions are those involving the lipid component phosphatidylinositol-4,5-bisphosphate (PIP2) and SNARE complex binding proteins complexin and synaptotagmin. Even though the regulatory function of these factors is indispensable for efficient membrane fusion and proper synaptic communication, the molecular mechanisms that underly their function have not been determined. Many previous study have focused on the interactions between these regulatory proteins and the SNARE complex; however, recent work indicates that the membrane interactions of these proteins may be critical to their function and are functionally indispensable. We speculate that part of the difficulty in understanding the molecular mechanisms of synaptic vesicle fusion originates from a lack of understanding regarding the membrane interactions made by complexin.

One of the main proposed functions of complexin-1 is to inhibit neurotransmitter release in the absence of Ca^{2+}, while synaptotagmin-1 overcomes this inhibition in the presence of Ca^{2+} to facilitate synchronous neurotransmitter release. Previous work from our lab shows that complexin-1 simultaneously binds both acceptor SNAREs and membranes, where the membrane interactions occur via the terminal domains of complexin-1 in a highly membrane curvature-sensitive manner. In a fusion assay, where the target membrane contains an acceptor SNARE complex consisting of syntaxin-1a and SNAP25, these interactions inhibit fusion by lowering the affinity of the v-SNARE synaptobrevin-2 to the acceptor SNAREs. In other work, the membrane interactions of synaptotagmin-1 were shown to alter the order of the lipid acyl chains, thereby catalyzing a conformational change in the linker region of the SNARE complex and triggering fusion. As a follow-up to this work, this thesis is focused on characterizing the interaction between complexin-1 membranes in lipids of varied composition and in the presence or absence of

the closely related players including synaptotagmin-1, PIP2, and the acceptor SNARE complex.

First, titration experiments using fluorescence anisotropy and electron paramagnetic resonance (EPR) demonstrate that complexin-1 not only senses but also modifies membrane curvature. This is evidenced by a self-competitive complexin-1/membrane interaction even at very low protein to lipid ratio. We propose that, in addition to preventing SNARE assembly, complexin-1 might inhibit spontaneous vesicle fusion via the introduction of curvature strain into the membrane bilayer.

Next, complexin-1 is shown to associate with PIP2 in bilayers. This has been observed using both vesicle binding assays that employ EPR or fluorescence anisotropy and using planar supported lipid bilayers that employ total internal reflection microscopy. This is the first time that a preferential association of complexin-1 for PIP2 containing bilayers has been characterized. We have observed that complexin-1 is recruited to the docking sites of dense core vesicles on planar supported bilayers reconstituted with the acceptor SNARE complex, which may be related to the curvature of the dense core vesicles or locally high concentrations of PIP2. We propose that the locally high concentration of complexin-1 at the site of vesicle docking might regulate fusion by locally modifying membrane curvature.

We also tested the idea that synaptotagmin-1 might compete with complexin-1 at the membrane interface and might modulate fusion through its membrane interaction. In a binding assay using total internal reflection microscopy, we find that complexin-1 competes with synaptotagmin-1 in either the presence or absence of the acceptor SNARE complex, but does so only when PIP2 is present in the membrane. Both complexin-1 and synaptotagmin-1 exhibit higher membrane affinity in the presence of PIP2, and we speculate that the competition for the membrane interface may in part be due to the ability of these proteins to sense and modulate membrane curvature.

TABLE OF CONTENTS

Page

LIST OF FIGURES

ABBREVIATIONS

AEBSF	4-(2-aminoethyl)benzenesulfonyl fluoride hydrochloride
Alexa546	Alexa Fluor 546 C5-maleimide
ATP	Adenosine triphosphate
bPC	Porcine brain L-α-phosphatidylcholine
bPE	Porcine brain L- α-phosphatidylethanolamine
bPS	Porcine brain L- α-phosphatidylserine
C2AB	Residues 136-421 of synaptotagmin-1
CAPS	Calcium-dependent activator protein for secretion
CATCHR	Complex associated with tethering containing helical rods
CCD	Charge coupled device
Chol	Cholesterol
CNS	Central nervous system
Cpx	Complexin
Cpx-1	Complexin-1
Cpx-2	Complexin-2
Cpx-3	Complexin-3
Cpx-4	Complexin-4
dCCpx	Residues 1-83 of complexin-1
DCV	Dense core vesicle purified from rat PC12 cells
DNA	Deoxyribonucleic acid
dNCpx	Residues 27-134 of complexin-1
dNTP	dinucleotidetriphosphate

DOPC	1,2-Dioleoyl-sn-glycero-3-phosphocholine
DOPE	1,2-Dioleoyl-sn-glycero-3-phospho-L-serine
DOPS	1,2-Dioleoyl-sn-glycero-3-phosphoethanolamine
DPPC	1,2-Dipalmitoyl-sn-glycero-3-phosphocholine
DPPE	1,2-Dipalmitoyl-sn-glycero-3-phosphoethanolamine
DPPS	1,2-Dipalmitoyl-sn-glycero-3-phospho-L-serine
dSNAP25	Dodecylated SNAP25
DTT	Dithiothreitol
EDTA	Ethylenediaminetetraacetic acid
EMCCD	Electron multiplying charge coupled device
EPR	Electron paramagnetic resonance
HEPES	2-[4-(2-hydroxyethyl)piperazin-1-yl]ethanesulfonic acid
IPTG	Isopropyl-β-D-thiogalacto-pyranoside
MARCKS	Myristoylated alanine rich C-kinase substrate
MARCKS-ED	Myristoylated alanine rich C-kinase substrate effector domain
MOPS	3-(N-morpholino)propanesulfonic acid
mRNA	Messenger ribonucleic acid
MTSL	S-(1-oxyl-2,2,5,5–tetramethyl-2,5–dihydro-1H–pyrrol–3-yl)methylmethanethiosulfonate
Munc13	Mammalian uncoordinated-13
Munc18	Mammalian uncoordinated 18
NMR	Nuclear magnetic resonance
PIP2	Porcine brain L-α-phosphatidylinositol-4,5-bisphosphate

POPC	1-Palmitoyl-2-oleoyl-sn-glycero-3-phosphocholine
POPE	1-Palmitoyl-2-oleoyl-sn-glycero-3-phosphoethanolamine
POPS	1-Palmitoyl-2-oleoyl-sn-glycero-3-phospho-L-serine
PSLBs	Planar supported lipid bilayers
Q-SNAREs	Proteins that contribute a glutamine (Q) residue in the assembled core SNARE complex, such as syntaxin and SNAP25
R-SNARE	Proteins that contribute a glutamine (Q) residue in the assembled core SNARE complex, such as synaptobrevin
RIM-BP	RIM binding proteins
RIMs	Rab3-interacting molecules
SDSL	Site directed spin labeling
shCpx	Residues 27-83 of complexin-1
SM	Sec-1/Munc18
SNAP25	Synaptosome associated protein 25
SNARE	Soluble N-ethylmaleimide–sensitive factor attachment protein receptors
SUV	Small unilamellar vesicle
Syb-2	Synaptobrevin-2 or vesicle associated membrane protein-2
Syt-1	Synaptotagmin-1
Syx-1a	Syntaxin-1a
t-SNARE	Target SNARE
TIRF	Total internal reflection fluorescence
Tris	tris(hydroxymethyl)aminomethane hydrochloride

v-SNARE	Vesicle SNARE

ACKNOWLEDGEMENTS

First and foremost, I would like to express my heartfelt appreciation and gratitude to Prof. David S. Cafiso, for accepting me to join his group, guiding me into the field, showing me how wonderful biophysics is, and supporting me all the way through during these past six years. This thesis would not have been possible without Dave's thoughtful guidance, constructive feedback, and endless encouragement. Additionally, Dave has also generously given me the freedom to explore ideas I am interested in. I could not have imagined having a better advisor and mentor for my PhD study.

This thesis would not be possible without the collaboration with Prof. Lukas K. Tamm, who is also my committee member. Thanks to Lukas for allowing me to conduct all the total internal reflection microscopy measurements and part of the fluorescence anisotropy measurements in his lab.

I would also like to acknowledge my other committee members, Prof. Eric Herbst and Prof. Lin Pu for their insightful comments, hard questions, and kind feedback on my candidacy exams.

Tremendous thanks to Dr. Volker Kiessling from the Tamm lab for teaching me the planar supported lipid bilayer techniques, training me on the microscopes, and always being a crucial source of help and advice. I would not have the binding assays under microscope done without Volker's help. Thanks to Dr. Binyong Liang and Dr. Chris Stroupe for providing me with the purified syntaxin-1a and dodecylated SNAP25. Thanks also to Dr. Alex Kreutzberger and Jacob Wolpe, who always provide informative conversations. I would also like to acknowledge all current and past members of the Cafiso laboratory for both friendship and support over the years. An extra acknowledgement is well deserved for Rafal Zdanowicz, who trained me and prepared me for the necessary lab skills to work with complexin at the point I did not have any biochemistry or biophysics background. I am also grateful to Sarah Nyenhuis for teaching me to purify the soluble fragment of synaptotagmin-1, C2AB. Thanks to my candid friend, Vanessa Bijak, for sharing the tears and laughs. To Dr. Lishan Liu, Dr. Sara Blankenship, Dr. Arthur Sikora, Abigail Graham, Akosua Ofosuhene, Jacob Stanley, thank you for making the days in the lab so enjoyable! I would also like to acknowledge Dr. Meagan Belcher Dufrisne from Prof.

Linda Columbus' lab for giving me kind suggestions on how to start with writing this thesis. Special thanks to my roommate Jianhao Zeng for his help with processing the images presented in this dissertation as Fig. 3.14.

I would not have been able to begin this amazing academic career in chemistry without the wonderful teachers and staff I met both in China and the United States. Thanks to Prof. Xiguang Du and Prof. Wendong Sun for showing me the elegance of organic synthesis and physical chemistry. Thank Prof. Shuangxi Xing for recommending me to join Prof. Bukuo Ni's lab in Texas A&M University-Commerce. Prof. Ni's hands-on mentorship and patient guidance motivated me to pursue my PhD degree.

Thanks to the professors I have TAed for, Prof. Allan D. Headley, Prof. Rebecca Pompano, Prof. Kateri DuBay and Dr. Carol Price. Being your teaching assistant was such wonderful experiences! I would also like to acknowledge the directors of graduate studies Prof. Ian Harrison and Prof. Thomas Brent Gunnoe, the department chair Prof. Jill Venton, and the graduate studies coordinator Susie Marshall for answering my questions along the way. It was all your smiling faces, warm responses, and thoughtful help that makes the department home to me.

Finally, I would love to acknowledge my family, and dedicate this thesis to my parents Xiushan Liang and Tianyan Huang. Thanks to my brother Dong Liang for the happiness in our childhood. My parents taught me the value of knowledge and the importance of hardworking. Over the years I studied abroad, my family supported me spiritually and financially with all their efforts. I would also like to thank my uncle, Tianlin Huang for sowing the seed of curiosity for nature and science in my heart since I was a kid. Last but not the least, thanks to my then-boyfriend-now-husband, Dr. Baojun Cai for always being patient with me and inspiring me to not give up when the experiments did not work.

1. INTRODUCTION AND BACKGROUND

1.1 Introduction

1.1.1 Rationale

All aspects of bodily function are controlled and regulated by the nervous system, in which neurons or nerve cells play a central role. Neurons communicate via synapses, which are structures that allow one neuron to pass a chemical signal to another neuron. Proper neuron to neuron communication is of fundamental importance for the normal function of the nervous system. When an external stimulus induces an action potential, membrane depolarization followed by the influx of Ca^{2+} ions into the neuron triggers the secretion of signaling carrying molecules known as neurotransmitters (Katz, 1969). Neurotransmitters are stored in synaptic vesicles and neurotransmitter release depends on the membrane fusion between the synaptic vesicle and the plasma membrane at the axonal terminus. Neurotransmitter release proceeds with astonishing speed: the postsynaptic activity responds to the presynaptic signal within a millisecond (Sabatini and Regehr, 1996). Besides temporal precision, neuronal exocytosis also proceeds with a high spatial specificity. Moreover, the synaptic connectivity and strength changes with experience through a process known as synaptic plasticity. It is for these essential characteristics that neuronal exocytosis becomes the vulnerable target for a range of neurological disorders including Alzheimer's disease, autism, Huntington's disease, bipolar disorder, Parkinson's disease, and Amyotrophic lateral sclerosis.

As the most rapid and highly coordinated form of exocytosis, neuronal exocytosis is mainly driven by the assembly of Soluble *N*-ethylmaleimide-sensitive factor Attachment protein Receptors (SNAREs). The SNAREs that mediate synaptic transmission include the synaptic vesicle protein synaptobrevin-2 (Syb-2), and the presynaptic plasma membrane proteins syntaxin-1a (Syx-1a) and SNAP-25. They each contribute one or two conserved stretches of 60-70 amino acids termed "SNARE motifs" to the formation of the assembled SNARE complex (Jahn and Fasshauer, 2012; Südhof, 2013). While Syb-2 and Syx-1a are anchored on the synaptic vesicle membrane and plasma membrane respectively via C-

terminal transmembrane domains, SNAP-25 is attached to the plasma membrane via palmitoylation of cysteine residues on the linker region between its two SNARE motifs. The SNAREs are designated by their location, where Syb-2 is called a vesicle- or v-SNARE, and SNAP25 and Syx-1a are termed target- or t-SNAREs. SNAREs assemble into a core complex that involves assembly from the N- to C-terminal direction to form a four-stranded coiled-coil, and this coiled-coil is stabilized by interactions between evolutionarily conserved hydrophobic side chains. This assembly is highly exergonic, and it brings the opposing vesicle and plasma membranes into close contact and initiates membrane fusion. In many systems, SNARE proteins are constitutively active and intrinsically competent to drive membrane fusion in a variety of slow processes such as intracellular cargo transport and hormone secretion. The speed and specificity of fusion in neurotransmission involves a regulatory system that performs several functions, including tethering and docking a pool of synaptic vesicles near voltage gated calcium channels, clamping or preventing the full assembly of the SNARE proteins until a triggering signal arrives, preparing the synaptic vesicles so that the vesicles are in a release-ready or primed state, and finally driving membrane fusion to respond to the trigger. In the past three decades, great progress has been made and investigators have found that it is via various protein-protein and protein-membrane interactions that these functions are coordinated to produce a sophisticated regulatory machine.

Unlike in constitutive fusion, the fusogenic SNARE complex in neuronal exocytosis were thought to be clamped in a partially assembled *trans* complex in the prefusion primed state, where Ca^{2+} influx releases this clamp to allow full assembly of SNARE complex and initiate membrane fusion. Among the regulatory proteins that control this process, complexins (Cpx) and synaptotagmins (Syt) are the most extensively studied and it is widely accepted that both proteins play critical roles in neuronal exocytosis.

Synaptotagmin-1 (Syt-1) is a vesicle anchored protein that contains tandem C2A and C2B domains that bind 3 and 2 Ca^{2+} ions respectively, and it is widely established as the major Ca^{2+} sensor for fast synchronous release in neurons and neuroendocrine cells (Brose et al., 1992; Littleton et al., 1993; Geppert et al., 1994; Fernandez et al., 2001). Complexin-1 (Cpx-1) is a cytosolic peptide that is specifically expressed in the central

nervous system and is suggested to bind and arrest the *trans*-SNARE complex to prevent its full fusion until this clamping is released after activation Syt by influx of Ca^{2+} ions (Brose, 2008; Mohrmann et al., 2015; Trimbuch and Rosenmund, 2016). Cpx-1 and Syt-1 function in parallel; they both inhibit spontaneous release and facilitate the evoked release. Both Cpx-1 and Syt-1 interact with membranes as well as the SNARE complex, although they bind with different affinities and through different types of interactions.

The membrane interactions of both Syt-1 and Cpx-1 are essential for the regulation of neuronal exocytosis. In the absence of Ca^{2+}, the polybasic face of C2B domain of Syt-1 binds electrostatically to negatively charged membranes containing phosphoinositide 4,5-biphosphate (PIP2) and phosphatidylserine (PS) (Bai et al., 2004; Kuo et al., 2009; Pérez-Lara et al., 2016). In the presence of Ca^{2+}, the membrane interaction of Syt-1 is greatly enhanced as Ca^{2+} binding loops in both C2 domains insert into the membrane. Additionally, Syt-1 prefers to bind more curved membrane vesicles and conversely, Syt-1 not only senses but also induces highly positive curvatures as it binds to the target membranes (Martens et al., 2007). Similarly, Cpx-1 is reported to exhibit a curvature sensitivity when it binds to the membranes via its terminal domains (Snead et al., 2014; Zdanowicz et al., 2017). Despite this similarity and their co-existence in the presynaptic terminal regions, it is not clear how Syt-1 and Cpx-1 might interfere with each other in terms of their membrane affinity.

In addition to membranes, the SNARE complex is the other common target that both Cpx-1 and Syt-1 interact with. Cpx-1 binds to the assembled SNARE complex with nanomolar affinity, and it was first identified because it was copurified with the SNARE complex (Ishizuka et al., 1995; Pabst et al., 2002). In addition to the post-fusion SNARE complex, Cpx-1 was suggested to insert into and arrest the assembly of the *trans*-SNARE mimicking a SNAREΔ60 complex that suppresses spontaneous fusion (Kümmel et al., 2011; Krishnakumar et al., 2015). Syt-1 also binds to SNAREs, and it has been co-crystalized either with the SNARE complex or together with Cpx-1 and the SNARE complex (Zhou et al., 2015; Zhou et al., 2017). It is worth mentioning that the unstructured terminal domains of Cpx-1 that binding membranes have always been truncated in the crystal structures, and the structures have been obtained in a non-membranous environment.

This is one reason why controversial and conflicting models based on Cpx/SNARE complex have been proposed (Kümmel et al., 2011; Trimbuch et al., 2014).

Lipids are intrinsically involved in the membrane fusion processes, and membrane composition is proposed to modulate membrane fusion by modifying the biophysical properties of lipid bilayers (Puchkov and Haucke, 2013; Meher and Chakraborty, 2019). As a special component of the inner leaflet of the presynaptic plasma membrane, phosphatidylinositol-4,5-bisphosphate (PIP2) is essential for efficient vesicle docking, priming and fusion (Martin, 2012; Martin, 2015). The multiple roles of PIP2 in the exocytosis are possibly mediated by the interactions of PIP2 with a range of proteins in the regulated fusion machinery including, but not limited to, Syt-1, Syx-1a, CAPS, rabphilin, Doc2β, α-synuclein, granuphilin and Mints (Martin, 2012; Wen et al., 2011, Bradberry et al., 2019; Schechter et al., 2020). Planar supported lipid bilayer based total internal reflection fluorescence (TIRF) microscopy and electron paramagnetic resonance (EPR) are techniques well suited to investigate protein membrane interaction in physiologically relevant conditions. Taking advantage of TIRF microscopy, previous work from the Tamm lab has not only identified the role of phosphatidylethanolamine in controlling the fusion pore lifetime and probability (Kreutzberger et al., 2017) but also reported recently that Syt-1/Ca^{2+} catalyzed the transition of SNARE complex to a more fusogenic conformation (Kiessling et al., 2018). Using EPR, the Cafiso lab established that Syt-1 bridges across the vesicle and the plasma membrane surfaces (Herrick, et al., 2009), and intriguingly, the Syt-1 interaction with PIP2 and phosphatidylserine might mediates the vesicle plasma membrane fusion event by regulating the distance between the two (Pérez-Lara et al., 2016; Nyenhuis et al., 2019). Moreover, using a combination of EPR and TIRF, collaboration of the two labs built a molecular model in which the spontaneous fusion might be clamped by simultaneous membrane and t-SNARE interaction of Cpx (Zdanowicz et al., 2017).

Whether indirectly involved by interacting with relevant proteins or directly involved by modifying biophysical properties of the bilayer, lipids are indispensable in understanding the molecular mechanisms of neuronal exocytosis, which is exquisitely regulated by proteins including Cpx and Syt. In particular, it remains unknown how the Cpx-1/membrane interaction regulates the synaptic vesicle fusion process. Part of the

difficulty in identifying the role of Cpx-1/membrane interaction in neuronal exocytosis is likely due to an insufficient characterization of the Cpx membrane interaction.

1.1.2 Objective

This dissertation was directed in part at quantitively characterizing the interaction of Cpx with membranes, and we took advantage of techniques including fluorescence anisotropy, EPR and TIRF. Focusing on the Cpx-1/membrane interaction in the presence/absence of factors like PIP2, Syt-1, t-SNARE complex, the ultimate goal was to achieve a better understanding of its regulatory machinery in neurotransmission. Specifically, this goal used a step-wisely approach with the following sets of objectives:

The first objective was to quantitate the interaction of Cpx-1 with vesicles made of different lipid headgroups and acyl chains and providing insights into the mechanism of its curvature-dependent membrane binding pattern. Titrations monitored by fluorescence anisotropy reveal that Cpx-1 prefers binding to vesicles containing more disordered acyl chains. Moreover, our data indicated that Cpx-1 not only senses curvature but also modifies it. Most strikingly, Cpx-1 interferes with its own membrane binding mode at low protein:lipid ratios of 1:6000. These ratios indicate that Cpx-1 exerts a a long range effect on the membrane to modify curvature or introduce curvature strain; as a result, Cpx-1 appears to change the properties of the membrane or bind to limited sites on the membrane interface.

The second objective was to investigate the potential influence of PIP2 on the Cpx-1 membrane interaction, considering the special architecture and multiplex activity of this functionally essential lipid molecule. EPR and TIRF measurements of the Cpx-1 membrane binding demonstrate that PIP2 enhances membrane affinity of Cpx-1. Notably, proteins that interact with PIP2 alter the Cpx-1 membrane affinity. When PIP2 on the planar supported bilayers is sequestered by the Myristoylated Alanine Rich C-kinase Substrate-Effector Domain (MARCKS-ED) (Wang et al., 2002), the intensity of bound Cpx-1 dropped to the level similar to that of membranes without PIP2. This is the first time that a sensitivity of Cpx-1 for PIP2 has been demonstrated.

Several studies have reported that the different domains of Cpx-1 have different functions (Trimbuch and Rosenmund, 2016), we therefore sought to precisely locate the region that dictates this PIP2 sensitivity. To this end, we designed Cpx-1 mutants lacking N-terminal sequences (dNCpx: 27-134), C-terminal sequences (dCCpx: 1-83), or both (shCpx: 27-83) and then measured the intensity of each fluorescently labeled mutant that associated to the planar supported bilayers containing 0, 1 and 5 mol% of PIP2 respectively. Compared with the full length Cpx-1, the intensity of dNCpx did not change very much, but the truncation of the C-terminal domain abolished most of the peptide membrane interaction. Additionally, compared to the binding to the membranes without PIP2, shCpx and dCCpx didn't not show higher affinity when 1 mol% PIP2 was included. These data indicate that the sensitivity of Cpx-1 towards PIP2 originates in its C-terminal domain.

The third objective was to access how the Cpx-1 membrane interaction would be modulated in the presence of Syt given that both proteins show a curvature- and PIP2-sensitive membrane binding pattern. By incubating the planar supported bilayers with C2AB, the soluble fragment of Syt-1, we observed that the Cpx-1 membrane interaction was dramatically suppressed, but this only occurs when PIP2 was included in the membrane. We conclude that Cpx-1 and C2AB compete for membrane binding in a PIP2-dependent manner. Additionally, we observed that Cpx-1 is recruited to the dense core vesicle (DCV) docking sites. Cpx-1 association to PIP2 might be one of the factors that contributes to the DCV/Cpx colocalization, and this observation also suggests that locally high concentrations of Cpx at vesicle docking sites might be functionally important in modulating synaptic vesicle fusion.

1.1.3 Organization

There are four chapters in this dissertation. This first chapter covers a general rationale, the objectives, and main results, as well as a more in detail background about neuronal exocytosis. The second chapter covers the materials, methodology including theories and instrumentation, and experimental procedures that were utilized to obtain the results that are presented in chapter 3. To be specific, chapter 3 describes and interprets the data, which were obtained via EPR, TIRF and fluorescence anisotropy, showing that Cpx-1: modifies membrane curvature, associates with PIP2, and can be recruited the vesicle docking site.

The final chapter summarizes my thesis work and sketches possible extensions in the future based on our current progress.

1.2 Background: Neuronal Exocytosis

Neuronal exocytosis is a highly regulated process that underlies information processing and transfer in the nervous system. Via synaptic vesicle fusion with the presynaptic plasma membrane at the junction between two nerve cells, neurotransmitters that can either excite or inhibit the next neuron are released. Proper synaptic communication relies on proper protein-protein and protein-lipid interactions in a time-sensitive manner in the complex neuronal wiring scheme. Synaptic dysfunction is involved in a range of neurological disorders including autism, addiction, depression, and dementia. Thus, it is of paramount importance to understand the sophisticated molecular mechanisms underlying proper synaptic communication.

From the cell biology perspective, neuronal exocytosis is a form of intracellular vesicle trafficking. However, neurons have specialized proteins and unique membrane constituents at the presynaptic active zone to form the fundamental building blocks that performs the synaptic communication tasks properly. In this part, we introduce the basics of biomembranes, intracellular vesicle trafficking, and membrane fusion process in general. Then, we take a closer look at the presynaptic active zone, which consists unique protein components that accomplish synaptic vesicle fusion and neurotransmitter release. Among these proteins, we focus on regulatory proteins synaptotagmin-1 and complexin-1, which are neuronal specific and indispensable for proper synaptic functions: synaptotagmin-1 serves as the Ca^{2+}-sensor by coupling Ca^{2+}-influx tightly with vesicle fusion, and complexin-1 modulates neuronal exocytosis by suppressing spontaneous vesicle fusion (in the absence of Ca^{2+}) and facilitating Ca^{2+}-evoked release.

1.2.1 Biomembranes and Intracellular Membrane Trafficking

1.2.1.1 Biomembranes, lipid diversity and membrane curvature

Biomembranes. As the basic building blocks of living organisms, cells consist of cytoplasm enclosed within the plasma membranes. In eukaryotes, membrane bilayers also

define intracellular organelles such as the nucleus, Golgi apparatus, mitochondria, endoplasmic reticulum (ER), lysosome, and endosome. Each type of organelle or cellular

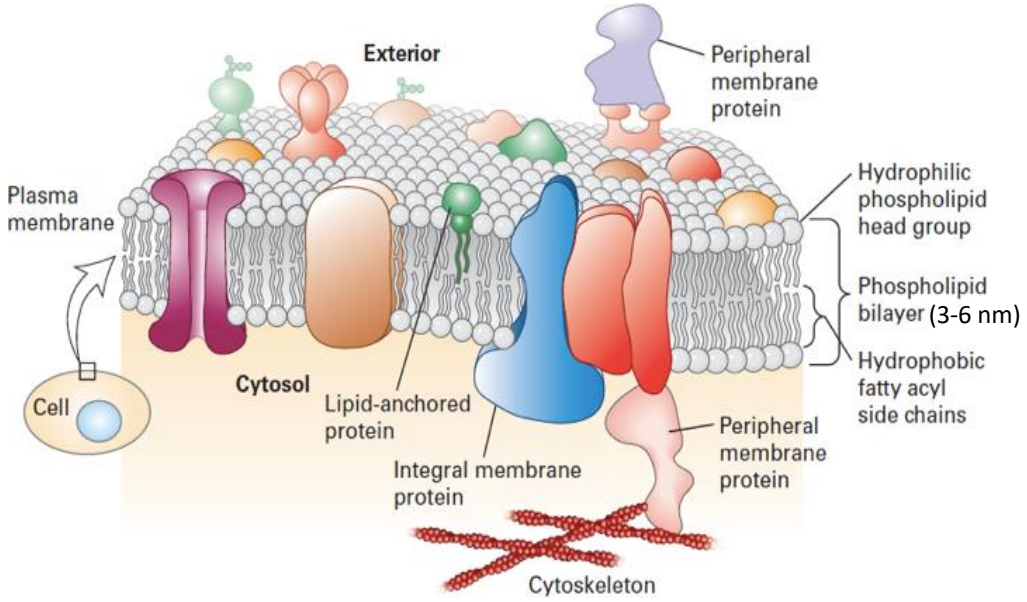

Figure 1.1 Biomembranes consists of lipids and membrane proteins. Figure from Molecular Cell Biology (Lodish et al, 2016).

membrane has a unique set of lipids and proteins that allow it to accomplish its characteristic cellular functions. Despite the diversified functions, all biomembranes have the same basic architecture: a thin film of lipid and protein molecules holding together mainly by non-covalent interactions (Figure 1.1). Under restrictions imposed by thermodynamics, the amphipathic lipid molecules arrange into a stable, continuous and water-impermeable double layer with a thickness of 4~5 nm. Non-covalent interactions enable the bilayers to bend, undulate, and flex while still maintaining their integrity. The fluid mosaic model of lipid bilayers describes biomembranes as a two-dimensional oriented solution of integral proteins in the viscous phospholipid bilayer solvent (Singer and Nicolson, 1972). While the double layer of lipid molecules mainly serves as a barrier to prevent passage of most water-soluble substances, some proteins embedded in the membrane can serve as membrane transporters to transport specific molecules across the membrane, some serve as ion channels to allow the passage of charged ions, some serve as receptor proteins to transduce and respond to external chemical signals, other membrane proteins may serve as structural links by binding components of the cytoskeleton.

Lipid Diversity. Cellular and subcellular membranes are formed from lipids with diverse chemical structures and widely varied abundances, and these diversities underlie many functions membrane lipids fulfill. Typically, the amphipathic molecules forming membranes in mammalian cells are grouped into three categories: glycerophospholipids, sphingolipids, and sterols (Harayama and Riezman, 2018). Compared to the relatively simple structure of sterols, glycerophospholipids and sphingolipids consist of hydrophobic tails composed of hydrocarbon acyl chains and a polar/hydrophilic headgroup. The structural diversity of lipid molecules generated from three different features of lipids: 1) there are multiple headgroups with distinct size and charge like choline, ethanolamine, serine, and inositol in glycerophospholipids and phosphoethanolamine, phosphocholine, glucose, phosphate, and oligosaccharides in sphingolipids; 2) fatty acids can vary in chain length, number of double bonds, position of double bond, hydroxylation etc.; 3) multiple linkages are employed for connecting the headgroups and the tails (blue and pink box in Figure 1.2 A and B). It is worth mentioning that the inositol headgroup in glycerophospholipids is a polyol cyclohexane of which positions 3, 4 and 5 can be phosphorylated or dephosphorylated by lipid kinases or phosphatases respectively, producing seven possible isomers of phosphoinositides (given that they all have the same acyl chains) (Figure 1.2 E). Through interaction with different kinases in the cytosol or on the membrane, phosphoinositides regulate a series of cellular processes including activity of ion channels, membrane trafficking and lipid signaling pathways (Falkenburger et al., 2010; De Craene et al., 2017). In particular, phosphatidylinositol 4,5-bisphosphate (PIP2) is an extensively investigated lipid messenger that has been demonstrated to play crucial roles in neuronal exocytosis. It interacts with multiple effector proteins such as the Ca^{2+}-sensor synaptotagmin-1, syntaxin-1a, and calcium activated protein for secretion (CAPS) and these protein-lipid interactions are suggested to play crucial roles in regulating neurotransmission (Martin, 2012).

To sustain distinct cellular functions, lipid compositions vary significantly within a cell depending on the organelle, across different cells depending on cell stage, the tissue and cell type, and across different organs within a living body. There are examples for this diversity. First, the acyl chains of phosphatidylcholine in mouse brain are predominantly 1-palmitoyl-2-oleoyl (16-0/18-1), in contrast to the acyl chain compositions in organs like

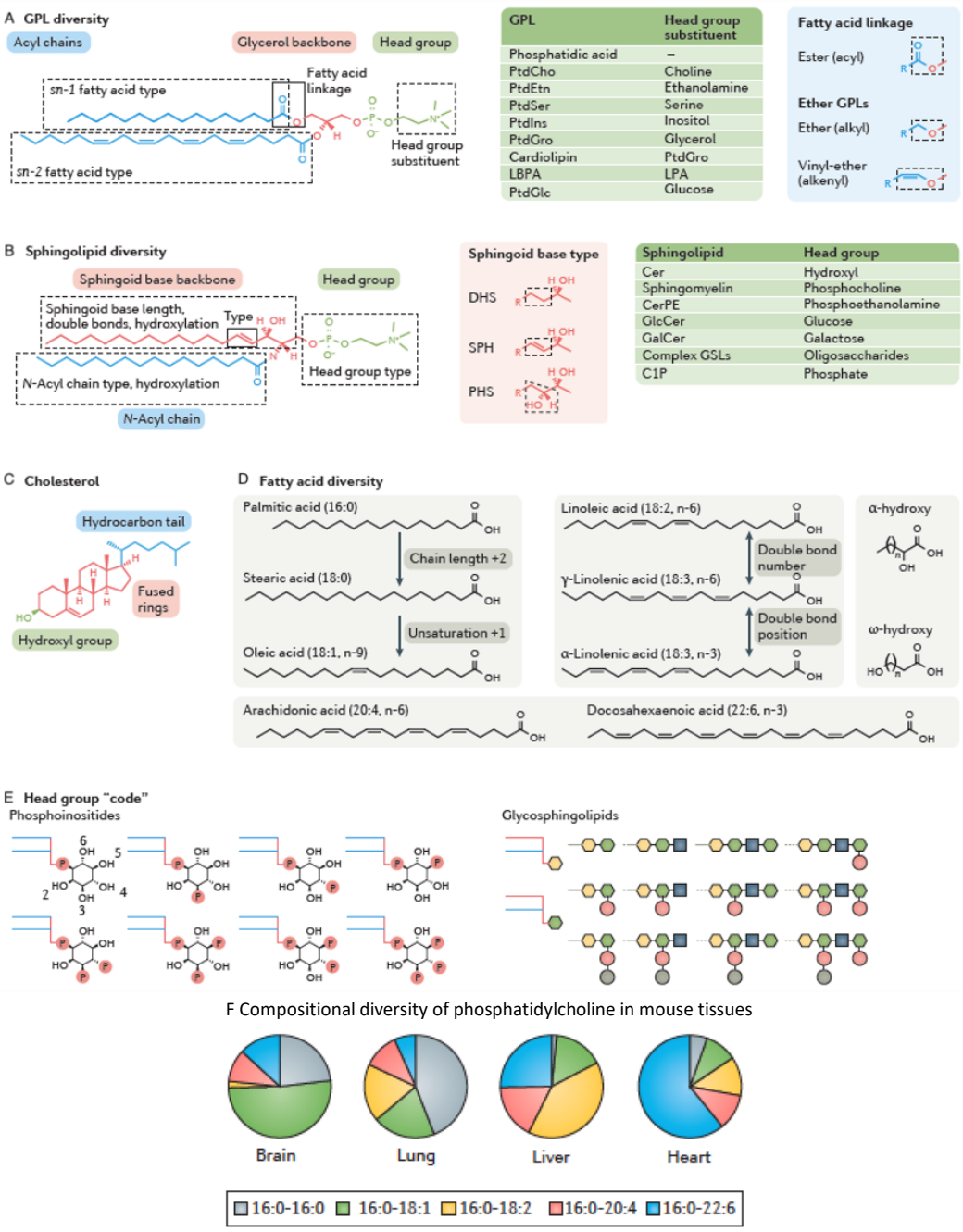

Figure 1.2 Chemical and compositional diversity of membrane lipids in mammals. (A) Glycerophospholipids consist of a glycerol backbone connected with two fatty acids and the headgroup. (B) Sphingolipids are made of a sphingoid base, which contains one fatty acid, another fatty acid and a headgroup. (C) Cholesterol (D) Fatty acids differ in unsaturation (both position and number of *cis* double bond) and chain length. (E) Head group structure of phosphoinositides headgroups and sphingolipids (F) Acyl chain composition of POPC differ in different tissues. Figure is from Harayama and Riezman, 2018.

lung, liver and heart (Figure 1.2 F). Second, in neurons, arachidonic acid containing phosphatidylcholine exhibited a gradient of increasing intensity along the axon terminus and it is enriched within the axon according to imaging mass spectrometry (Yang et al., 2012). Third, a recent computational lipidomics study showed that higher cholesterol levels and increased acyl chain saturation in the brain compared with the average mammalian plasma membrane enable the brain mixture to undulate with higher amplitudes (Ingólfsson

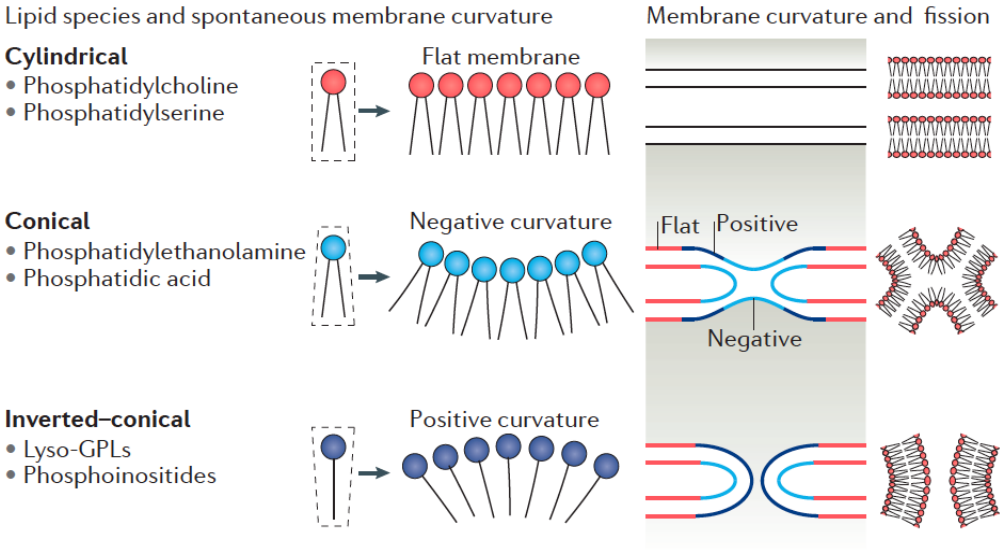

Figure 1.3 Molecular shape and its effect on spontaneous curvature of membranes. Lipids with headgroup and fatty acid tails about the same size assembles into non-curved bilayers, small headgroup but large tails contribute to negative curvature, and large headgroup but small tailed creates positive curvature respectively. Spontaneous curvatures might be important for the formation of non-bilayer intermediates during membrane remodeling processes such as fusion and fission. Figure is from Harayama and Riezman, 2018.

et al., 2017). Dysregulation of lipid composition, particularly in the brain, contributes to neurological disorders such as anxiety, depression, and cerebral ischemia (Müller et al., 2015; Waugh, 2015).

Membrane Curvature. Membrane curvature, which can be generated directly by lipid shape or indirectly by effector protein binding, mediates a series of important biological activities including membrane trafficking and signaling pathways. The effective spontaneous membrane curvature is defined as the curvature a one monolayer in a lipid bilayer would adopt in the absence of external constraints, and it is determined by the lipid composition as well as the lipid interaction within the leaflet. When the lipids have a

headgroup about the same volume as its nonpolar tails, such as phosphatidylcholine and phosphatidylserine, the self-assembly of the lipids will generate a planar bilayer without any curvature (Figure 1.3, top). Cone-shape lipids with a small headgroup and long unsaturated hydrocarbon chains, such as diacylglycerol and phosphatidylethanolamine, tend to form monolayers of a negative curvature, whereas these lipids alone do not form bilayers easily (Figure 1.3, middle). On the contrary, inverted cone-shape lipids such as lysophophatidylcholine and phosphoinositide with large headgroups and relatively small tails tend to self-assemble into micelles or monolayers with positive curvature (Figure 1.3, bottom). In membrane remodeling processes such as fusion and fission, spontaneous membrane curvature plays direct roles in the formation of and transitions between non-bilayer intermediate states. Additionally, membrane curvature mediates membrane fission or fusion indirectly by affecting processes including protein concentration and enzyme activation (McMahon and Boucrot, 2015).

Tissues, cells and subcellular organelles actively maintain characteristic lipid compositions to preserve membrane physicochemical properties like membrane curvature, membrane thickness, fluidity or viscosity and membrane packing pattern. Membranes containing fewer double bonds and long acyl chains in the lipids pack tightly to give bilayers with enhanced membrane thickness and viscosity, whereas small headgroup and high fatty acids unsaturation creates packing defects. All the changes in membrane physicochemical properties, which depend largely on the lipid composition, influence the distribution and function of both integral membrane proteins and certain cytosolic effector proteins that has specific lipid interactions. Specific membranes embedded with particular proteins jointly carry out their biological functions via both lipid-lipid interaction and lipid-protein interactions.

1.2.1.2 Intracellular Vesicle Trafficking

To adapt to changes in the environment and maintain proper electrochemical balances across the plasma membrane, cells including neurons must communicate and exchange with its surroundings. This is realized via exocytosis and endocytosis. Following the central dogma in molecular biology, transcription of the template DNA and splicing of

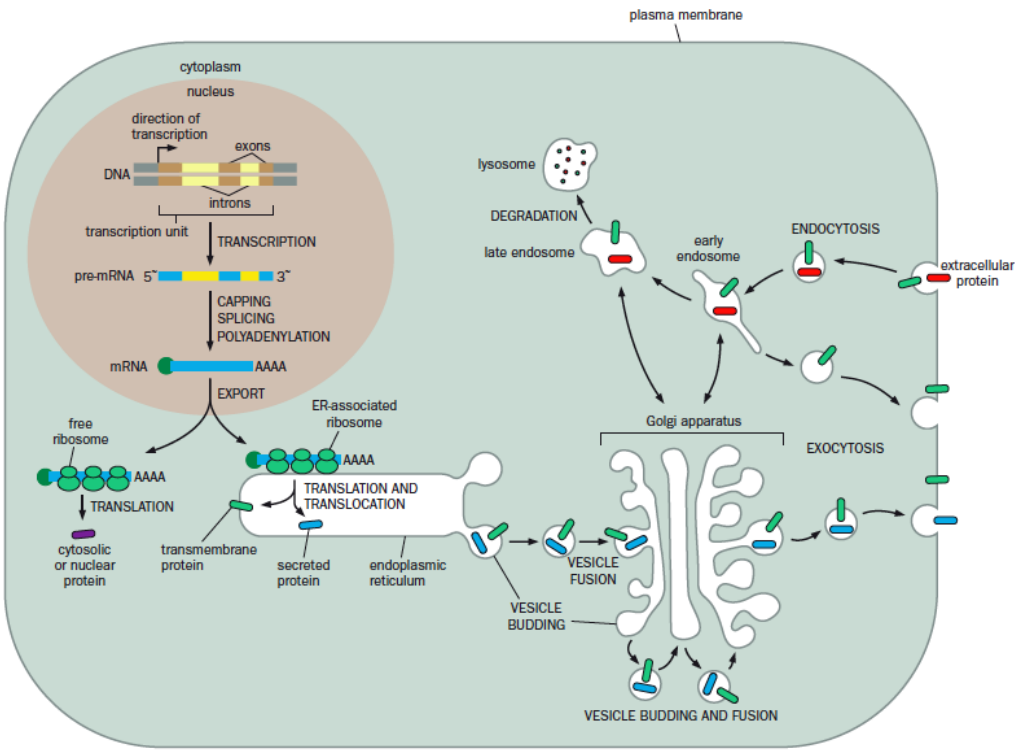

Figure 1.4 Schematic view of the central dogma of molecular biology and intracellular vesicle trafficking. In the nucleus, transcription converts the DNA template into a pre-mRNA, which is then spliced and capped to produce the mature mRNA (top left). Mature mRNAs encoding nucleus and cytosolic protein (purple) are translated in soluble ribosomes (bottom left), while mRNAs encoding the secreted proteins (blue) and transmembrane proteins (green) are translated in the ribosomes on the ER. Transmembrane and secretory proteins exit the ER via vesicle budding, pass through the Golgi apparatus via vesicle fusion and budding process, fuse with the plasma membrane to add transmembrane protein and vesicle membrane to the plasma membrane and release its content (bottom right). On the other hand, extracellular contents and membrane proteins could be delivered to the intracellular space by budding off the plasma membrane via the process of endocytosis (top right). Figure is from Principles of Neurobiology (Luo, 2020).

pre-RNA are performed in the nucleus following by export of the mature mRNAs to the cytosol (Figure 1.4, top left). Translation occurs and proteins are synthesized in distinct locations depending on the destination of the protein: soluble proteins in the cytosol or nucleus are synthesized on free ribosomes (Figure 1.4 bottom left), while transmembrane proteins or proteins destined for secretion are synthesized on ribosomes attached to the endoplasmic reticulum, or ER (Figure 1.4, middle). For the latter, after the translation and synthesis, proteins are translocated across the ER membrane and then budded off the ER

as transport vesicles with secreted protein being encapsulated. These vesicles, carrying the cargo including soluble proteins and membrane components, undergo a series of fusion and budding off until they reach the plasma membrane. At the plasma membrane, the vesicles release their cargo to the extracellular space and add its membrane components to the plasma membrane via fusion with plasma membrane. This process is called exocytosis (Figure 1.4, bottom right). Exocytosis is not only the mechanism cells communicate with the environment, but also the process how synaptic communications occurs. Additionally, exocytosis also deposits receptors, transporters, channels or adhesion molecules into the plasma membrane. On the other hand, through the process of endocytosis, substances like plasma membrane components on the cell surface, extracellular proteins or nutrients outside of a cell are taken up and delivered into the cell via plasma membrane invagination and internalization (Figure 1.4, top right). Both reuse of molecules in the endocytic vesicles and release of secretary cargos in the exocytotic pathway are accomplished via membrane fusion, which will be discussed in next section.

1.2.2 Membrane Fusion

As discussed in the previous section, membrane fusion is a vital process for intracellular membrane trafficking. Additionally, membrane fusion is also the underlying process that enables fertilization, formation of syncytia in muscle cells, development and carcinogenesis, and viral infection. Membrane fusion occurs when two distinct lipid bilayers merge their hydrophobic cores to form a single continuous bilayer. Membrane fusions can be triggered by constitutive proteins (SNAREs), fusion peptides, laser irradiation, electric pulses, plasmonic and nanoheater and polymers (Lira et al., 2019). Despite the high energy transitional state, the whole process of fusion is governed by the second law of thermodynamics: in order to minimize the free energy of the system, the hydrophobic acyl chains of the phospholipids minimize their interaction with the polar aqueous solution. According to the stalk intermediate hypothesis, even with different triggering mechanisms and distinct fusion dynamics, most, if not all, biological membrane fusion reactions in aqueous environment proceeds through similar stages including membrane bending and merging of the proximal leaflets, formation of hemifusion stalk,

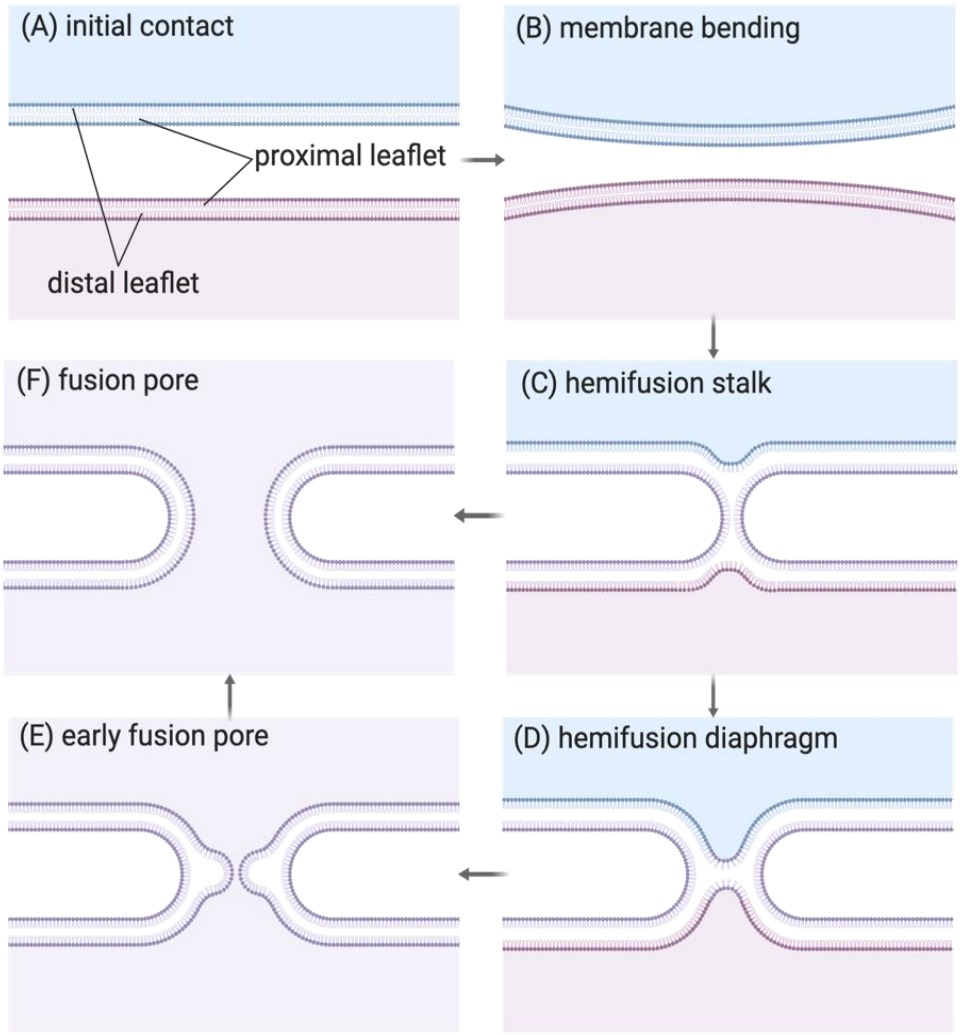

Figure 1.5 Intermediates in membrane fusion process in the stalk hypothesis. (A) The bilayers are brought into close proximity by docking and tethering of one membrane to its fusion target. (B) As hydration repulsion between the two leaflets is overcome, the proximal leaflets are in immediate contact. (C) As provided force continues to distort the boundary between hydrophobic and hydrophilic portion of the membrane, lipids in the proximal leaflets start to mix and form the hemifusion stalk. The distal leaflets remain separate at this stage. (D) Axially expansion of the hemifusion stalk results in the optional hemifusion diaphragm. (E) Merging of the distal leaflets creates an aqueous connection, which is the early fusion pore, across the fusing bilayers and enables content exchange between the two compartments. (F) Either dilation of the early fusion pore or direct expansion of the hemifusion stalk promotes further mix of the distal leaflets and stabilize the fusion pore until the two membranes are fully incorporated into each other. This figure was created with BioRender.com.

hemifusion diaphragm as an optional pathway, and finally fusion pore opening (Kozlov and Markin, 1983; Jahn et al., 2003; Tamm et al., 2003; Chernomordik and Kozlov, 2008).

To fuse, bilayers need to be brought into close proximity: the counteracting hydration repulsion force arising from the water molecules bound to the hydrophilic lipid headgroups needs to be overcome so that the proximal leaflets can get close enough to each other. This initial close contact is essential but not sufficient for membrane fusion. Furtherly, the attractive force of the hydrophobic lipid acyl chains interior of a single leaflet should be disrupted before the approximal leaflets start to distort and join each other to form the hemifusion stalk, which is a hour-glass shaped connection between the apposed distal monolayers. Back in 1983, based on theoretical modeling, hemifusion stalk was first proposed to be an intermediate state membrane fusion proceeds with (Kozlov and Markin, 1983). After the proposal of the stalk hypothesis, basically all the different simulation models of membrane fusion supported the presence of this intermediate structure and the hemifusion stalk arrangement was finally confirmed by direct observation via X-ray diffraction (Yang and Huang, 2002). In contrast to the consensus about the hemifusion stalk, the transitional pathway of the stalk structure into a fusion pore remains controversial. There are mainly two suggested approaches through which a fusion stalk develops into the fusion pore: 1) axially symmetric expansion of the hemifusion stalk leads to a round hemifusion diaphragm followed by breaching of this structure to form a hydrophilic fusion pore; or 2) bypassing stalk expansion to the hemifusion diaphragm, the stalk direct decays into a hydrophilic fusion pore. Experimental results indicate that both the early fusion pore and the hemifusion connections are reversible structures (Yoon et al., 2006; Zhao et al., 2016). Finally, expansion of the early fusion pore will allow full fusion and content exchange. These intermediates and pathways are illustrated in Figure 1.5.

1.2.3 Molecular Anatomy of the Synapse

The most rapid and highly coordinated form of membrane fusion occurs in synaptic vesicle fusion, noting that insulin release from β-cells and neuropeptide release from dense core vesicles share similarities with synaptic vesicle fusion. The vertebrate nervous system consists of central nervous system (CNS), which is located mainly inside the brain and the spinal cord, and peripheral nervous system that serves to connect the CNS to the limbs and

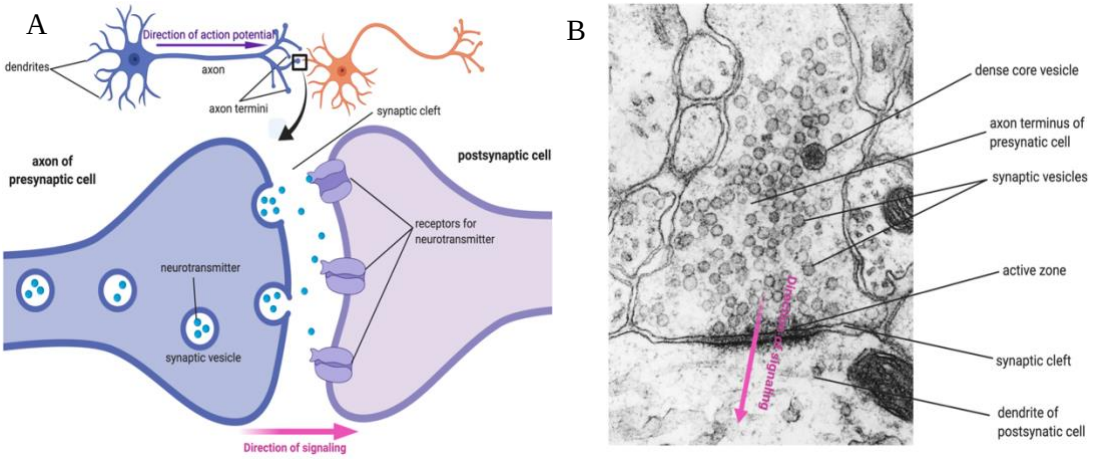

Figure 1.6 The chemical synapse. (A) Cartoon showing a synapse formed by an axon terminal of a presynaptic cell and a dendrite of the post synaptic cell. The region between the axon terminus and the dendrite is termed synaptic cleft. When an action potential travels down the axon of the presynaptic cell unidirectionally, it depolarizes the axon termini and opens the voltage-gated Ca^{2+} channels. The influx of Ca^{2+} triggers the release of neurotransmitters (cyan dots) via membrane fusion between the vesicle and the presynaptic plasma membrane. After diffusing across the narrow synaptic cleft, the neurotransmitters bind to specific receptors on plasma membrane of the dendrite of the postsynaptic cell. Figure was created with BioRender.com. (B) Transmission electron micrograph of an excitatory synapse from the human central nervous system. Besides synaptic vesicles, the dense core vesicles and the active zone are clearly observed. Figure was from Dennis Kunkel Microscopy/Science Photo Library. (C) Synaptic vesicle fusion was observed at frog neuromuscular junction. Image is from Heuser and Reese, 1981.

organs. In an adult human brain, there are around 100 billion nerve cells or neurons, and each neuron forms up to 10,000 synapses. Synapses are junction points where a postsynaptic cell, usually a dendrite of one neuron, is closely opposed to axon termini of

another one or more neurons (Figure 1.6 A) At each axon terminus of a presynaptic cell, synaptic vesicles loaded with small signaling molecules called neurotransmitters cluster at the active zone, which is a specialized area that appears dense in electron microscopy pictures of fixed tissue and is localized precisely opposite to postsynaptic receptor clusters (Figure 1.6 B). Being interconnected by nearly 100 trillion synapses, neurons transfer information to as well as receive signal from a large number of neurons. When a nerve cell receives an external trigger, it transforms the trigger into electrical signals called action potentials in the dendrites followed by the propagation of action potentials to the nerve termini. Action potentials with characteristic frequencies open the voltage-gated calcium channels at the presynaptic plasma membrane and trigger the fusion of synaptic vesicles with the plasma membrane at the presynaptic active zone, resulting the release of the neurotransmitters into the synaptic cleft (Figure 1.6 B and C). At the postsynaptic plasma membrane, neurotransmitter-binding activates ligand-gated ion channels, converting the extracellular neurotransmitter signal back into an intracellular ionic signal or an action potential. Proteins on the vesicle membrane and part of the neurotransmitters are then recycled via endocytosis (Südhof, 2004).

1.2.3.1 SNARE Proteins

SNAREs, which is an abbreviation for soluble NSF attachment receptor proteins, are the minimal protein machinery for the fusion of synaptic vesicles as well as other cellular membranes (Weber et al., 1998). Thus, SNAREs are at the core of synaptic vesicle fusion. SNARE proteins are a large protein family in all eukaryotes that primarily function to mediate vesicle fusion both in intracellular trafficking and exocytosis. SNAREs were first identified because neurotoxins from the bacteria *Clostridium tetani* and *Clostridium botulinum* block synaptic vesicle fusion with presynaptic membrane via specifically cleaving SNARE proteins (Link et al, 1992; Schiavo et al, 1992). SNAREs classified into v-SNARE if it is associated with the vesicle, and t-SNARE if it is on the target plasma membrane (Söllner el al., 1993). SNAREs from distinct organism possess evolutionarily conserved SNARE motifs consisting repeat heptad sequences and these motifs are mainly engaged in coiling one around another to form a four-helix bundle. At the center of the

coiled-coil, conserved ionic interactions between three glutamine (Q) and one arginine (R) reclassified the SNAREs into Q- and R-SNAREs (Fasshauer et al, 1998).

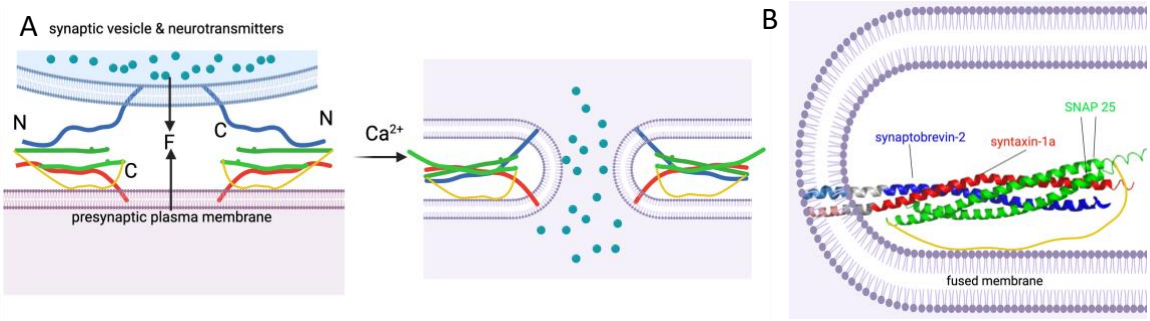

Figure 1.7 SNARE assemble drives synaptic vesicle fusion. (A) Upon a trigger, SNARE proteins assemble from the N- to C-terminus, forming a coiled-coil. This highly exergonic process created a force, F, that brings the synaptic vesicle and plasma membrane together, distorts the membrane surface, fuses the opposing membranes and releases the neurotransmitters. (B) Crystal structure of fully assembled SNARE complex after fusion. SNARE motifs of synaptobrevin-2, syntaxin-1a, and SNAP25 are in blue, red, and green respectively. While synaptobrevin-2 and syntaxin-1a are anchored on the synaptic vesicle and plasma membrane via their transmembrane domains (light blue and pink helices) respectively, SNAP 25 associates to the plasma membrane via its unstructured long linker region (yellow loop) between its two SNARE motifs via four palmitoylated cysteines. Figure is created with BioRender.com and the crystal structure in panel B is from PDB 3IPD.

SNARE proteins involved in neuronal exocytosis are synaptic vesicle membrane anchored synaptobrevin-2, presynaptic plasma membrane anchored syntaxin-1a and presynaptic plasma membrane associated SNAP25 (Figure 1.7 B). Being different from syntaxin-1a and synaptobrevin, SNAP25 contributes two SNARE motifs during SNARE complex formation and SNAP25 is associated with the membrane via its palmitoylated linker region. Once synaptic vesicles come close to the plasma membrane, trans-SNARE complex forms when only the N-terminal part of the SNARE are assembled (Ellena et al., 2009; Liang et al., 2013). Further conformation change occurs upon a trigger and progressive zippering of the four-helix SNARE motifs from N- to C-terminus generates a force that pulls the vesicle closer to the plasma membrane. Energy released from formation of the SNARE complex fuses the opposing membranes, opens the fusion pore and releases the neurotransmitters into the synaptic cleft (1.7 A). It is also suggested that formation of

the SNARE complex facilitates membrane fusion by destabilizing the membrane surfaces via the transmembrane domains (Jahn and Scheller, 2006). SNAREs are essential but far from sufficient to mediate synaptic vesicle fusion and many other proteins at the active zone also play crucial roles in mediating synaptic vesicle fusion.

1.2.3.2 The Presynaptic Active Zone

One of the most important properties of synaptic transmission is its ultrafast speed compared with constitutive vesicle fusion: synaptic vesicles fuse with the plasma membrane in less than a millisecond following the Ca^{2+}-influx (Sabatini and Regehr, 1996). The major reason for the precise excitation-secretion coupling is the unique morphology and organization of the presynaptic active zone.

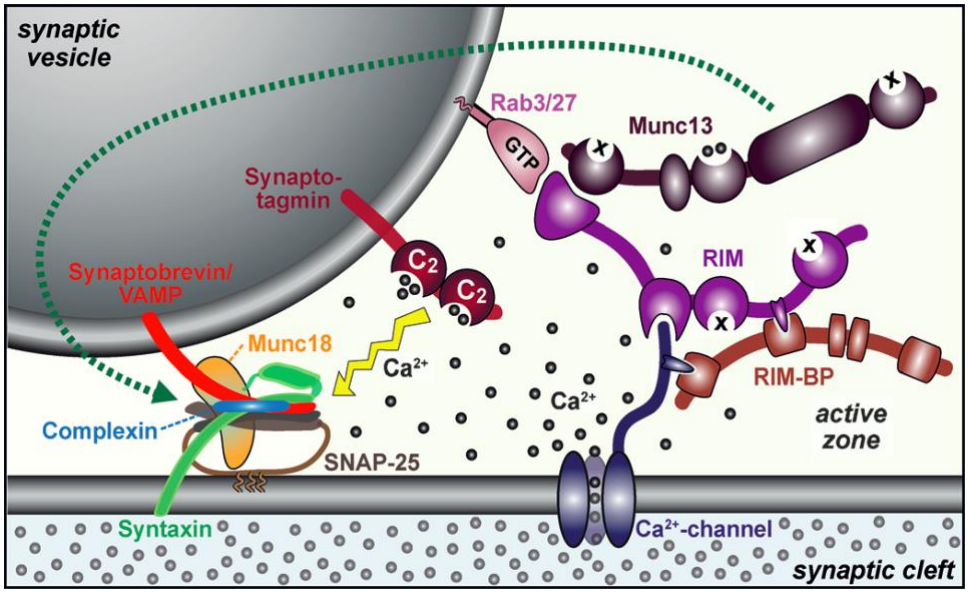

Figure 1.8 Molecular organization of the presynaptic active zone. Synaptic vesicles are brought close to the plasma membrane by RIMs. Munc13 is also suggested to mediate vesicle docking and priming, while it acts to orchestrate SNARE complex assembly together with Munc18. A complex formed by RIM and RIM-BP recruits the Ca^{2+}-channels to the active zone, shortening the distance Ca^{2+} ions diffuse. Synaptotagmin is the Ca^{2+}-sensor and complexin is believed to arrest SANREs in a partially assembled state during vesicle priming. Figure is a courtesy of Professor Thomas C. Südhof, and it is from Südhof , 2014.

SNARE chaperones at the active zone play fundamental roles for exocytosis at a millisecond time scale. Sec-1/Munc18 (SM) like proteins are essential components for

proper neurotransmission as they bind the core fusion machinery and regulate proper assembly of the SNARE complex. A heterogenous off-pathway 2:1 syntaxin-1a/SNAP25 complex can be easily formed and it competes with the formation of the fusion-competent 1:1:1 syntaxin-1a/SNAP25/synaptobrevin-2 complex (Pobbati et al., 2006). EPR spectroscopy demonstrated that Munc18-1 dissociates the 2:1 complex and stabilizes a 1:1 complex of the t-SNAREs (Dawidowski and Cafiso, 2016). Munc13-1, which belongs to the complex associated with tethering containing helical rods (CATCHR) family, is another protein that plays indispensable roles in regulating neuronal exocytosis (Rizo and Südhof, 2012). Evidence has revealed that Munc13-1 promotes the transition from Munc18-1/syntaxin-1a complex to the SNARE complex (Ma et al., 2013), and a recent work suggested that Munc18-1 and Munc13-1 together serve as a template to orchestrate the SNARE complex assembly (Wang et al., 2019).

The speed of neurotransmitter release requires a quick response to the Ca^{2+}-trigger. The active zone always maintains a pool of release-ready synaptic vesicles, which are vesicles in a 'primed' state immediately ready for fusion with the plasma membrane upon a stimulation (Rosenmund and Stevens, 1996). Meanwhile, a second pool of docked vesicles is essential to compensate the primed vesicles once they are depleted upon exocytosis. Synaptic vesicles at the axon terminus must dock to the active zone before vesicle priming and multiple molecules can contribute to the stable attachment of the vesicles to the plasma membrane. One of the most important docking contributors are Rab3-interacting molecules (RIMs), although the molecular mechanisms that determine docking remain unclear. Besides vesicle docking, RIMs recruit Ca^{2+}-channels to the vesicle docking sites via a tripartite interaction with RIM-BP and Ca^{2+}-channels, minimizing the time Ca^{2+} ions diffuse (Kaeser et al., 2011; Han et al., 2011) (Figure 1.8). The C_1C_2BMUNC_2C domains of Munc13 were also implicated to play a role in bridging the synaptic vesicles and the plasma membrane (Quade et al., 2019). Additionally, cell adhesion proteins like cadherins on both pre- and post-synaptic membranes, presynaptic neurexins and postsynaptic neuroligins tightly control the width of the synaptic cleft and minimize the distance neurotransmitters diffuse across (Craig and Kang, 2007; Jontes, 2018).

With an understanding about the sophisticated molecular organization of the presynaptic active zone, two major questions remain unanswered. First, as SNAREs are insensitive to the second messenger Ca^{2+}, how does the neuron couple the Ca^{2+}-trigger with synaptic vesicle fusion? Second, considering that the SNARE assembly is spontaneous and highly exergonic, it raises the question how a complete fusion is arrested half-way at the vesicle priming state, waiting for the Ca^{2+}-trigger. To answer these questions, we now turn to two of the most extensively examined regulatory proteins in the presynaptic active zone: complexin-1 and the Ca^{2+}-sensor synaptotagmin-1. Like SM proteins and the core fusion machinery SNAREs, complexin and synaptotagmin protein families are functionally indispensable. But unlike SM and SNARE proteins, these two regulators are not expressed in yeast and they're evolved as neuro-specific regulators in the synaptic vesicle fusion machinery exclusively.

1.2.4 Synaptotagmin-1

Synaptotagmins are a family of proteins with an N-terminal transmembrane domain and two C2 domains, which often function to mediate Ca^{2+}-dependent binding to negatively charged membranes. Among the 16 mammalian members, synaptotagmin-1 is the Ca^{2+}-sensor for fast synchronous exocytosis in neurons and neuroendocrine cells, and other members are involved in asynchronous release (Brose et al., 1992; Fernández-Chacón et al., 2001; Walter el al., 2011). Similar to most C2 domains, C2A and C2B domains of synaptotagmin-1 bind 3 and 2 Ca^{2+} ions respectively, and the Ca^{2+}-dependent membrane penetration of Ca^{2+}-binding loops on both domains is critical for Ca^{2+}-triggered vesicle fusion. Electrophysical recordings showed that point mutations that disrupt Ca^{2+} binding without inducing structural or conformational changes in synaptotagmin-1 decrease the Ca^{2+}-sensitivity of neurotransmitter release accordingly (Fernández-Chacón et al., 2001; Shin et al., 2009).

Synaptotagmin-1 interacts with membrane via different modes. In addition to the Ca^{2+}-binding loops, the C2B domain has a polybasic face that is known to interact with negatively charged membrane interfaces, but in a Ca^{2+}-independent manner (Kuo et al., 2009), and such electrostatical interactions get more pronounced when PIP2 is included in the membrane bilayers (Pérez-Lara et al., 2016). Moreover, recent EPR spectra revealed

that the conserved arginine residues (referred to here as the arginine apex) on the opposite side of the Ca^{2+}-binding loops in C2B domain also make contacts with the membrane, and simultaneous membrane contact at the arginine apex, the polybasic face and the Ca^{2+}-binding loops could be accommodated only when the membrane surface is curved (Nyenhuis et al., 2021) (Figure 1.9).

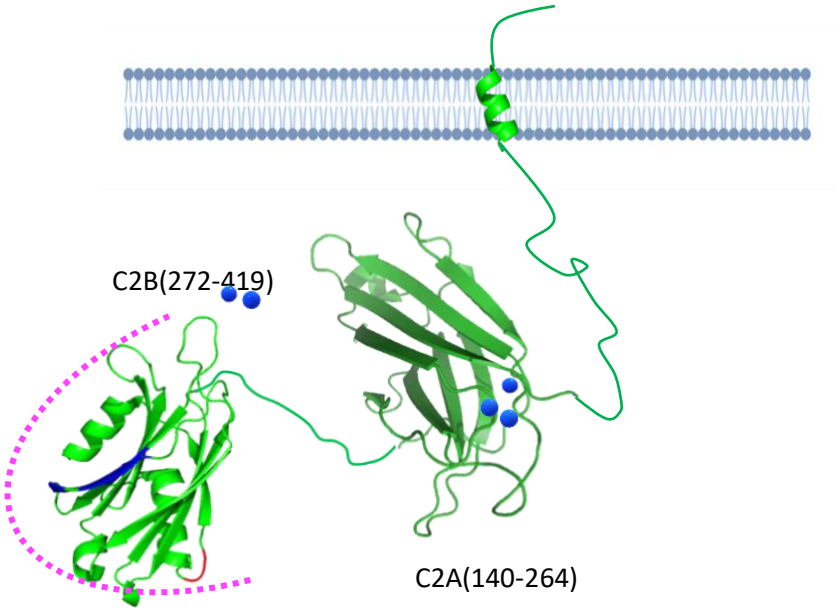

Figure 1. 9 Structure of synaptotagmin-1. Synaptotagmin-1 is a transmembrane protein anchored on the synaptic vesicle membrane, and its C2A and C2B domains are connected via an unstructured linker. The C2A and C2B domains can bind 3 and 2 Ca^{2+} ions (blue spheres) respectively. The polybasic face of the C2B domain is labeled in blue, while the arginine apex on the opposite end of the Ca^{2+}-binding loops are colored in red. The magenta dashed line represents an imaginary membrane surface when C2B makes membrane contacts at Ca^{2+}-binding loops, the polybasic face and the arginine apex simultaneously. Figure is adapted from PDB 2R83.

The other binding partner of synaptotagmin is the SNARE complex, and several structures of synaptotagmin-1/SNARE complex have been proposed according to NMR spectroscopy and X-ray crystallography data. Such binding modes between synaptotagmin-1 and the SNARE complex involve the polybasic face and the arginine apex in the C2B domain (Brewer et al., 2015; Zhou et al., 2015; Zhou et al., 2017). Intriguingly, the synaptotagmin-1/SNARE complex interaction turns out to be structurally heterogenous (Lai et al., 2011). Moreover, in a more physiological relevant condition, polyvalent ions

such as ATP and Mg^{2+} disrupt the synaptotagmin-1/SANRE interactions (Park et al., 2015; Voleti et al., 2020). In contrast to the weak protein/protein interactions, the polybasic face of C2B makes tight contact with PIP2-containing membranes in regardless of the presence of Ca^{2+} (Park et al., 2015). These results demonstrate that binding of synaptotagmin-1 to PIP2-contaning membranes might be a more physiologically relevant event than its heterogenous interaction with the SNARE complex.

Despite the tremendous progress that has been made, it remains controversial, from a molecular perspective, how synaptotagmin-1 triggers ultrafast synchronous release when Ca^{2+} ions influx into the active zone. Several molecular mechanisms based on synaptotagmin-1/membrane interactions are introduced here, while more models could found in Park and Ryu, 2018: 1) synaptotagmin-1 might trigger vesicle fusion by bridging between the vesicle and the plasma membrane and it could shorten the distance between the two to the level that promotes full assembly of the SNARE complex once it binds to the Ca^{2+} (Herrick et al., 2009; Lin et al., 2014; Nyenhuis et al., 2019); 2) synaptotagmin-1 triggers synchronous release by creating local positive curvatures and lowering the energy barrier for vesicle fusion when synaptotagmin-1 penetrates the membrane after Ca^{2+}-influx (Martens et al., 2007; Lai et al, 2011); 3) synaptotagmin-1/Ca^{2+} catalyzes vesicle fusion by induces a conformation change in the membrane anchored SNARE complex and (Kiessling et al., 2018); 4) recent progress in our lab has revealed another molecular role of synaptotagmin-1 in vesicle fusion as the arginine apex of the C2B domain seems to expand the fusion pore when the domain is positioned at a curved membrane surface (Nyenhuis et al., 2021).

1.2.5 Complexin-1

Complexins have been identified across the animal kingdom (Figure 1.10 A) and they have evolved to regulate neuronal exocytosis specifically. Genetic deletion of complexins causes profound damage in evoked neurotransmitter release and altered expression level of complexins have been suggested to contribute to the symptoms of psychiatric disorders including Alzheimer's disease, Huntington's disease, and Parkinson's disease (Brose, 2008). In mammals, the complexin family consists of 4 highly charged cytosolic proteins. Complexin-1 (Cpx-1, or synaphin-2) and complexin-2 (Cpx-2, synaphin-1) are closely

related isoforms, and they were discovered because of their ability to bind the SNARE complex (McMahon et al., 1995; Ishizuka et al., 1995; Ishizuka 1997). Cpx-1/2/3/4 are largely expressed in the central nervous system, while Cpx-3 and Cpx-4 are predominantly expressed in retinal ribbon synapses and Cpx-2 expression outside the neurons is occasionally detectable (Reim et al., 2005; McMahon et al., 1995). Cpx-3 and Cpx-4 isoforms only show limited homology to Cpx-1 and Cpx-2, and they mainly differ in the C-terminal domain. The CAAX box motifs (red box in Figure 1.10 A) at the C-terminal ends of mammalian Cpx-3/4, as well as some of the invertebrate complexin isoforms, mediate the presynaptic targeting by attaching hydrophilic complexins to the synapses via posttranslational farnesylation (Reim et al., 2005).

Similar to synaptotagmin-1, Cpx-1 binds both membranes and the SNARE complex. With a highly conserved central helix region, all Cpx isoforms bind the SNARE complex (Reim et al., 2005). A crystal structure obtained between mouse Cpx-1 (26-83) and the SANRE complex revealed a series of ionic interactions, hydrophobic interactions, and hydrogen bonding among Cpx 48-70, synaptobrevin-2 47-68, and syntaxin-1a 214-232 (Chen et al., 2002) (Figure 1.10 C). Cpx-1 not only binds to the SNARE complex, but it also interacts with the membranes via its unstructured terminal domains (Seiler et al., 2009; Wragg et al., 2013; Zdanowicz et al., 2017).

1.2.5.1 Dual Function of Cpx

Functional impact of Cpx has been examined in liposomes, neurons and neuroendocrine cells across several species via techniques including lipid mixing assay, reconstituted vesicle fusion, antibody perturbation, gene knockout and overexpression (Brose, 2008; Trimbuch and Rosenmund, 2016). The results of these efforts are convincing yet contradictory, since Cpx has both a facilitatory role and an inhibitory effect on vesicle fusion. On the one hand, Cpx was observed to always facilitate evoked, Ca^{2+}-triggered, synchronous neurotransmitter release. Double knockout of Cpx-1/2 reduced the vesicle release probability in response to action potential stimulations by 50% in cultured hippocampal neurons from mice, and triple knockout of Cpx1/2/3 in mice reduced evoked as well as spontaneous release at both excitatory and inhibitory synapses (Reim et al., 2001;

Xue et al., 2008). A fusion facilitating role is also demonstrated in experiments examining vesicle fusion in PC12 cells and chromaffin cells (An et al., 2010; Lin et al, 2013). Recent evidence is that acute genetic deletion of Cpx decreases rates of all forms of neurotransmitter release in forebrain neurons in mouse (López-Murcia et al., 2019). On the other hand, a clamping effect of the spontaneous release was revealed in invertebrate neurons in *D. melanogaster* and *C. elegans* since Cpx deficits lead to significant increase in spontaneous release, in addition to the reduced evoked release (Huntwork and Littleton, 2007; Martin et al., 2011). This clamping effect has also been supported by vesicle fusion studies *in vitro*. Lipid mixing between synaptobrevin-reconstituted liposomes with target proteoliposomes reconstituted with t-SNARE complex decreases in a Cpx-concentration dependent manner (Zdanowicz et al., 2017). Similarly, fusion between dense core vesicles and t-SNARE reconstituted planar supported lipid bilayers in the absence of Ca^{2+} was reduced when Cpx-1 and Munc18-1 are included in the system (Kreutzberger et al., 2017).

The dual function of Cpx could be reconciled if it is recognized that complexins have evolved differentially in different species (Trimbuch and Rosenmund, 2016). Regardless, the physiological recordings *in vivo*, reconstituted vesicle fusion assays and the 3-D crystal structure of SNARE/Cpx complex all provided guidance as well as insights for scientists who are pursuing an understanding about the mechanism how Cpx functions from a molecular level.

1.2.5.2 Molecular Mechanisms of Cpx

To address the janus-faced actions of Cpx during vesicle fusion from a molecular perspective, different hypotheses have been proposed. The positive of role of Cpx on Ca^{2+}-trigger release has been explained by the interaction between Cpx and the SNARE complex. It was proposed the strong interaction between Cpx central helix, which is highly conserved, and the SNARE complex stabilizes the interaction between synaptobrevin-2 and syntaxin-1a in the assembled SNARE complex, especially at its C-terminal end, by preventing potential local unfolding events (Chen et al., 2002).

Despite the controversy about the negative role of Cpx in neurotransmission, a fusion clamping is intuitively indispensable since the SNARE core fusion machinery is

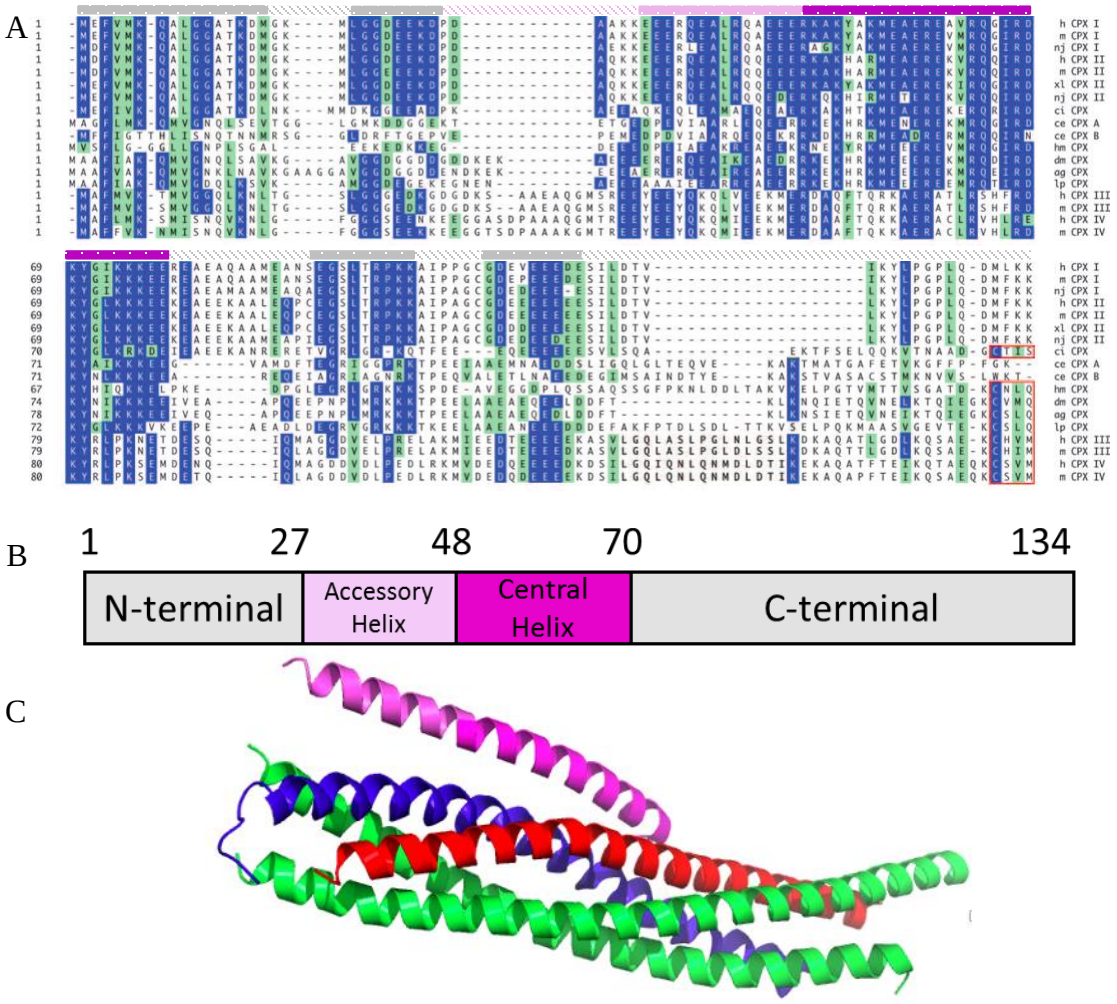

Figure 1.10 The complexin protein family and the interaction of Cpx-1 with the SNARE complex. (A) Sequence alignment of selected complexin paralogs and orthologs. Identical and similar residues across the sequences are shown in blue and green background respectively, and highly conserved regions are shown under bars filled with dotted pattern following the color code according to panel (B). CAAX-box motifs are shown in red boxes. ag, *A. gambia*; ce, *C. elegans*; ci, *C. intestinalis*; dm, *D. melanogaster*; h, human; hm, *H. medicinalis*; lp, *L. pealei*; m, mouse; nj, *Narke japonica*; xl, *X. laevis*. Figure is adapted from Brose, 2008. (B) Domain diagram of *Rattus norvegicus* complexin-1. The central helix (48-70, magenta) binds to the SNARE complex; the accessory helix (27-48, pink) might stabilize the binding of the central helix with the SNARE complex; and the unstructured N-terminal and C-terminal domains bind to the membranes. (C) The complexin-1/SNARE complex. Shown here is the Cpx fragment including the central helix and the accessory helix (26-83) only. The central helix domain binds to a grove between synaptobrevin-2 (blue) and syntaxin-1 (red). Figure is from PDB: 1KIL.

constitutively capable of catalyzing membrane fusion and assembly of SNAREs occurs spontaneously in constitutive secretions, which are much slower than neuronal exocytosis. Besides the assembled SNARE complex, Cpx also binds the binary t-SNARE complex consisting of syntaxin-1 and SNAP25 (Weninger et al., 2008; Zdanowicz et al., 2017). This interaction not only stabilizes the acceptor complex, but also contributes to a fusion clamp by preventing assembly of the SNARE complex in the presence of synaptobrevin.

Tang and coworkers once proposed that Cpx binding prepares SNARE complexes into a metastable states and synaptotagmin-1/Ca^{2+} triggers the fusion by displacing Cpx from metastable SNARE complexes. The evidence supports this model was the observations that synaptotagmin-1 displaces Cpx from the SNARE complex in a Ca^{2+}-dependent manner according to fluorescence intensities (Tang et al., 2006). However, crystal structures including synaptotagmin-1, Cpx and SNARE complex show that Cpx and synaptotagmin-1 can bind simultaneously to the SNARE complex (Zhou et al., 2017). This model is neither supported by the fact that the synaptotagmin-1/SNARE complex interaction is heterogenous and can be disrupted in a membranous environment in the presence of physiological concentrations of ATP and Mg^{2+} ions (Park et al., 2015).

Cpx was also proposed to clamp the spontaneous SNARE assembly by organizing prefusion SNAREpin into a zigzag topology interposed between vesicle and plasma membranes (Kümmel et al., 2011). According to this model, by inserting the accessory helix into one SNAREpin and the central helix into another, spontaneous SNARE assembly is clamped. 'Superclamping' Cpx mutant (D27L/E34F/R37A) that enhances Cpx/SNAREpin interaction showed higher clamping efficiency, whereas 'nonclamping' Cpx mutant (L41E/A44E/A30E/A31E) that disrupts Cpx insertion into the SNAREpin failed in clamping cell-cell fusion. In this model, synaptobrevin 29-60 instead of its full SNARE motif was used to mimic the prefusion SNARE complex, and Cpx(26-83) without the terminal domains was used. The author did not examine if the zigzag structure could be possible when full length Cpx and a complete synaptobrevin SNARE motif are used. Moreover, NMR data using the short constructs showed that the accessory helix of Cpx did not insert into the SNAREpin in solution and the cell-cell fusion results were not repeatable in electrophysiological recordings (Trimbuch et al., 2014). Alternatively, Trimbuch and

coworkers found that increasing and decreasing the negative charge of Cpx accessory helix inhibits or stimulates release. They proposed that Cpx inhibits release by stabilizing and modulating the electrostatic repulsion between the opposing synaptic vesicle and plasma membranes.

While acknowledging that structural information obtained from X-ray crystallography and NMR are important, unresolvable flexible loops flanking the helical region of Cpx are equally important for its regulating efficiency. Multiple studies showed that the central helix, which confers its SNARE interaction, is essential but not sufficient for the precise processes of vesicle fusion and content release. C-terminal domain truncation mutant of *C. elegans* complexin failed in rescuing inhibition of spontaneous fusion, suggesting that the C-terminal domain might be essential for suppressing spontaneous fusion (Martin et al., 2011; Wragg et al., 2013). Meanwhile, mutant Cpx without the N-terminal sequences did not rescue Ca^{2+}-triggered neurotransmitter release defects in Cpx-1/2 double knockout mouse in hippocampal neurons, and the N-terminal domain was even suggested to independently activate Ca^{2+}-triggered fusion *in vitro* (Xue et al., 2007; Xue et al., 2010; Lai et al., 2016). The regulatory role of Cpx in synaptic vesicle fusion arises from cooperative interactions made by its four domains, each of which might invoke distinct functions (Trimbuch and Rosenmund, 2016), and it is likely that the unstructured domains flanking the central helical region are functionally essential for understanding the overall molecular role of complexin in synaptic vesicle fusion.

According to the sequence alignment analysis, complexin paralogs contain a conserved N-terminal domain and a well-conserved region in the C-terminal domain (Figure 1.10, sequence under grey bars filled with dotted pattern). Helical wheel analysis of the conserved regions from mice Cpx-1 indicates that both motifs have the potential to form amphipathic helices (Figure 3.4). Amphipathic helices are known structures that interacts with membranes and alter membrane curvature (Grin and Antonny, 2010). Several studies have reported that the amphipathic regions in complexins from different species bind membranes and that mutations that alter Cpx membrane affinity affect membrane fusion efficiencies *in vitro* or *in vivo*. The C-terminal amphipathic helix in human Cpx-1 was demonstrated to bind the liposomes in a co-flotation assay, and a point mutation

L117W, which enhances the Cpx-1 membrane binding, facilitates fusion between vesicles reconstituted with v- and t-SNAREs respectively (Seiler et al., 2009). *C elegans* Cpx also contains an amphipathic region that binds the membranes and membrane binding of the C-terminal domain is required to inhibit spontaneous synaptic vesicle fusion (Wragg et al., 2013). The same group later reported that NMR and circular dichroism data revealed helix formation upon membrane binding in the amphipathic region in the C-terminal domain (Snead et al., 2014). Membrane binding of the mouse Cpx-1 N-terminal domain was also observed and a mutagenesis study demonstrated that such a membrane interaction is essential for Cpx-1 to activate Ca^{2+}-triggered vesicle fusion *in vitro* (Lai et al., 2016). Progress in our lab found that both terminal domains of Cpx-1 from *Rattus Norvegicus* bind to membranes in a curvature sensitive manner since the binding gets stronger with smaller vesicles (Zdanowicz et al., 2017). Despite the importance of the Cpx/membrane interaction, it remains largely unknown through what mechanism this interaction mediates the formation of and transition between the membrane fusion intermediates.

2. MATERIALS, METHODOLODY AND EXPERIMENTAL PROCEDURES

2.1. Materials

2.1.1 Materials for Membrane Preparation

The following lipids were purchased from Avanti Polar Lipids and used without further purification: 1,2-dipalmitoyl-*sn*-glycero-3-phosphocholine (DPPC), 1,2-dipalmitoyl-*sn*-glycero-3-phospho-L-serine (DPPS), 1,2-dipalmitoyl-*sn*-glycero-3-phosphoethanolamine (DPPE), 1-palmitoyl-2-oleoylphosphatidylcholine (POPC), 1-palmitoyl-2-oleoyl-phosphatidylserine (POPS), 1-palmitoyl-2-oleoyl-*sn*-glycero-3-phosphoethanolamine (POPE), 1,2-dioleoyl-*sn*-glycero-3-phosphocholine (DOPC), 1,2-dioleoyl-*sn*-glycero-3-phospho-L-serine (DOPS), 1,2-dioleoyl-*sn*-glycero-3-phosphoethanolamine (DOPE), porcine brain L- α -phosphatidylcholine (bPC), porcine brain L- α -phosphatidylethanolamine (bPE), porcine brain L- α-phosphatidylserine (bPS), and porcine brain L-α-phosphatidylinositol-4,5-bisphosphate (bPIP2). Cholesterol (powder) was from Sigma. Chloroform, ethanol, and methanol, acetic acid, hydrogen peroxide, contrad detergent were from Fisher Scientific.

2.1.2 Materials for Cell Culture

Competent cells were homemade starting from *Escherichia coli* strain Top10 and BL21(DE3) (Invitrogen). Yeast extract and tryptone were from IBI Scientific. Isopropyl-β-D-thiogalacto-pyranoside (IPTG), ampicillin sodium salt, and kanamycin were from Gold Biotechnologies. Water was purified with three deionizing and organic-free filters (Virginia Water Systems) followed by running through a NanoPure system from Barnstead to achieve a resistivity of 18.2 MΩ/cm.

2.1.3 Buffers and Chemical Reagents

Ethylenediaminetetraacetic acid (EDTA), calcium chloride, potassium chloride, sodium chloride, tris(hydroxymethyl)aminomethane hydrochloride (Tris), sodium cholate, 3-(N-morpholino)propanesulfonic acid (MOPS), glycerol, and triton X-100 were from Sigma. 2-[4-(2-hydroxyethyl)piperazin-1-yl]ethanesulfonic acid (HEPES) were from Research Products International. Alexa Fluor 546 C5 maleimide was from Thermo Fisher Scientific. Primers for PCR were ordered from Integrated IDT Technologies, PfuUltra High-Fidelity DNA Polymerase was from Agilent, and DpnI restriction endonuclease was from New England Biolabs. Benzonase nuclease and 4-(2-aminoethyl) benzenesulfonyl fluoride hydrochloride (AEBSF) were from EMD Millipore/Sigma. Aprotinin and dNTP mixes were from Gold Biotechnologies. Thrombin was from MP Biomedicals.

2.2 Methodology and Experimental Procedures

2.2.1 Protein Expression, Purification and Labeling

Complexin and soluble fragment of synaptotagmin, C2AB were cloned into suitable vectors, and then the plasmids were transformed into *Escherichia coli* strain BL21(DE3) with certain antibiotics. Single colony was picked and inoculated into mini-culture and then main-culture to get the proteins expressed, followed by induction by IPTG. The proteins were then purified following previously reported procedures (Zdanzowicz et al., 2017; Nyenhuis et al., 2019). Certain protein constructs were either labeled with spin label or fluorophore label.

2.2.1.1 Complexin-1

Plasmid mutagenesis and cloning. The plasmids for *Rattus norvegicus* wild-type complexin-1 and Cpx(27-134) were kindly provided by Dr. Binyong Liang from Prof. Lukas Tamm lab. Genes encoding *Rattus norvegicus* complexin-1 were cloned downstream of the T7lac promoter in the pET-28a expression construct. The N-terminal his-tag and a thrombin cleavage site (MGSSHHHHHHSSGLVPRGSH) were inserted for isolation purposes. Single cysteine mutations, including E2C, T13C, K18C, E47C, and T119C, were produced by site-specific mutagenesis based polymerase chain reaction, after the native cysteine at 105 was mutated into serine, using mutation-carrying primers

(Integrated DNA technologies, Coralville, IA). Mutants including fragments containing residues 27-134 (dNCpx), 27-83 (shCpx), and 1-83 (dCCpx) were prepared in the same way. The plasmids were amplified in homemade and chemically competent *Escherichia coli* strain TOP 10 cells, isolated using QIAprep Spin Miniprep Kit (Qiagen, Germantown, MD), and then sequenced via sanger sequencing (GENEWIZ, South Plainfield, NJ).

Protein Expression and purification. Recombinant protein expression was started with transformation of homemade *Escherichia coli* strain BL21 (ED3) with desired plasmids using LB plates with antibiotic kanamycin. A single colony was then picked and inoculated into 50 ml of autoclaved LB media containing 40 mg/L kanamycin. After growing about 6 hours at 37 °C with shaking at 200 rpm, the mini-culture was inoculated into 1 L LB media with 40 mg/L kanamycin and this main culture was kept at 37 °C with shaking at 200 rpm for ~2 hours until it was induced at log phase (OD: 0.6~1) with isopropyl β-D-1-thiogalactopyranoside (IPTG). After induction, the culture were left shaking at 20 °C overnight. Cells were harvested by spinning the culture at 7000 rpm at 4 °C for 20 min with a Sorvall SLA-3000 rotor in Sorvall DuPont RC-5C plus Superspeed Refrigerated Floor Centrifuge (New Life Scientific, Cridersville, OH). The cell pellets were resuspended in extraction buffer (20 mM HEPEs, 500 mM NaCl, 8 mM imidazole, pH 7.4). To prevent protein degradation during cell lysis, protease inhibitors 4-(2-aminoethyl)benzenesulfonyl fluoride hydrochloride (AEBSF) and leupeptin were added to the resuspension with a concentration of 10 μg/mL respectively. Additionally, benzonase nuclease was added to hydrolyze the nucleic acids to aid their further removal in the subsequent steps. The cells were then lysed in a French press and the cell debris after lysis was pelleted under ultracentrifugation (Beckman Coulter, Brea, CA) at 27800 rmp (rotor Ti45) at 4 °C for an hour. After incubating the supernatant from the previous step with Ni^{2+}-NTA resins (Thermo Fisher Scientific, Waltham, MA) for 1 hour at 4 °C, the beads were washed extensively with wash buffer (20 mM HEPEs, 500 mM NaCl, 20 mM imidazole, pH 7.4) to remove any contaminants that bind unspecifically. The recombinant protein was then eluted in fractions of 3 mL with elution buffer (20 mM HEPEs, 500 mM NaCl, 400 mM imidazole, pH 7.4). The fractions were examined by Pierce™ Coomassie Plus (Bradford) Assay reagent (Thermo Fisher Scientific, Waltham, MA) and the fractions

containing proteins were collected and transferred into a dialysis tubing with molecular weight cut off of 3 kDa (SpectraPor, Phoenix, AZ). To cleave the his-tag, 0.5 mg thrombin in glycerol buffer was added to the protein sample right before dialysis. The sample was then dialyzed against dialysis buffer I (20 mM tris, 1 mM DTT, 50 mM NaCl, 1 mM EDTA, pH 7.4) and dialysis buffer II (20 mM tris, 1 mM DTT, 1 mM EDTA, pH 7.4) to remove the extra salt and imidazole. Further purification procedures depend on the isoelectric point of the peptide.

For all the mutants except shCpx, the protein sample was further purified by ion-exchange chromatography on a HiTrap Q HP column (GE Healthcare Life Science, Chicago, IL) with tris and tris/NaCl buffer. The fractions indicated by the chromatogram that containing proteins were further verified by SDS polyacrylamide electrophoresis with either 12 or 4~20 % gel (Bio-Rad, Hercules, CA). According to the gel, the fractions with pure and desired protein were collected and dialyzed into reconstitution buffer (20 mM HEPEs, 150 mM KCl, pH 7.4) followed by concentration via centrifugation using Amicon Ultra centrifugal filters (Millipore Sigma, Burlington, MA). The concentrated and pure protein was then stored at -80 °C.

Due to a neutral isoelectric point, shCpx does not bind Q HP or SP ion exchange columns. Therefore, after isolating the protein via the Ni^{2+}-NTA column, the his-tag was removed by incubating the recombinant protein with thrombin during dialysis in reconstitution buffer. After dialysis, the protein sample was reapplied to the Ni^{2+}-NTA column so that the protein could flow through and his-tag binds to the resin. The thrombin coming together with the protein was then removed by applying the sample to the p-aminobenzamidine agarose beads (GE Healthcare Life Science, Chicago, IL). The pure protein was then concentrated and stored at -80 °C.

2.2.1.2 Soluble Synaptotagmin Fragment C2AB

Plasmid mutagenesis and cloning. Plasmid of soluble synaptotagmin fragment C2AB (136-421) was kindly provided by Dr. Sarah Nyenhuis. Sequences encoding C2AB were cloned into a pGEX-KG vector and a N-terminal GST-tag with a thrombin cleavage site was inserted to facilitate protein purification.

Protein Expression and purification. Homemade and chemically competent *Escherichia coli* strain BL21 (DE3) was transformed with the plasmid of C2AB using ampicillin plates. A single colony was selected to inoculate 50 mL preculture of standard LB media with 50 mg/mL ampicillin and the culture was shaking at 200 rpm under 37˚C for 6 hours to overnight. The main culture was then inoculated with the pre-culture and grew under 37˚C with shaking at 200 rpm, until induced with 0.1 mM IPTG at OD ~0.6. The induced culture was left to grow at 20 °C with 200 rpm shaking overnight to maximize protein overexpression. Once the optimal protein expression is achieved, the cells were pelleted down and separated from the medium by spinning the culture at 7000 rpm under 4 °C for 15 min. The cells were then resuspended in PBS buffer (140 mM NaCl, 2.7 mM KCl, 10 mM Na_2HPO_4, 1.8 mM KH_2PO_4, pH 7.3) containing 2 mM EGTA and 2% triton X-100. Protease inhibitors leupeptin, aprotinin, and AEBSF were added to the resuspension to prevent protein degradation. Benzonase nuclease was added to facilitate purification by hydrolyze double or single stranded DNA and RNA. With the presence of the reagents mentioned above, the cells were ruptured via French press. The recombinant protein together with other soluble components in the lysed cells were separate from the cell debris via ultracentrifugation at 18000 rpm for 40 min under 4 °C. The supernatant was loaded to a GST Prep FF 16/10 column (GE Healthcare Life Science, Chicago, IL) pre-equilibrated with bead wash buffer (PBS, 1% triton X-100, 2 mM EGTA) using AKTA prime (GE Healthcare Life Science, Chicago, IL), so that the recombinant protein could be isolated by binding to the column. The column was then rinsed with 3 column volume (CV) of bead wash buffer, 2 CV of prep buffer (50 mM Tris, 150 mM NaCl, pH 8.4), and 2 CV of cleavage buffer (50 mM Tris base, 150 mM NaCl, 4 mM $CaCl_2$, pH 8.4) to remove any proteins bound unspecifically as well as prepare the column for the cleavage of the GST-tag. Once washed, 0.5 mg thrombin dissolved freshly in 20 mL cleavage buffer was injected manually into the GST Prep column at flow rate 1 mL/min. The column was left at room temperature to cleave the GST tag. The second morning, two GST-Trap FF columns (GE Healthcare Life Science, Chicago, IL) and a HiTrap benzamidine FF(HS) column (GE Healthcare Life Science, Chicago, IL) were attached to the GST Prep column, followed by attaching all the columns to ÄKTA to remove the GST tag and thrombin respectively. The protein C2AB was then eluted with elution buffer (50 mM Tris, 750 mM

NaCl, 25 mM EGTA). To remove any nucleic acids contaminations binding to the polybasic face of C2B domain, protein obtained from the previous step was applied to ion exchange column. A buffer exchange was performed, via a HiPrep 26/10 desalting column (GE Healthcare Life Science, Chicago, IL), to dissolved C2AB into low salt SPA buffer (50 mM MOPS, 1 mM $CaCl_2$, 150 mM NaCl, pH 7.2) to permit binding to the cation exchange SP column. SPA and SPB buffer (50 mM MOPS, 1 mM $CaCl_2$, 800 mM NaCl, pH 7.2) were used for continuous salt gradients to elute C2AB. The fractions containing C2AB as indicated by the UV absorption on the chromatography were further screened by NanoDrop to make sure the collected fractions does not have any nucleic acids(260/280 ratio ≤ 0.6). 12% SDS polyacrylamide gel electrophoresis was used to monitor protein isolation from the lysate, GST Prep column binding, thrombin cleavage as well as the purity of the final fractions.

2.2.1.3 Protein Labeling

Protein labeling were carried out according to a protocol offered by Dr. Binyong Liang generously. The purified proteins were concentrated and buffer exchanged into

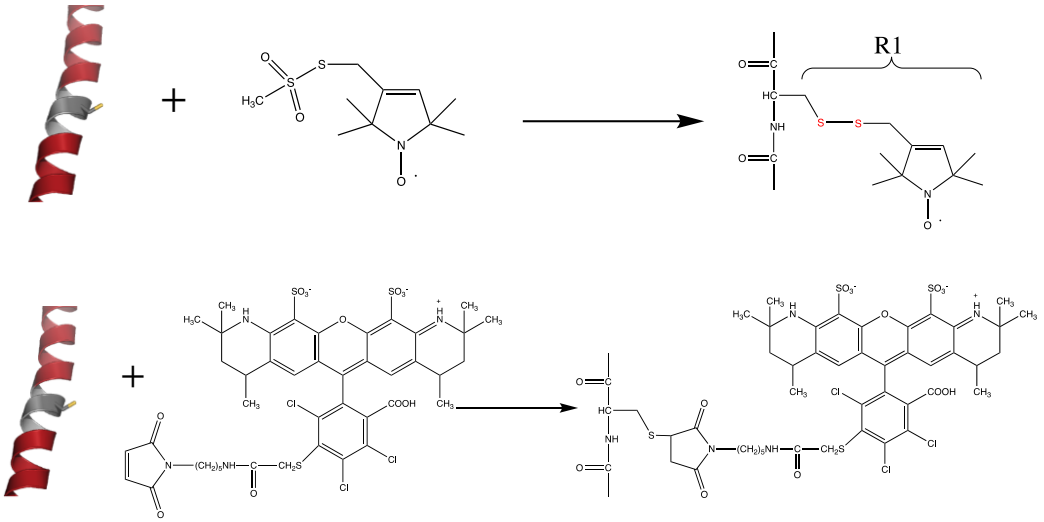

Figure 2.1 Chemical reaction involved in protein labeling at chosen site that has been mutated to a cysteine. (A) Spin labeling of a peptide by MTSL. MTSL reacts with the cysteine residue in the protein to generate a disulfide bond. Once the label is attached to the protein, it is abbreviated as R1 group. The dot represents the free electron in the NO bond. The single election is stable as it is protected by the neighboring methyl groups. (B) Fluorophore labeling of a peptide by Alexa546 maleimide.

labeling buffer (20 mM HEPEs, 500 mM NaCl, pH 7.0) via 3 kD 4 mL Amicon Ultra centrifugal filters (MilliporeSigma, Burlington, MA). The concentrated protein was activated by shaking with 20-fold molar excess of dithiothreitol (DTT) at room temperature for 30 min. The mixture was then applied to Sephadex PD-10 columns (GE Healthcare Life Science, Chicago, IL) to remove extra DTT. It is very important to make sure that the fractions used for the reaction in the next step do not contain any DTT contamination, since even residual amount of DTT will reduce and deactivate the maleimide or thiosulfonate ester groups. 1.5-fold Alexa 546 C5 maleimide or 10-fold molar excess of S-(1-oxyl-2,2,5,5-tetramethyl-2,5-dihydro-1H-pyrrol-3-yl)methyl methanesulfonothioate (MTSL) were added respectively to the DTT-activated protein fractions (Figure 2.1). The reaction with Alexa546 was placed on a shaker for 1 hour at room temperature while the reaction with MTSL was shaking at 4 °C overnight. After the complete reaction, free label was removed by applying the reaction mixture to PD-10 columns and the fractions of labeled protein were further dialyzed extensively into reconstitution buffer (20 mM HEPEs, 150 mM KCl, pH 7.4) with buffer swaps every 4 hours at 4 °C in dark environment.

2.2.2 Lipid Vesicles

2.2.2.1 Formation of Lipid Vesicles

Lipid vesicles or liposomes are spherical structures that enclose an aqueous solution with a bilayer, where the bilayers may be composed of one or multiple types of lipid molecules. Liposomes are widely used as models for artificial membranes to examine the protein lipid interactions and they are also used as vesicles for drug delivery. Liposomes may be used as mimics of a synaptic vesicle or the plasma membrane when formed and reconstituted with appropriate SNARE proteins, and they may be used to study the molecular mechanism of vesicle docking and membrane fusion in using assays, such as a lipid mixing assay. In this case, methods such as total internal reflection fluorescence microscopy or Förster resonance energy transfer may be employed. Because they have been used in a wide range of applications and for many different membrane systems, a wide variety of methods have been developed to prepare liposomes (Lasic, 1988; Patil and Jadhav, 2014). In this thesis, vesicles were used in several different ways. Unilamellar vesicles from small to medium

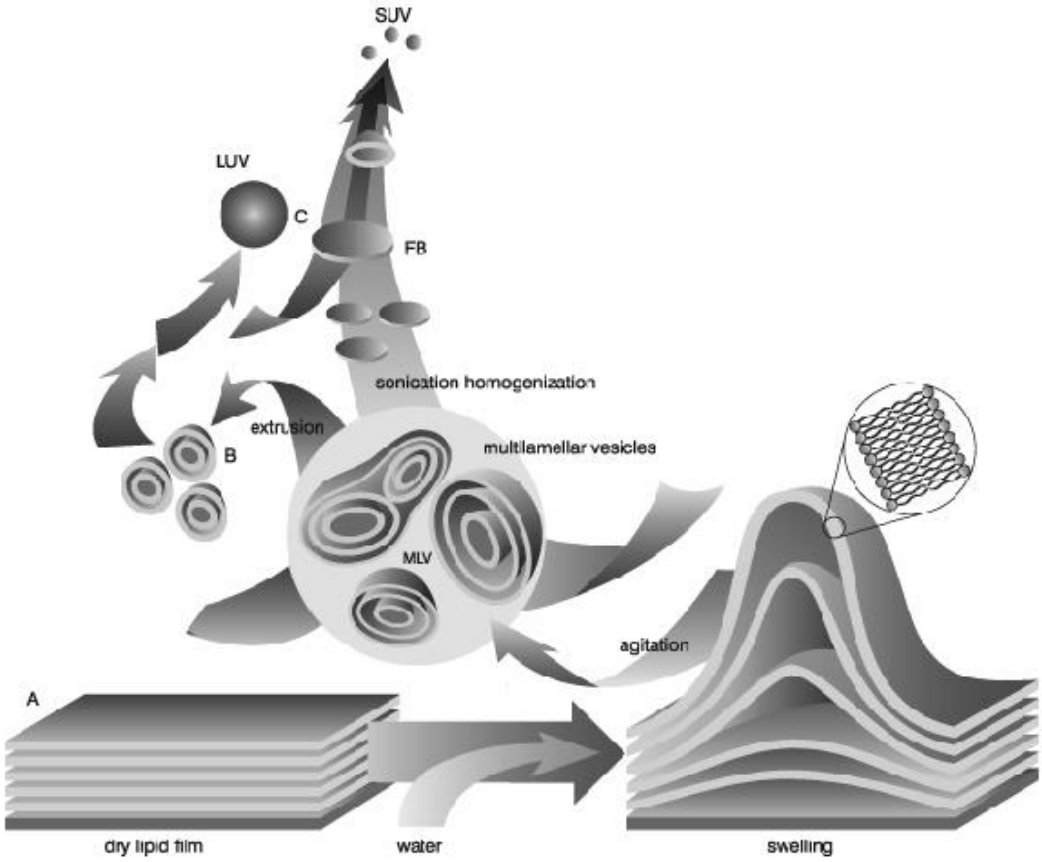

Figure 2.2 The mechanism of formation of vesicles. After removal of organic solvents, lipid stacks/films are left in the container. Once buffer was added, the dry lipid film starts swelling and hydration and becomes fluid and swell. During agitation by vortexing, the hydrated lipid leaflets undergo self-assembly to form multilamellar vesicles to minimize the interaction between the aqueous solution and the hydrophobic acyl chains of the lipid molecules. To break up the multilamellar vesicles and form unilamellar vesicles of desired size, energy input either in the form of sonic energy (sonication) or mechanical force (extrusion) should be provided (Lasic D. D. 1988).

size with varying lipid compositions were prepared via sonication and extrusion following a basic procedure for vesicle formation (Figure 2.2). Sonication was primarily utilized to produce small unilamellar vesicles with diameters ranging from 20 to 50 nm, and extrusion of multilamellar liposomal suspension was used to produce unilamellar vesicles with diameters ranging from 50 to 200 nm. Additionally, whenever vesicles were prepared with membrane proteins incorporated (sometimes termed proteoliposomes), a reconstitution

procedure involving detergent solubilization was used to prepare vesicles. The size distribution of reconstituted vesicles is dependent on the lipid composition of the vesicle and the detergent used, but those produced here were similar in size to sonicated vesicles (Kreutzberger et al., 2015).

2.2.2.2 Experimental Procedures

For all three methods mentioned above, the phospholipids (Avanti Polar Lipids, Alabaster, AL) in chloroform and cholesterol were combined and thoroughly mixed in desired ratios in a glass test tube. To make sure that all the lipids are mixed evenly to give a homogenous mixture, methanol was added to facilitate the solvation of phosphatidylinositol 4,5-bisphosphate (PIP2) whenever PIP2 is needed in the lipid mixture. The chloroform was then evaporated carefully under a directed nitrogen gas flow. To further remove the residual organic solvents, the lipid cake was left under high vacuum for at least an hour. The derived lipid film was then extensively hydrated into reconstitution buffer (20 mM HEPEs, 150 mM KCl, pH 7.4) to reach desired concentration and the mixture was allowed to hydrate thoroughly above the transition temperature (water bath is needed for vesicles made of mainly DP lipids) for 30 min with vortexing occasionally. The resultant milky (due to light scattering) large multilamellar liposomal suspension was directly used in the next steps.

Extrusion. Before extrusion, the large multilamellar vesicles were disrupted by at least five freeze-thawed cycles with help of liquid nitrogen to facilitate the formation of unilamellar vesicles. Prefiltering the resuspension through a larger pore size gives similar results. The extrusion was then performed on an extruder (Avanti Polar Lipids, Alabaster, AL) at a temperature above the phase transition temperature by manually forcing the mixture passing through a filter with desired pore size (MilliporeSigma, Burlington, MA) repeatedly for at least 21 times. Odd times of extrusion are always preferable in order to avoid any insoluble contaminants in the final product. A successful extrusion will give a hazy transparent solution of vesicles with relative small dispersity regarding size distribution.

Sonication. Extrusion does not apply to the preparation of highly curved vesicles with diameter smaller than 50 nm, since the pressure for pushing the multilamellar liposomal resuspension increases beyond the handleable level as the pore size of the filter is smaller than 50 nm. Alternatively, sonication is adopted to produce smaller unilamellar vesicle. Though sonication giving smaller vesicles, the sonicated vesicles show the same molecular and nanoscale organization as extruded vesicles, thus the data obtained from sonicated vesicles can be directly compared with data obtained on extruded vesicles (Lapinski et al., 2007). A 125 W probe-tip sonicator (QSonica Q125, Newtown, CT) is used to deliver energy into the multilamellar vesicle resuspension. The tip should be placed under the lipid suspension level at a fixed height among different batches without touching the walls of the test tube. To prevent over-heating or potential oxidation of the lipid molecules, the sample tube was merged in ice-water bath and sonication was set to pulse 30 sec after every 30 sec of sonication. It usually takes 15~30 min total sonication time for the opaque lipid suspension to clarify into a slight hazy transparent solution of vesicles. The solution can get even clear by ultracentrifugation the vesicles under 20000 rpm for 20 min at 20 °C to remove both the titanium particles released from the sonicator tip during sonication and the residual large vesicles in the solution. Due to the high curvatures and small size, small unilamellar vesicles derived from sonication tend to fuse into larger sizes even being stored at 4 °C. Normally, small unilamellar vesicles were be used in no more than 2 days since preparation.

The size distribution of sonicated vesicles is dependent on several factors including the relative position of the sonicator tip in the sample, lipid composition, sample volume, power and temperature. However, if these factors are carefully controlled among different batches, vesicles with reproducible mean size and size distribution could be obtained. The final lipid concentration of both sonicated and extruded vesicles was quantified via a phosphate assay as described in section 2.2.7.

Reconstitution. One of the most commonly used techniques for preparation of planar supported lipid bilayer is Langmuir-Blodgett/vesicles fusion (section 2.2.3 and Fig 2.3 B). In this thesis, vesicles used for preparation of planar supported lipid bilayer were all prepared by reconstitution, in regardless of the restitution of the t-SNARE complex.

While protein reconstitution into model membranes via detergents is a widely used technique to retain and investigate the functions of membrane proteins, the reason for preparing vesicles without any SNAREs via reconstitution is to make sure the planar supported bilayers made from these vesicles could be most comparable to planar supported bilayers made from vesicles reconstituted with certain SNARE proteins.

The vesicles for preparation of planar supported lipid bilayers were prepared via detergent mediated reconstitution as previously reported (Wagner and Tamm, 2001; Domanska et al., 2009). The dried lipids with desired lipid composition was solubilized in 350 µl of 25 mM sodium cholate in reconstitution buffer (20 mM HEPEs, 150 KCl, pH 7.4). Whenever t-SNAREs were reconstituted, proper volumes of SNARE proteins in their respective detergents were added to reach a final lipid/protein ratio of 3000:1. After an hour incubation at room temperature, the mixture was diluted by addition of another 200 µL reconstitution buffer to reach a sodium cholate concentration of 16 mM, which is close to the critical micellar concentration. The sample was then dialyzed against 1 L reconstitution buffer with one buffer exchange after 4 hours.

2.2.3 Planar Supported Lipid Bilayers

2.2.3.1 Fabrication of Planar Supported Lipid Bilayers

Planar supported lipid bilayers (PSLBs) are bilayers assembled *in vitro* on a planar solid surface such as quartz or silicon dioxide slides. PSLBs exhibit a number of features that make them very attractive as mimics of the plasma membrane, including the ability to create bilayers having an asymmetric composition between leaflets, the ability to incorporate membrane proteins, and the ability to use compositions that can form lipid domains (Kiessling et al., 2015). In addition to these advantages, the very low lipid concentrations used in PSLBs systems and their attachment to a solid support avoids problems that might arise with lipid aggregation by proteins such as synaptotagmin-1 in a bulk assay. Consequently, PSLB reconstituted with certain SNARE proteins are well suited to study protein-lipid interactions as well as the molecular mechanisms of vesicle docking and fusion.

Different methods have been utilized to prepare a PSLB (Figure 2.3). In direct vesicle fusion method (panel A), continuous bilayers can be formed by incubating

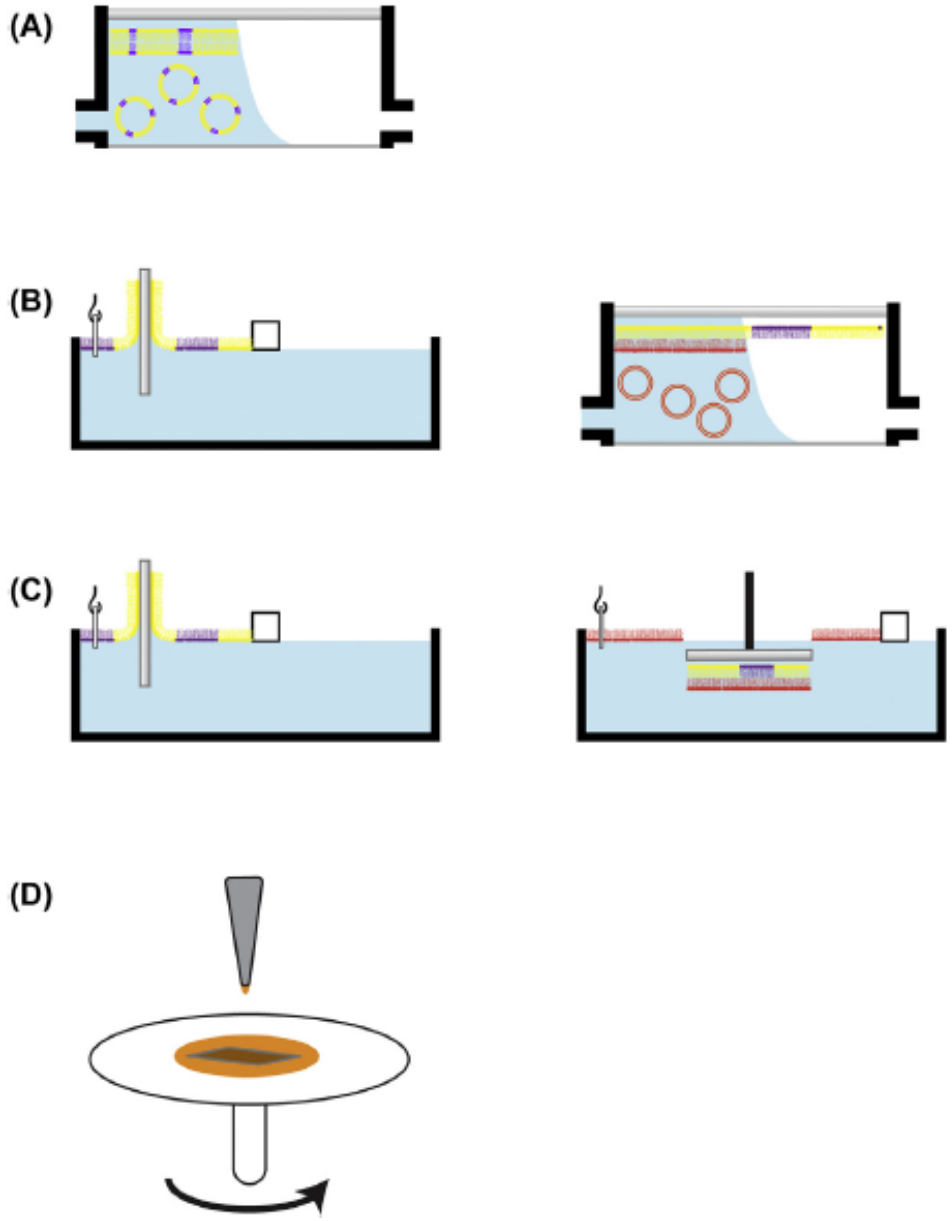

Figure 2.3 Methods for preparation of planar supported lipid bilayers. (A) Direct vesicle fusion/deposition. (B) Langmuir-Blodgett/vesicle fusion. The first layer is prepared by dipping the slide in a trough and the second layer is assembled from vesicle fusion. (C) Langmuir-Blodgett/Schaefer transfer. (D) Spin coating. Figure is from Kiessling et al., 2015.

unilamellar vesicles with the hydrophilic quartz slides so that the vesicles rupture and adhere to the surface. Another common technique for the preparation of a PSLB is spin coating (panel D), in which lipids together with proteins dissolved in organic solvents are

dropped onto a spinning surface. PSLBs may be obtained after the organic solvent is evaporated, the surface gets hydrated and rinsed by buffers sequentially. However, neither direct vesicle fusion nor spin coating allows lateral diffusibility of integral membrane proteins on the lipid bilayer due to non-physiological interactions between integral membrane proteins and the solid support. It is neither possible to prepare PSLB with asymmetric lipid compositions between different leaflets. To get around these limitations, the two leaflets of the PSLBs can be prepared with better control in two separate steps: the first layer is assembled by dipping a hydrophilic quartz slide in a Langmuir-Blodgett trough so that a Langmuir monolayer can be transferred to the hydrophilic surface; and the second leaflet can be formed either via vesicle fusion (panel B, Langmuir-Blodgett/vesicle-fusion) or direct transfer of another monolayer on the Langmuir-Blodgett trough (panel C, Langmuir-Blodgett/Shaefer-transfer). In these two techniques, a polymer-supported planar lipid bilayer system has been developed by conjugating polymer chains, such as polyethylene glycol (PEG) and PEG based DPS, with lipid molecules (Wagner and Tamm, 2000). DPS polymers covalently tethered to the hydrophilic surfaces efficiently lift the bilayers away from the solid surface, providing buffer region between the first leaflet and the solid support so that integral membrane protein can diffuse laterally.

2.2.3.2 Experimental Procedures

In this thesis, we chose the Langmuir-Blodgett/vesicle fusion technique to fabricate the planar supported lipid bilayers reconstituted with or without plasma membrane SNARE proteins as described previously (Kalb et al., 1992; Wagner and Tamm, 2001; Domanska et al., 2009; Kiessling et al., 2015). We first cleaned quartz slides loaded on a teflon holder by boiling in 5% contrad for 30 min, and the slides were sonicated for 15 min while still in the hot detergent solution right after boiling. After sonication, the detergent was thoroughly removed by extensive rinsing with deionized water. Immediately before dipping, the slides were cleaned by etching in a freshly mixed piranha solution (a mixture of 3 volume of concentrated sulfuric acid and 1 volume of 30% hydrogen peroxide) for at least 15 min. After etching, the slides were removed from the piranha solution with the help of the teflon holder, and residual acids were cleaned by rinsing extensively with Milli-Q water (Millipore, Billerica, MD). Besides removing any organic contaminants on the slides

during etching, the surface of the quartz slides has been thoroughly hydroxylated and becomes hydrophilic. After cleaning, the slides were stored in Milli-Q water. While cleaning the quartz slides, a Langmuir-Blodgett monolayer can be formed by adding the lipid mixture of POPC:cholesterol:DPS = 80:20:3 in chloroform to the water surface in a Nima 611 Langmuir-Blodgett trough via a Hamilton syringe. A Wilhelmy plate and a teflon surface blockade have been installed on the trough to monitor and control the surface tension respectively. Ideally, the amount of the lipid mixture added should be controlled so that the initial surface pressure falls in the range of 10~15 mN/m. After evaporation of chloroform, a compression rate of 10 cm^2/min was used to record surface pressure-area isotherms until a final surface tension of 32 mN/m had been reached. After equilibration for 5 min, a freshly cleaned quartz slide dried with directed nitrogen gas flow was quickly (200 mm/min) dipped through the monolayer and into the trough. Lipid transfer did not happen during insertion due to the repulsion between the hydrophilic quartz slide surface and the nonpolar lipid acyl chains. While a constant surface tension of 32 mN/m was maintained via a computer, monolayer transfer evenly occurred when the slide was slowly (5 mm/min) pulled out through the monolayer from the trough. During the process of withdrawing the slide, the polar lipid head groups adhered to the hydrophilic quartz slide surface. The monolayer loaded slides were store in a desiccator until the slide was assembled into a homemade cassette for assembly of the second monolayer. 77 μM liposomes with or without SNARE proteins were then injected into the chamber carefully and the liposomes were incubated with the monolayer on the slide in the cassette to form the second leaflet via vesicle rupture and self-assembly. After incubation of 1 hour for liposomes without protein and 1.5 hours for proteoliposomes respectively, the PSLBs were obtained by removing the extra unfused liposomes via perfusion with at least 5 chamber volumes of reconstitution buffer.

2.2.4 Total Internal Reflection Fluorescence (TIRF) Microscopy

2.2.4.1 Configuration of TIRF Microscopy

Total internal reflection fluorescence (TIRF) microscopy is an optical technique based on the principle that when the excitation wave gets totally reflected at the glass-water interface,

an evanescent wave/field, from which the light intensity decays exponentially, can be induced across the interface by the reflected light. Accordingly, TIRF selectively images a thin layer of fluorophores within the evanescent field that are immediately located adjacent to the glass-water surface, and it thus improves the signal-to-noise ratio by effectively eliminating the background fluorescence intensity. Penetration depth of the evanescent field normally ranges from 100 to 200 nm, depending on the angle and wavelength of the excitation wave as well as the refractive indices of the media. TIRF was initially described by E. J. Ambrose to study cell movements (Ambrose, 1956), and it was further developed then by Daniel Axelrod to visualize the contact between cultured cells and the substrate (Axelrod, 1981). A combination with planar supported lipid bilayers has greatly expanded the application of TIRF, making it well-suited to investigating certain membrane

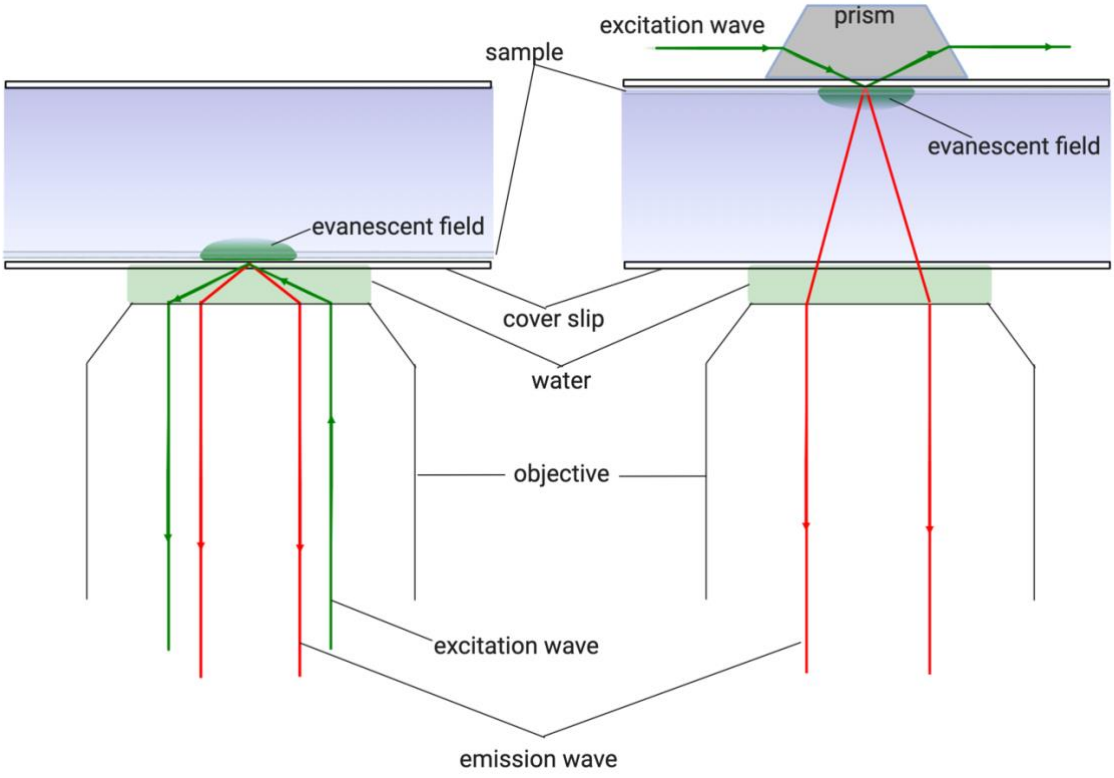

Figure 2.4 *Cis* and *trans* configurations of total internal reflection microscopy. In the *cis* geometry, both the excitation and emission wave are guided through the objective lens (left panel). In the *trans* geometry, the excitation wave is guided through a quartz prism on the opposite side of the objective lens (right panel). This figure was created with BioRender.com.

interactions that would otherwise be difficult or impossible to observe. The examples include but are not limited to determining the equilibrium binding constants of proteins for

the membrane or receptors on the membrane (Kalb et al., 1990); characterizing protein binding and protein partitioning between liquid-ordered and liquid-disordered membrane phases (Wan et al., 2011); and furtherly recording the kinetics of vesicle docking and fusion between dense core vesicles or vesicles reconstituted with synaptobrevin and planar supported membranes reconstituted with the acceptor SNARE complex (Domanska et al., 2009; Kreutzberger et al., 2017).

There are two geometries, *trans* and *cis*, in which a TIRF microscope can be configured (Figure 2.4). In the *trans*-geometry, the incidental wave is guided through a prism on the opposite side of the objective lens, and this is also known as the prism method. In contrast, in the *cis*-geometry, or the objective lens method, the incidental wave is guided through the objective lens. In our research, the prism-based technique was used preferentially to introduce the excitation wave so that the excitation light path and the emission channel are separated, the evanescent field is not contaminated, and the angle of the incident wave is better controlled. The experimental procedure and parameter settings of TIRF microscopy will be introduced in more detail in the next sub-section.

2.2.4.2 Experimental Procedures of TIRF Microscopy

In this thesis, TIRF has been used to investigate the interaction between complexin (or complexin mutants) and the planar supported bilayers in the presence or absence of several factors such as PIP2, C2AB, MARCKS-ED, and the acceptor SNARE complex. The fluorophore label Alexa546 was attached at CpxE47 after the site was mutated to a cysteine.

The planar supported bilayers with desired lipid composition were prepared as described in the previous section. All experiments examining the interaction between complexin and planar bilayers were carried out on an Axiovert 35 Fluorescence Microscope (Carl Zeiss, Thornwood, NY), equipped with a 40× water immersion objective (N.A. = 0.95; Carl Zeiss, Thornwood, NY) and prism based TIRF illumination. The prism-quartz interface was lubricated with glycerol to allow easy translocation of the sample chamber on the microscope stage. The light source was an OBIS 532 LS laser (Coherent, Santa Clara, CA). The beam was totally reflected an angle of 72° from the surface normal,

resulting in an evanescent wave that decays exponentially with a characteristic penetration depth of ~100 nm. Fluorescence was observed through a 610-nm band-pass filter (D610/60, Chroma Technology, Brattleboro, VT) by an electron multiplying CCD camera (DU-860E, Andor Technology, Belfast, Northern Ireland), which was cooled to -70℃ normally. The gain was set to an electron gain factor of ~100. An elliptical area of 250 × 65 μm^2 was illuminated. The laser intensity, shutter, and camera were controlled by a homemade program written in LabVIEW (National Instruments, Austin, TX). The fluorescence intensity in the field was recorded every 15 sec for 2 min before the addition of 1 μM complexin $E47A_{546}$ to get the baseline. During and after addition of the complexin in reconstitution buffer (150 mM KCl, 20 mM HEPES, pH 7.4) with 100 μM EDTA or Ca^{2+}, the measurements were taken constantly every 15 sec for at least 20 min to get a binding curve. When the effect of C2AB on the complexin membrane binding was examined, the planar supported bilayer was incubated with 0.4 μM C2AB for 15 min, after which the C2AB was washed away by 2 chamber volumes of reconstitution buffer. The sample chamber was then loaded to the microscope stage to start intensity-recording following procedures described above. For complexin interaction with planar supported bilayers in the presence of the effector domain of myristoylated alanine-rich C-kinase substrate (MARCKS-ED), before intensity-recording, the supported bilayer was incubated with 1 μM MARCKS-ED for 15 min. The sample chamber was then directly loaded to the microscope stage and intensity-recording was started before 2 chamber volumes of 1 μM complexin $E47A_{546}$ containing 1 μM MARCKS-ED was injected.

Experiments examining the Cpx membrane binding in the presence of docked dense core vesicles (DCVs) were performed on a Zeiss Axiovert 200 fluorescence microscope (Carl Zeiss), equipped with a 63× water immersion objective (Zeiss; N.A.=0.95) and a prism-based TIRF illumination (Kreutzberger et al., 2017). The light source was a 514 nm beamline of an argon ion laser (Innova 90C, Coherent), controlled through an acousto-optic modulator (Isomet), and a diode laser (Cube 640, Coherent) emitting light at 640 nm. Fluorescence signals were recorded by an EMCCD (iXon DV887ESC-BV, Andor Technology). The EMCCD camera was cooled to −70°C, and the electron gain factor was set between 200 and 220. The prism-quartz interface was lubricated with glycerol to allow easy translocation of the sample cell on the microscope stage. The beam was totally

internally reflected at an angle of 72° from the surface normal, and the characteristic penetration depth was ~102 and ~130 nm for the 514- and 640-nm lasers, respectively. The laser intensity, shutter, and camera were controlled by a homemade program written in LabVIEW (National Instruments). An OptoSplit (Andor Technology) was used to separate the fluorescence from Alexa546 (complexin) and Cy5 (DCV) fluorescence. Acceptor t-SNARE proteins containing planar supported bilayers were washed with fusion buffer (120 mM potassium glutamate, 20 mM potassium acetate, and 20 mM HEPES, pH 7.4) containing 100 μM EDTA, and then incubated for 20 min with 0.5 μM Munc18, 2 μM CpxE47Alexa$_{546}$, and 100 μM EDTA. During the incubation, the sample chamber was loaded to the microscope, the microscope was focused, and the recording was started by taking one image per second. The DCV sample (50 to 100 μL depending on preparation was diluted into 2 mL fusion buffer) was then perfused in while keeping the concentrations of Munc18-1 and complexin-1 constant. Both the complexin membrane binding and DCV docking were recorded for 20 min, and images were spooled directly to the hard drive.

2.2.5 Fluorescence Anisotropy

As a powerful tool to measure the binding constant and kinetics of reactions, fluorescence anisotropy is originated from the existence of transition moments for absorption and emission that lie along specific directions within the fluorophore structure. It is the phenomena when exposed to polarized light, those fluorophores that have their absorption transition moments aligned within a range of the electric vector of the incident light are preferentially excited, and the emission of most samples are polarized consequently. While anisotropy is defined as $r = (I_{VV}-G*I_{VH}) / (I_{VV}+2G*I_{VH})$, anisotropy measurements reveal the average angular displacement of the fluorophore that occurs between absorption and subsequent emission of a photon. When fluorophores are chemically linked to a protein, fluorescence anisotropy reflect the local conformational motion of the labeled residue and can be used to probe for changes such as complex formation or dissociation of a labeled protein (Lakowicz, 2006).

In this thesis work, all anisotropy measurements were performed in a FluoroMax®-3 spectrofluorometer (HORIBA scientific, Kyoto, Japan) installed with a magnetic stir, an

in-built L-format dual polarizer (Model FL-1044, Jobin Yvon), and a temperature bath (Model F-1000/1). The binding of complexin and its mutants to the vesicles were monitored with a Alexa546 label at positions like E2, K18, C105, and T119. The excitation and emission wavelength was set to 556 nm and 573 nm respectively. 50 nM of labeled complexin or its mutants were utilized in each titration experiment, and all the measurements were taken at a temperature of 20 ℃ in a reaction volume range of 1150 ~ 1250 μL as more vesicles were added gradually.

Following a previously developed method using continuous wave electron paramagnetic resonance to measure the partition coefficients, the complexin membrane interactions were quantitatively examined (Victor and Cafiso, 2001). The anisotropy readout at each lipid concentration was contributed by two components, the free fraction in the aqueous solution and the membrane bound fraction:

$$Ani = f_{bound} * Ani_{bound} + f_{free} * Ani_{free} \qquad \text{Equation 2.1}$$

where f_{free} represents the fraction of complexin that is in the aqueous solution, f_{bound} represents the fraction of complexin that is membrane bound, Ani_{free} is the anisotropy of complexin that is free in solution, and Ani_{bound} represents the anisotropy when complexin is fully bound to the membrane. In this equation the sum of f_{free} and f_{bound} should always be 1. The partition coefficient, which is the reciprocal of dissociation constant and represents the ratio of concentrations of complexin in the two phases, is used as the parameter to measure the membrane affinity of complexin as given in equation 2.2.

$$K_p = \frac{[Cpx_{bound}]/[AccLip]}{[Cpx_{free}]} \qquad \text{Equation 2.2}$$

In equation 2.2, [AccLip] represents the lipid concentration that is accessible for complexin interaction, $[Cpx_{bound}]$ represents the concentration of membrane bound complexin, and $[Cpx_{free}]$ represents complexin concentration in the aqueous phase. From equation 2.2, f_{bound} can be expressed in terms of K_p and $[AccLip]$ as shown in equation 2.3.

$$f_{bound} = \frac{[Cpx_{bound}]}{[Cpx_{bound}]+[Cpx_{free}]} = \frac{K_p[AccLip]}{1+K_p[AccLip]} \qquad \text{Equation 2.3}$$

While Ani_{free} can be directly measured before addition of vesicles, Ani_{bound}cannot be measured due to limited vesicle concentration in the assay or in a situation where the

partition coefficient of the peptide goes below 100 M^{-1}. Accordingly, K_p and Ani_{bound} are determined indirectly by least-squares using equation 2.4.

$$Ani = \frac{K_p[AccLip]}{1+K_p[AccLip]} * Ani_{bound} + \frac{1}{1+K_p[AccLip]} * Ani_{free} \qquad \text{Equation 2.4}$$

2.2.6 Site Directed Spin Labeling and Electron Paramagnetic Resonance

2.2.6.1 Theory of EPR

Electron paramagnetic resonance (EPR), also called electron spin resonance, is a spectroscopic technique works by examining the interaction between an external electromagnetic field and its induced magnetic moments on a paramagnetic material, and it can be used for a variety of applications in physics, chemistry and biology. The first EPR spectrum was observed by the Soviet physicist Yevgeny Zavoisky in 1944 (Zavoisky, 1944) from a $CuCl_2 \cdot 2H_2O$ sample. After the development of radar systems during world war II, availability of the complete microwave range in the post-war era provided necessary components to build the first spectrometer. Early applications of EPR were limited to naturally occurring paramagnetic substances such as transition-ions and radical intermediates. EPR was not applicable to study biological materials, which show very rare occurrence of paramagnetism, until the successful synthesis introduction of nitroxide spin labels in the 1960s (Stone et al., 1965). By attaching the spin label to sites of interest in the protein or phospholipids, site directed spin labeling based continuous wave EPR has developed to be a powerful tool in solving biomedical and biological problems by providing information on the local environment of a selected site within a macromolecule or a complex. For example, secondary structure and tertiary contact of specific sites in a large protein and membrane penetration depth of a selected site in a membrane binding peptide can be revealed or derived from continuous wave EPR spectra (Mchaourab et al., 1996; Hubbell et al., 2000). Pulse EPR provides further structural information by measuring distances and distance distributions between two labeled sites (Jeschke, 2012).

As previously mentioned, in order to perform EPR experiments, a paramagnetic probe at the site of interest in the protein is essential. Since the majority of substances, including biochemical and biological samples, are diamagnetic and have no magnetic

moments in the electronic ground state, a paramagnetic tracking molecule is introduced into studied systems at particular sites and this technique is called site-direct spin labeling. In our research, a thoroughly characterized spin label S-(1-oxyl-2,2,5,5-tetramethyl-2,5-dihydro-1H-pyrrol-3-yl) methyl methanethiosulfonate (MTSL) is introduced to the particular sites of complexin via a disulfide bond (Berliner et al., 1982) (Figure 2.1 A). For free radicals such as the nitroxide label, there is a magnetic moment associated with the free unpaired electron. This intrinsic magnetic moment $\boldsymbol{\mu_e}$ is related with its spin angular momentum:

$$\boldsymbol{\mu_e} = g_e \beta_e \boldsymbol{S} \qquad \text{Equation 2.5}$$

where g_e is the dimensionless 'g-factor', also called Landè factor, β_e is the Bohr magneton, and $\boldsymbol{S}$ is the spin angular momentum of electrons respectively. In almost all EPR spectroscopy measurements on organic radicals, spin angular momentum contributes more than 99% to the overall induced electron magnetic dipole while the contribution of orbital

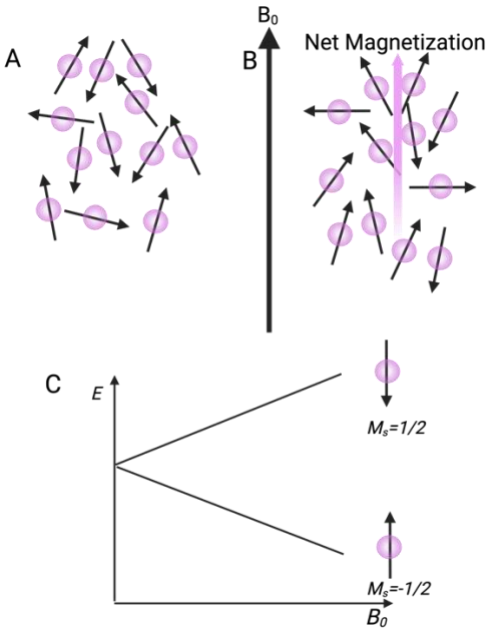

Figure 2.5 Electron Zeeman effect. (A) Every electron has an intrinsic magnetic moment. Since the electron is a spin ½ particle, the spins may assume one of two directions along any one axis, but there is no preferred direction and no net magnetization in the absence of a magnetic field. (B) As an external magnetic field B_0 is applied, more electron magnetic moments align with ($Ms = -\frac{1}{2}$) than against ($M_s=\frac{1}{2}$) the external field, resulting in a bulk net magnetization. Each alignment has a specific energy due to the Zeeman effect. (C) The energy diagram shows that the difference between two states is linearly proportional to the strength of the external magnetic field as equation 2.7 indicates. It is worth noted that 1) the magnetic moment of an electron is opposite in direction to its angular momentum; 2) the arrows in the figure represent the direction of electron magnetic moments instead of angular momentum; 3) nuclear Zeeman effect occurs similarly except the fact that nuclear magnetic moments and nuclear spin angular momenta point to the same direction for most nuclei. Figure was created with BioRender.com.

motion and spin-orbit interaction is negligible. When unpaired electrons are placed within an external magnetic field B_0, the magnetic moments will either align with or against the external magnetic field, giving rise to two different energy levels of the different spin states ($M_S = \pm\frac{1}{2}$), and this is called the Zeeman effect (Figure 2.5).

The energy level of the single electron depends on the spin quantum number and the strength of the external field, and the energy difference between the two states is correlated with the external magnetic field linearly:

$$E = M_S g_e \beta_e B_0 = \pm\frac{1}{2}\, g_e \beta_e B_0 \qquad \text{Equation 2.6}$$

and

$$\Delta E = h\nu = g_e \beta_e B_0 \qquad \text{Equation 2.7}$$

where h is the Plank's constant and ν is the frequency of a perpendicular (relative to the external field) incident magnetic radiation.

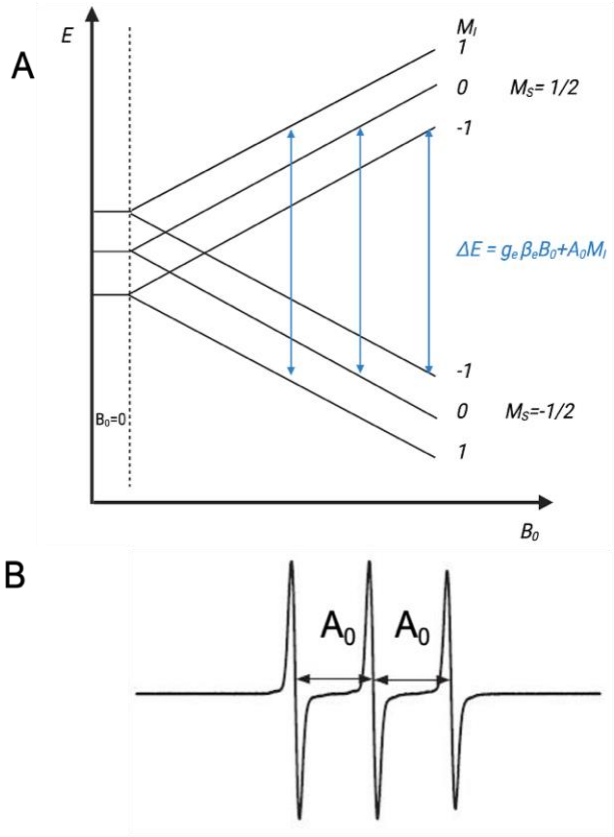

Figure 2.6 The hyperfine interaction of atoms with S= ½ and I=1, such as the nitroxide. (A) Energy diagram and allowed EPR transitions at constant frequency and sweeping magnetic field B_0. Following the selection rule, three transitions are possible as indicated by the blue arrows. (B) Three EPR peaks could be produced at low field (M_I=1), center field (M_I=0) and high field (M_I=−1) from left to right accordingly. The sharp peaks shown here is a simulated spectrum assuming that the label is moving freely in solution.

In addition to the contribution of the electron Zeeman effect, the unpaired electron in nitroxide label is also sensitive to the magnetic moments of the nuclei and such an interaction is called hyperfine interaction. Nuclei possess nuclear magnetic moments $\boldsymbol{\mu_I}$ intrinsically, just similarly to unpaired electrons:

$$\boldsymbol{\mu_I} = g_I \beta_I \boldsymbol{I} \qquad \text{Equation 2.8}$$

where g_I, β_I, and $\boldsymbol{I}$ are the 'g-factor', Bohr magneton and spin angular momentum of the nuclei respectively. In an external magnetic field, while parallelly aligned nuclei magnetic moments add to and increase the effective magnetic field experienced by the electron, antiparallel nuclei magnetic moments decrease the effective magnetic field strength. Consequently, the nuclei magnetic moments further split the energy levels, leading to more informative EPR spectra lineshape. When the nuclear Zeeman effect and hyperfine splitting are added to equation 2.6:

$$E = g_e \beta_e B_0 M_S + g_I \beta_I B_0 M_I + A_0 M_S M_I \qquad \text{Equation 2.9}$$

where M_I is the nuclear spin quantum number and A_0 is the isotropic hyperfine coupling constant. For the nitroxide radical utilized in this thesis, $S = \frac{1}{2}$ and $I = 1$, there can be six spin states, as $M_S = \pm\frac{1}{2}$ and $M_I = 1, 0, -1$. Transitions in EPR follow the selection rule $\Delta M_s = \pm 1$, and $\Delta M_I = 0$, meaning that only those transitions that flip the electron spin are allowed (Figure 2.6). Following this selection rule, only three transitions are allowed, and equation 2.7 will be expanded as:

$$\Delta E = h\nu = g_e \beta_e B_0 + A_0 M_I \qquad \text{Equation 2.10}$$

EPR spectra are recorded differently from some spectroscopic techniques. While a traditional absorption or emission spectrum might be recorded by scanning the frequency of the electromagnetic radiation to match the energy difference for spins in a fixed external magnetic field, EPR spectra are obtained by sweeping the magnetic field while keeping the frequency of the incident wave constant alternatively. Magnetic-field sweeping is favored over frequency sweeping simply because it is technically not feasible to change the microwave frequency in the instrument. The field strength which matches the energy difference is called the 'field of resonance'. For nitroxide radicals in aqueous solution, EPR spectra are recorded with 100 Gauss magnetic field sweeps centered around 3500 Gauss and electromagnetic resonance occurs primarily around the microwave frequency 9.5 GHz

in the medium microwave-frequency region. In order to filter out random noise and junk signal oscillates at different frequencies, another feature of EPR spectra is that it is the first derivative of a field-sweep absorption (Figure 2.6 B and Figure 2.7 line b) that is recorded during the field-sweeping. This is achieved by modulating the external magnetic field with an oscillating 1 Gauss amplitude field at a 100 kHz frequency while the main magnetic field is swept. The resulting signal is at 100 kHz and is detected using a phase-sensitive detector (Figure 2.7). Details about the experimental procedures are described in the next sub-section.

In comparison with techniques that are typically employed to investigate protein structure such as nuclear magnetic resonance (NMR) and x-ray chromatography, SDSL-based EPR has several advantages. SDSL has no molecular weight limitations, and it can be applied to small soluble proteins as well as to large membrane bound molecular complexes. Proteins do not need to be crystalized and can be examined under a native environment without the need for precipitants. EPR also provides information on conformational exchange in proteins and on protein dynamics (Hubbell et al., 1996), and does so in a way that is complementary to some NMR approaches without the same molecular weight limitations.

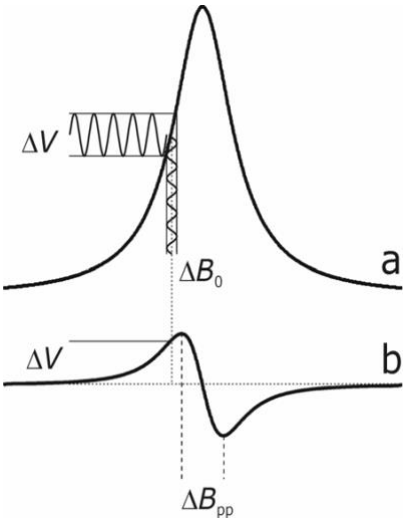

Figure 2.7 Field modulation and phase sensitive detection. In continuous wave EPR, the external magnetic field is modulated sinusoidally with amplitude ΔB_0 at proper modulation frequency so that the EPR signal is transformed into a sine wave with an amplitude ΔV, which is proportional to the slope of the absorption curve (line a). The first derivative of the absorption curve (line b) is recorded by comparing the phase of the signal with that of the modulation source. Details about instrumentation aspects can be found in Hemminga and Berliner, 2007.

2.2.6.2 Experimental Set Up of EPR

Complexin interaction with sonicated or extruded vesicles were quantified using site-directed spin labeling based EPR following a procedure reported before (Victor and Cafiso, 2001; Zdanowicz et al., 2017). Briefly, the EPR spectra were recorded when a specific concentration of spin labeled complexin was titrated with gradually increasing amount of lipid vesicles. For complexin concentration equal to or higher than 20 µM, spin labeled complexin and lipid vesicles were mixed in specified ratios with a final volume of 15 µL, and 6 µL of the sample was loaded with a Hamilton syringe into a 0.6 mm × 0.8 mm – 100 mm (inner diameter × outer diameter - length) borosilicate glass capillary (VitroCom, Mt. Lakes, NJ). For titrations with less than 20 µM complexin, 100 µL sample of spin labeled complexin and lipid vesicles mixture in specified ratios were loaded via Pasteur transfer pipette to a VT TE102 aqueous flat cell (Wilmad Lab Glass, Vineland, NJ). Spectra were recorded on an EMX X-band EPR spectrometer (Bruker, Billerica, MA) at 2 mW incident microwave power with modulation amplitude of 1 G and frequency of 100 kHz. The magnetic field was swept through 100 G and up to 30 scans were performed to improve the S/N ratio. The peak-to-peak amplitude of the $m_I = 0$ EPR resonance of complexin was then measured as a function of the concentration of lipid vesicles. The spectra were processed using LabVIEW programs provided by Christian Altenbach (University of California, Los Angeles, CA). The partition coefficients can be determined similarly as described in section 2.2.5 by fitting amplitudes of the spectra with respect to accessible lipid concentrations to a simple Langmuir isotherm.

2.2.7 Phosphate Assay

The final concentration of either the extruded or sonicated vesicles were quantified using the Bartlett phosphate assay (Bartlett, 1959) modified as described previously (Pokorny et al., 2002). Briefly, 0, 20, 40, 60, 80, 100, 150, 200 µL of 1 mM KH_2PO_4 standards were pipetted and adjusted to 300 µL in glass tubes with distilled water. For a vesicle sample with an expected lipid concentration of 10 mM, 15 µL sample was diluted to 300 µL in glass tubes for measurements. Each standard and each sample was prepared in sets of 3 for repetition purposes. 700 µL of 70% perchloric acid were added to each of the tube. The tubes were then covered with glass marbles and placed in a heating block at 200 ℃ for an hour so that organic sample could be digested into inorganic phosphate. The tubes then

were removed from the hot block and cooled down to room temperature before adding up of 2 mL of 1% ammonium molybdate. After vortexing, a colorless anion $PMo_{12}O_{40}^{3-}$ could be formed. 2 mL of freshly prepared 4% ascorbic acid was then added and mixed with the sample to reduce the colorless anion $PMo_{12}O_{40}^{3-}$ into an intensely colored mixed-valence complex: $PMo_4Mo_8O_{40}^{7-}$. By incubating the sample tubes in a water bath of 37 ℃ for 1 hour, the complex formation could be accomplished. The absorption of the standards as well as the samples were measured after the spectrophotometer was zeroed by measuring the blank standard at 800 nm. A standard curve could be generated by using the concentrations of the standards and the total lipid concentration could be determined based on the standard curve.

3. RESULTS

3.1 Effect of Lipid Composition on the Cpx Membrane Interaction

Complexin-1 (Cpx) is a highly charged soluble presynaptic peptide consists of a central helical domain flanked by unstructured N- and C-terminal domains. While the central helix domain bind to the assembled SNARE complex with nanomolar affinity (Pabst et al., 2002), previous work in our lab found that Cpx interacts simultaneously with the plasma membrane SNARE proteins and the lipid membrane (Zdanowicz et al., 2017). Cpx binds to the membrane via its terminal domains and both fusion assays and genetic studies show that the Cpx membrane interaction plays significant roles in mediating membrane fusion (Seiler et al., 2009; Wragg et al., 2013; Lai et al., 2016). On the one hand, the N-terminal domain of Cpx has been demonstrated to be essential to facilitate Ca^{2+}-triggered neurotransmitter release (Xue et al., 2009) and mutation of conserved hydrophobic amino acids into acidic ones abolished the Cpx-membrane interaction as well as the ability of Cpx to activate Ca^{2+}-triggered vesicle fusion (Lai et al., 2016). On the other hand, membrane interaction of the C-terminal domain of complexins from *C. elegans* and *D. melanogaster* has been implied to suppress the spontaneous release and mutations disrupting membrane interaction abolished the inhibitory function (Cho et al., 2010; Wragg et al., 2013). Despite the important roles of the Cpx membrane interaction, the molecular mechanism by which it acts remains unclear. Part of the difficulty in identifying the role of Cpx/membrane interaction in neuronal exocytosis is likely due to an insufficient characterization of the Cpx membrane interaction.

Computational work as well as experimental results show that lipids play key roles in membrane fusion. Molecular dynamic simulations indicate that the kinetics of fusion is dependent upon lipid composition (Kasson, 2007). Cholesterol is a critical lipid that plays multiple roles in membrane fusion as described in a recent review (Yang et al., 2016). In a hybrid membrane fusion system, asymmetric distribution of phosphatidylethanolamine was discovered to control the fusion pore lifetime and fusion probability (Kreutzberger et al., 2017). Recently, it was shown that the conformation of the SNARE complex can be mediated directly by an important plasma membrane component phosphatidylinositol (4,5)

bisphospate (PIP2) (Kiessling et al., 2018). Although particular membrane components play important roles when examined *in vitro* or *in vivo*, it is not clear how they mediate the Cpx membrane interaction. Here, the effect of membrane composition on the Cpx membrane interaction was systematically characterized and assessed using fluorescence anisotropy.

Fluorescence anisotropy is a sensitive and widely used tool to measure the binding constants between a fluorophore labeled ligand and corresponding receptors. Since previous work in our lab showed that Cpx interacts with the membranes mainly through its terminal domains, we chose to attach Alexa546 fluorophore label on the N-terminus of Cpx at K18. The effect of lipid composition on the Cpx membrane interaction was assessed by comparing the partition coefficients of Cpx when it binds to small unilamellar vesicles (SUVs) composed of lipids with either different acyl chain order or headgroups. Figure 3.1 shows an example of titration of Cpx with sonicated vesicles composed of 34 mol% 1-palmitoyl-2-oleoylphosphatidylcholine (POPC), 30 mol% 1-palmitoyl-2-oleoyl-sn-glycero-3-phosphoethanolamine (POPE), 15 mol% 1-palmitoyl-2-oleoyl-phosphatidylserine (POPS), 1 mol% porcine brain L-α-phosphatidylinositol-4,5-bisphosphate (bPIP2) and 20 mol% cholesterol (Chol). This lipid composition was

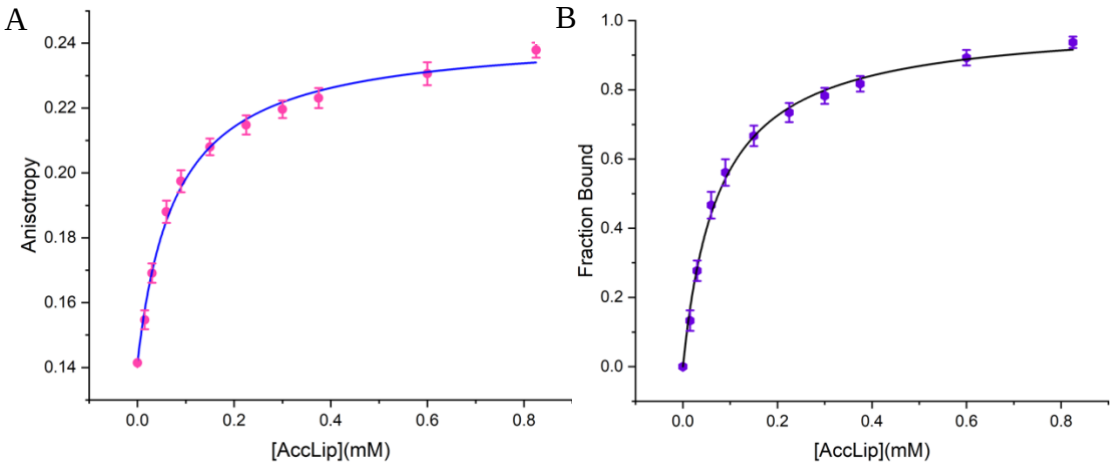

Figure 3.1 Titration of Cpx with sonicated PO vesicles via fluorescence anisotropy. (A) Fitting of the anisotropy versus accessible lipid concentration using equation 3.4. (B) The fraction of membrane bound Cpx as a function of accessible lipid concentration. Bound fraction of Cpx at each lipid concentration can be calculated via K_p. Error bars represent standard deviation from 3 to 5 repeats.

employed as a standard mixture in our initial studies. When gradually increasing concentrations of SUVs were titrated into 50 nM Cpx, the rotational diffusion rate of the fluorophore label on Cpx slows due to membrane association, leading to an increase in anisotropy. After fitting the anisotropy value at different vesicle concentrations to a simple binding isotherm (see section 2.2.5), the membrane partition coefficient for Cpx, K_p, is obtained (Figure 3.1 A). K_p is also the reciprocal molar binding affinity of Cpx. Larger partition coefficients represent stronger interactions between the peptide and the membrane. With a partition coefficient, the fraction of protein that is bound to the membrane at different lipid concentrations can be calculated accordingly (Figure 3.1 B). The derived partition coefficients are plotted and compared collectively in Figure 3.2 and 3.3.

3.1.1 The Effect of Headgroup

We began by examining the effect of headgroup on the Cpx-membrane interaction at physiological ionic strength, using a set of sonicated vesicles composed of lipids with

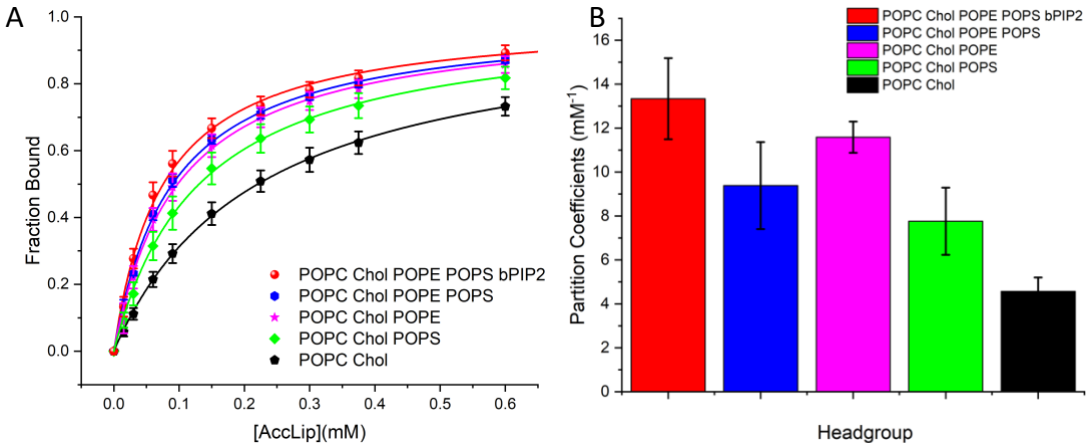

Figure 3.2 Effect of lipid headgroup on the Cpx membrane interaction. (A) Titration of POPC/Chol/POPE/POPS/bPIP2 (red spheres), POPC/Chol/POPE/POPS (blue hexagons), POPC/Chol/POPE (magenta stars), POPC/Chol/POPS (green diamonds), and POPC/Chol (black pentagons) vesicles yielded the membrane bound fraction of Cpx as a function of accessible lipid concentration. (B) Derived partition coefficients for Cpx binding to vesicles composed of POPC/Chol/POPE/POPS/bPIP2 (red), POPC/Chol/POPE/POPS (blue), POPC/Chol/POPE (magenta), POPC/Chol/POPS (green), and POPC/Chol (black). Error bars represent standard deviation from 3 to 5 repeats.

moderate chain order 1-palmitoyl-2-oleoyl (except for 1 mol% bPIP2), but different headgroups. Starting with the standard lipids composition as a neuronal plasma membrane mimic, POPC:POPE:POPS:bPIP2:Chol = 34:30:15:1:20, titrations were performed respectively with each lipid composition: whenever a certain component of headgroup was removed, corresponding molar percent of POPC was added and the minimal composition was POPC:Chol = 80:20. The titration curves for each lipid headgroup composition are shown in Figure 3.2 A, and the partition coefficients are compared in Figure 3.2 B. Taking the standard lipid composition (red spheres or bar) as the reference, it is interesting to notice that the bound fraction of Cpx at each particular lipid concentration drops slightly when 1 mol% of PIP2 was removed (blue hexagons or bar). Although this difference is just at the error limits (Figure 3.2 B), the result suggests that PIP2 may enhance the Cpx membrane interaction in this bulk system. Additional evidence for this sensitivity of the Cpx membrane to PIP2 will be presented in section 3.3 and 3.4. Compared to the minimal composition POPC/Chol vesicles (black pentagons or bar), addition of 30 mol% POPE (magenta stars or bar) facilitates the Cpx membrane interaction. The potential of POPE to boost the Cpx membrane interaction might be attributed to the small size of the ethanolamine group, which enhances the insertion of hydrophobic side chains into the membrane interior. The presence of POPS appears to slightly enhance the Cpx membrane interaction as indicated by a comparison of the titration curves for POPC/POPS/Chol (green diamonds) vesicles with the minimal composition POPC/Chol (blue pentagons). This effect might be the result of an altered electrostatic potential on the double layer when 15 mol% anionic POPS was included (Jurkiewicz et al., 2011). The results here indicates that headgroup of lipids has minimal effect on the Cpx membrane interaction.

3.1.2 Cpx Preferentially Binds to Membranes with More Disordered Acyl Chains

Previous work proposed that the C-terminal domain of Cpx binds to the bilayers by inserting its hydrophobic residues into the small packing defects on the membrane surfaces (Snead et al., 2014). Unsaturation of acyl chains and small headgroups are sources for packing defects. However, the effect of acyl chain order on the Cpx membrane interaction

has never been compared directly. Moreover, acyl chain order has been shown to have a profound effect on some components of the fusion machinery. For example, the orientation of the SNARE complex in the bilayer is heavily influenced by the lipid acyl chains: the more disordered lipids cause the SNARE complex to favor an orientation that promotes

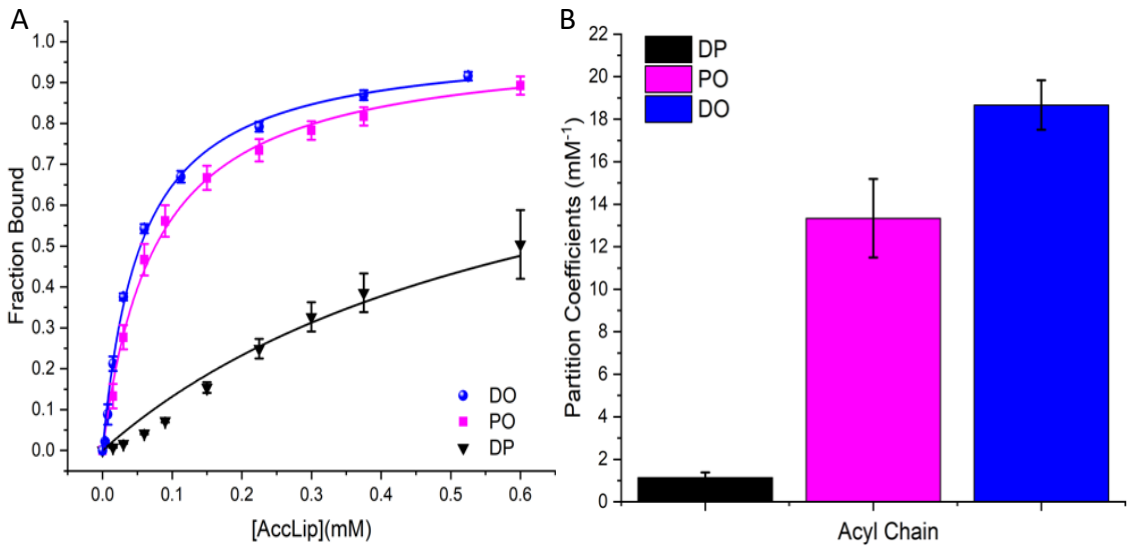

Figure 3.3 Effect of acyl chain order on the Cpx membrane interaction. (A) Titration of CpxK18 with vesicles consisting the same headgroup, namely PC:Chol:PE:PS:bPIP2 = 34:20:30:15:1, but different acyl chains 1,2-dipalmitoyl (black triangles), mixed 1-palmitoyl-2-oleoyl (magenta squares) and both unsaturated 1,2-dioleoyl (blue spheres) yielded the fraction of membrane bound Cpx as a function of accessible lipid concentration. (B) Derived partition coefficients for Cpx binding to vesicles composed of 1,2-dipalmitoyl (black bar), mixed 1-palmitoyl-2-oleoyl (magenta bar), and 1,2-dioleoyl (blue bar). Error bars represent standard deviation from 3 to 5 repeats.

SNARE assembly and zippering, which in turn enhances fusion in a reconstitution assay (Kiessling et al., 2018). To further explore the potential effects that the fatty acyl chain saturation might have on regulatory proteins like Cpx, we altered the acyl chains composition while keeping the headgroup components unchanged as a mimic of the neuronal plasma membrane: PC:PE:PS:bPIP2:Chol = 34:30:15:1:20. We chose three sets of lipid acyl chains: both saturated 1,2-dipalmitoyl (16:0, DP), mixed 1-palmitoyl-2-oleoyl (16:0/18:1, PO) and both unsaturated 1,2-dioleoyl (18:1, DO). Titrations using fluorescence anisotropy showed that Cpx binds the most unsaturated/disordered DO vesicles (blue spheres or bar) with a higher affinity than either the more saturated/ordered PO (magenta squares or bar) or DP (black triangles or bar) vesicles (Figure 3.3). In 100

μM EDTA buffer, the binding affinity of Cpx to DO vesicles is 16-fold stronger than to DP vesicles with the fully saturated acyl chains, and this difference corresponds to a free energy difference of 6.9 kJ/mol. A similar trend was observed in 100 μM Ca^{2+}: the Cpx binding to DP vesicles with most ordered acyls chains is 12.84-fold weaker than to the DO vesicles with the lowest order of acyl chains (data not shown).

We think that the preference of Cpx for vesicles with smaller headgroups or more disordered acyl chains correlates well with its sensitivity to membranes of different curvatures, as smaller headgroup structure, more disordered acyl chain and higher membrane curvature all could favor the exposure of the acyl chains to the aqueous environment and facilitate the interaction between the membrane interior and hydrophobic residues on the Cpx terminal domains. Mutagenesis and circular dichroism studies showed that an amphipathic region near the C-terminus of human or *C. elegans* Cpx binds liposomes (Seiler et al., 2009; Wragg et al., 2013). This amphipathic region is normally unstructured in solution, but it folds into an α-helix upon membrane association, reducing the energy penalty of exposing the peptide bonds to a hydrophobic environment and creating a segregation of hydrophilic and hydrophobic residues between the opposite faces of the α-helix (Grin and Antonny, 2010). Insertion of the hydrophobic residues into the nonpolar acyl chains of lipids would account for the ability of these amphipathic regions

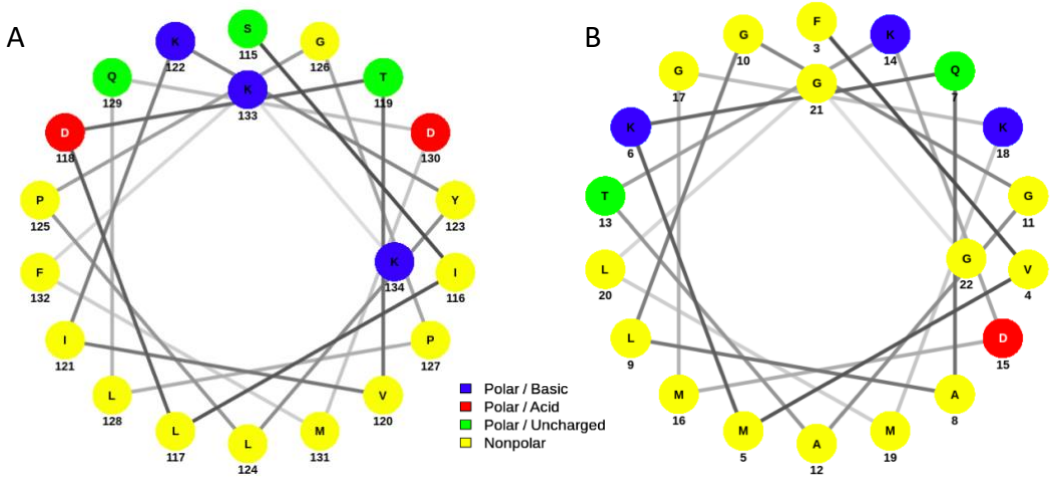

Figure 3.4 Helical wheel diagrams of the amphipathic region for the C-terminal domain (A) and the N-terminal domain (B) of *Rattus norvegicus* Cpx. Color code for residues: yellow, hydrophobic; green, polar but uncharged; red, acidic; blue, basic. Figure was made at *http://lbqp.unb.br/NetWheels/*.

to

sense membrane curvature and recognize lipid composition. Given that our previous work found that N-terminal domain of Cpx binds to the membrane in a curvature sensitive manner as well, we did a sequence analysis on both ends of Cpx. Helical wheel diagrams show that not only the C-terminal domain has a amphipathic region (Figure 3.4 A), but the N-terminal domain also has the potential to be transformed into laterally amphipathic helix upon membrane interaction (Figure 3.4 B). Sequences of both ends show that the hydrophobic and polar residues are towards either the lipid surface or the aqueous solution once a helix is formed.

3.2 Cpx Interferes with Itself in Membrane Binding

3.2.1 The Terminal Domains of Cpx Compete for Membrane Binding

During the investigation Cpx-membrane interaction, we noticed that the partition coefficients were dependent on the Cpx concentration that is used in the titration experiments. At the very beginning, titration of Cpx with SUVs was performed to test if the two ends of Cpx bind to the membrane cooperatively, independently of competitively. The titrations were performed using site directed spin labeling based electron paramagnetic resonance (EPR) and we placed the spin label at position T119 for both peptides. EPR is a well-suited technique to probe local environment of macromolecules in physiological conditions that are compatible with a membranous environment and spectra lineshape is sensitive to changes in including backbone motion and tertiary contact (section 2.2.6.1). We truncated the first 26 amino acids at the N-terminus of Cpx (dNCpx), and compared the membrane binding affinity of the C-terminal domain of this peptide with that of the full length Cpx.

Figure 3.5 A shows that the EPR spectra of CpxT119R1 broaden gradually as increasing concentrations of SUVs are added. As described in section 2.2.6, the amplitudes of the spectra were extracted and fitted as a function of the accessible lipid concentration and the bound fraction of Cpx can be calculated according to the partition coefficients derived from the fitting (Figure 3.5 B and C). Titrations were done for both CpxT119R1 (black squares) and dNCpxT119R1 (green dots) and their binding curves are compared in

Figure 3.5 D. Surprisingly, the full length Cpx shows stronger membrane affinity than the N-terminal domain truncated peptide. This trend illustrates that the two end of Cpx might be competing with each other for membrane binding. Actually, our previous work has

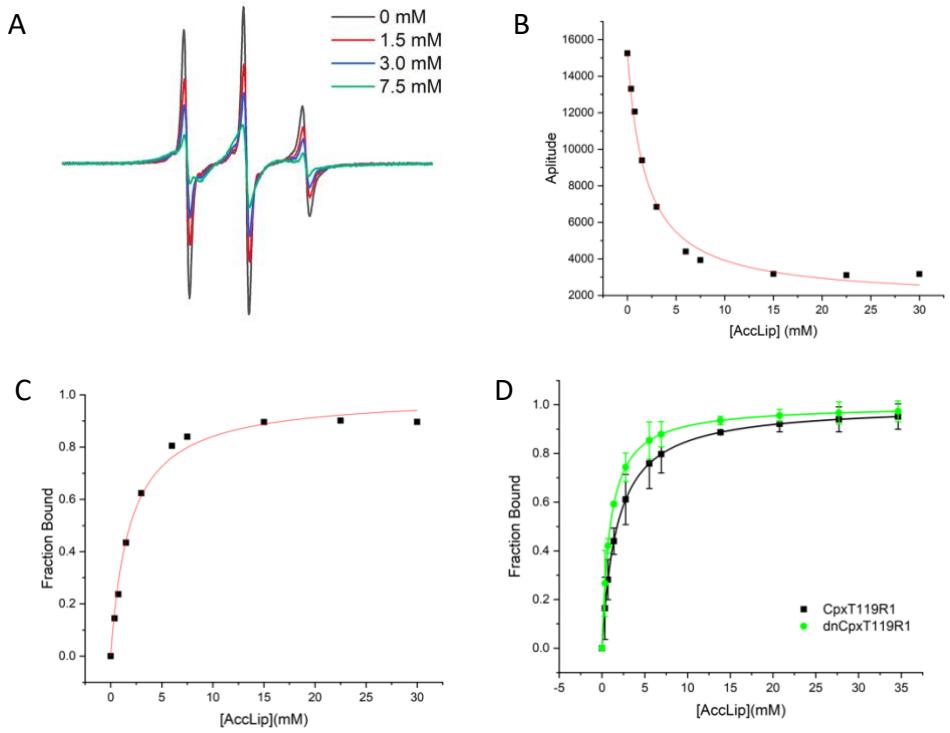

Figure 3.5 Titration of Cpx with SUVs via EPR shows that truncation of the N-terminal domain enhances membrane affinity of the C-terminal domain of Cpx. EPR spectra of CpxT119R1 (black) broadens as 1.5 mM (red), 3.0 mM (blue), and 7.5 mM (green) sonicated vesicles were added. (B) The amplitude of the spectra were utilized to determine Cpx-membrane partition coefficients by fitting to the accessible lipid concentration using equation 2.4. (C) Bound fraction of Cpx at each lipid concentration can be calculated via K_p, and the fraction of membrane bound Cpx as a function of accessible lipid concentration were plotted. (D) The binding of CpxT119R1 (black squares) in full length was compared with that for an N-terminal domain truncated version (dNCpxT119) (green dots) to SUVs. Error bars represent standard deviation from 3 repeats.

reported that the two ends of Cpx act independently in binding to membrane (Zdanowicz et al., 2017). The discrepancy here might result from a much higher concentration of Cpx that was used in the previous work. High Cpx concentrations in titration might give lower membrane affinity for both mutants and hence relatively small differences between full

length and N-terminal domain truncated Cpx could fall into the range of the error (data not shown). This self-competitive binding will be more clearly justified in the next section.

3.2.2 Cpx Interferes with Its Own Membrane Binding at Low Protein:Lipid Ratios

We explored the self-competitive membrane binding pattern further by examining how the membrane partition coefficient changes as a series of Cpx concentrations were used in the titration. We have titrated 2, 20, 40, and 80 μM Cpx respectively, and the binding curves show that the vesicle concentration that gets half of the Cpx bound decreases dramatically when Cpx concentration decreases. This reveals an inverse correlation between the partition coefficients and the Cpx concentrations because Cpx easily suffice to saturate limited binding sites on the vesicles. In Figure 3.6 B, the membrane partition coefficient of Cpx increases 44 times when the Cpx concentration decreased from 80 to 2 uM. Despite the fact that Alexa546 label is larger than the spin label and the fluorophore label is placed at the N-terminal domain, the affinity obtained with 50 nM CpxK18Alexa$_{546}$ using fluorescence anisotropy (13.34 mM^{-1}) is even stronger than that with 2 μM CpxT119R1 in EPR titration (8.28 mM^{-1}). The high membrane affinity at low Cpx concentration suggests that Cpx competes with itself for limited binding sites on the membrane surfaces.

To further verify the idea that Cpx is competing with itself on the membrane surface, we also took advantage of the fluorescence anisotropy measurements, which allows us to lower the Cpx concentration to nanomolar levels in the titration. We then tested for competition by adding non-labeled wild-type Cpx into mixture to see if membrane bound fluorescently labeled Cpx could be displaced from the membrane by wild-type Cpx. The left panel in Figure 3.6 C shows a titration carried out in a manner similar to the previously described titration experiments. As the concentration of sonicated vesicles is increased in the presence of fluorescently labeled CpxT119, an increase in anisotropy is observed as Cpx binds to the added vesicles. Then, wild-type Cpx was added into this mixture at the highest point in the titration. As seen in Figure 3.6 C (right panel), there is a dramatic drop in anisotropy as soon as the wild-type Cpx is added. Similar results were observed at the

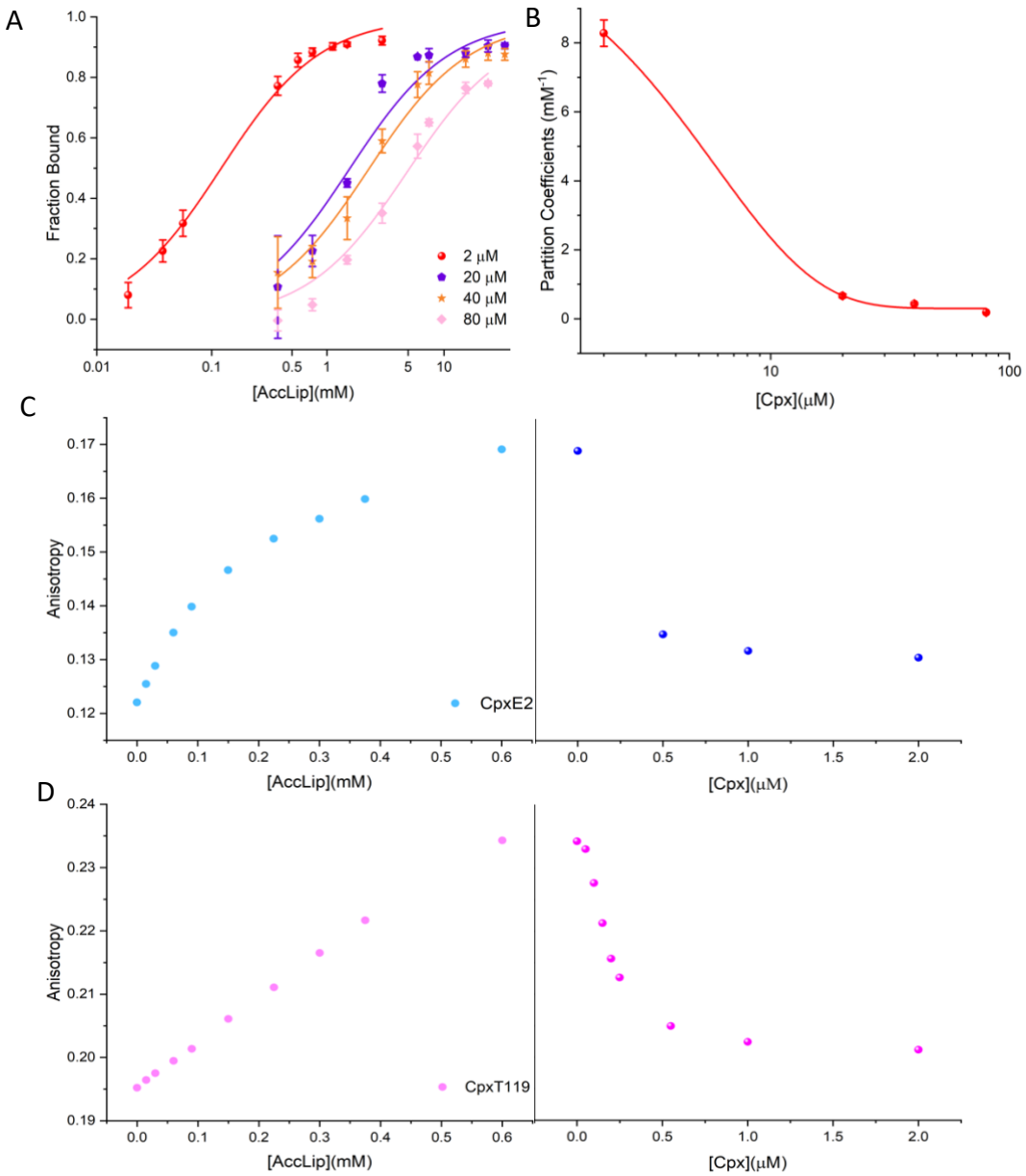

Figure 3.6 Self-competitive Cpx membrane binding. (A) Binding curves of 2 μM (red sphere), 20 μM (purple hexagon), 40 μM (orange star), 80 μM (pink diamonds) CpxT119R1 to sonicated PO-PM1 vesicles. (B) Partition coefficients of 2, 20, 40, 80 μM CpxT119R1 in sonicated PO-PM1 vesicles. Error bars represent standard error of the mean. (C and D) In the left panels, fluorescence of anisotropy of 50 nM CpxE2Alexa$_{546}$ (light blue dots, C) or CpxT119Alexa$_{546}$ (light magenta dots, D) increases with respect to increasing concentrations of sonicated vesicles that was added; at the highest point of the titrations, in the right panels, fluorescence anisotropy of CpxE2Alexa$_{546}$ (blue spheres, C) or CpxT119Alexa$_{546}$ (magenta spheres, D) decreases gradually as a function of the concentration of wild-type Cpx that was added to the system.

opposite end of the peptide when CpxE2Alexa$_{546}$ was examined (Figure 3.6 D). Remarkably, this drop occurs at relatively low Cpx concentrations that correspond to protein:lipid ratios of ~1: 6000 (Figure 3.6 D, right panel). Assuming the average surface area per lipid is 0.7 nm^2 (Lewis and Engelman, 1983), this ratio corresponds to an area of 4200 nm^2, which means Cpx modifies its own binding by reducing the affinity of Cpx for the membrane over a distance of ~65 nm. Considering that the Cpx-membrane interaction is highly sensitive to membrane curvature, this phenomenon might be explained by the altered membrane curvature strain. Once some Cpx has bound, the insertion of its hydrophobic residues into the membrane creates strain in the bilayer, making it less positively curved but more difficult for further Cpx binding.

3.3 The Cpx Membrane Interaction Is Sensitive to PIP2

In the bulk titration experiments examining the effect of lipid headgroup on the Cpx membrane interaction, we observed that PIP2 enhances the Cpx-membrane interaction (section 3.1.1). As a special membrane component in neuronal exocytosis (reviewed in Martin., 2012), PIP2 was shown to enhance both docking and fusion in the presence of Ca^{2+} (Hay, 1995) and inhibit spontaneous fusion when it is included in the t-SNARE containing liposomes (Vicogne, 2006). This regulatory behavior of PIP2 is very similar to the function of Cpx in clamping spontaneous release as well as facilitating evoked release. Although a moderate enhancement by PIP2 on the Cpx-membrane interaction using SUVs has been observed with anisotropy measurements, factors like very high membrane curvature in SUVs might interfere with the potential effect of PIP2. Accordingly, we further explored the effect of PIP2 on the Cpx membrane interaction using another two different approaches.

3.3.1 Cpx Binds to Vesicles Containing PIP2 with a Higher Affinity

First, to get around the extreme curvatures but also avoid any potential light scattering that could occur in anisotropy measurements, we examined the effect of PIP2 on the Cpx membrane interaction using slightly larger vesicles and the titrations were performed using EPR. We measured the partition coefficients of spin labeled Cpx, E2R1 as well as T13R1,

when it interacts with 100 nm extruded vesicles containing 2 mol% bPIP2 (POPC:POPS:bPIP2 = 68:30:2, green) or in the absence of PIP2 (POPC:POPS=70:30, peach) (Figure 3.7). In agreement with previous results, the titration curves below show that, at the same accessible lipid composition for both CpxE2R1 (Figure 3.7 A) and CpxT13R1 (Figure 3.7 B), the bound fraction of Cpx is higher for PIP2 containing vesicles. The Cpx membrane partition coefficient increases by 2.5-fold when measured using CpxE2R1 and by almost double when measured using another mutant CpxT13R1 (Figure 3.7 C). The stronger interaction observed when using the E2R1 label compared to the T13R1 label might be a result of the neighboring residues around E2 site, which are more hydrophobic. The other possible reason is that at the very N-terminal end, E2 has less steric

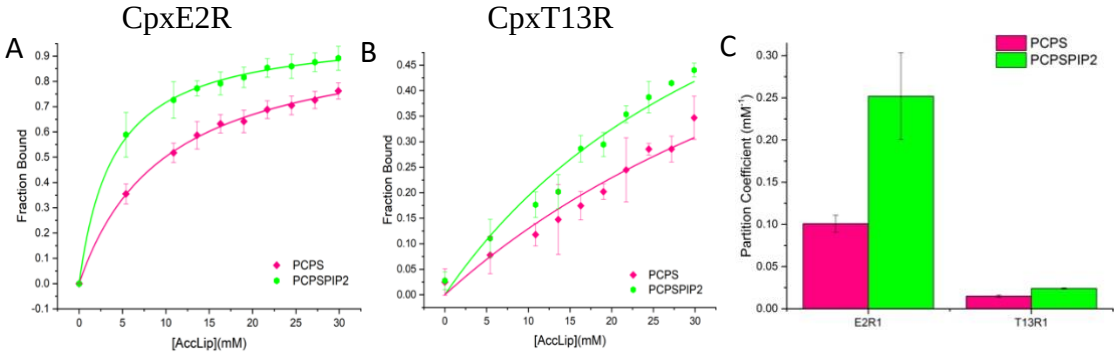

Figure 3.7 PIP2 enhances the Cpx membrane interaction, according to EPR titrations. Bound fraction of CpxE2R1 (A) or CpxT13R1 (B) as a function of accessible lipid concentration. The extruded vesicles have diameters around 100 nm, and the lipid composition of the vesicles were POPC:POPS = 70:30 (peach squares), or POPC:POPS:bPIP2 = 68:30:2 (green hexagons). (C) Shown here are partition coefficients obtained from the titration curves of CpxE2R1 or CpxT13R1 by fitting the amplitudes of EPR spectra to the accessible lipid concentration with a simple isotherm.

hindrance for inserting into the membrane interface. The effect of PIP2 on enhancing the Cpx membrane interaction is stronger using 100 nm vesicles than that was observed in titrations using SUVs. One possible explanation might be that curvature dominates the Cpx membrane interaction in SUVs and we also used slightly different lipid composition in two sets of titrations.

3.3.2 Cpx Binds to Planar Supported Lipid Bilayers Containing PIP2 with a Higher Affinity

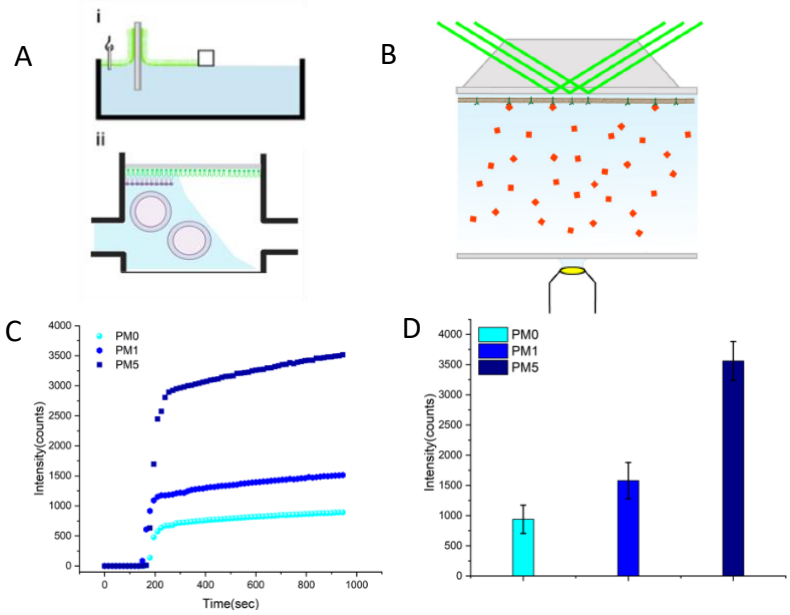

Figure 3.8 PIP2 enhances the Cpx membrane binding according to TIRF microscopy. (A) Preparation of planar supported lipid bilayers can be accomplished in two steps via Langmuir-Blodgett/vesicle fusion technique. Lipid vesicles with desired lipid composition fuse with the first layer of lipid on a quartz slide in a flow-through chamber to form the asymmetric bilayer. (B) TIRF microscopy was used to record the binding of fluorescently labeled proteins to planar supported lipid bilayer. Total reflection of the incident laser generates an exponentially decaying evanescent field at the water/glass surface. Only molecules bind to the membrane surface within the evanescent field can be excited and the intensities are recorded over time. (C) Shown here are the exemplary binding curves of CpxE47A$_{546}$ to the planar supported lipid bilayers containing varying amount of PIP2, POPC:POPE:POPS:bPIP2:Chol= 35-x:30:15:x:20, where x is 0 (cyan spheres), 1 (blue hexagons), 5 (royal squares) as indicated in the figure legend. (D) Binding curve with each particular PIP2 molar percent was repeated more 4~10 times, and the maximum binding intensities of Cpx in 15 min were averaged and plotted in bar chart. Error bars represent standard error. Panel A and B are adapted via Biorender.com from Kiessling et al., 2017.

Based on the enhanced Cpx-membrane affinity by PIP2, we were wondering if this effect will persist when the bilayer is asymmetric and more similar to the neuronal plasma membrane. Planar supported lipid bilayer based total internal reflection microscopy (TIRF)

is a well-established and widely used technique to record protein binding to the membrane surfaces (see section 2.2.4). Taking advantage of the Langmuir-Blodgett/vesicle fusion technique, asymmetric planar supported bilayers can be easily prepared (Figure 3.8 A). An exponentially decaying evanescent field at the water/glass surface can be generated when the incident light gets totally reflected (section 2.2.4). Fluorescent molecules bind to the membrane in the evanescent field can be excited and the intensities over time are recorded (Figure 3.8 B). Bilayers containing POPC and cholesterol (80:20) in the extracellular-face-mimicking leaflet, and 0, 1, and 5 mol% PIP2 in the cytoplasmic-face-mimicking leaflet were prepared respectively (PO-PM0, PO-PM1, PO-PM5). The exemplary binding curves of CpxE47A$_{546}$ to these different bilayers were recorded and represented in Figure 3.8 C. In line with previously observed PIP2 sensitivity, PO-PM1 (blue hexagons) gives stronger Cpx intensity than PO-PM0 (cyan spheres) and Cpx binding to PO-PM5 is the highest (royal squares). The binding curve with each PIP2 concentration were repeated 4~10 time to eliminate measurement error, and the fluorescence intensities at 15 min were averaged for each set of lipid bilayers, and the resulting intensities are graphed in Figure 3.8 D. The trend shown here illustrates that Cpx shows a preference for PIP2 in the asymmetric planar supported bilayers.

PIP2 has a unique structure: large headgroup with multiple negative charges at physiological conditions (Figure 3.9), and PIP2 alone in solution forms micelles (Hindrickson, 1969; Janmey et al., 1987). There might be three contributing factors accounting for the fact that PIP2 facilitates Cpx interaction with either highly curved SUVs or flat membrane surfaces like planar supported lipid bilayers. First, the anionic headgroup of PIP2 might attract basic residues that are positively charged on the peptide via long-

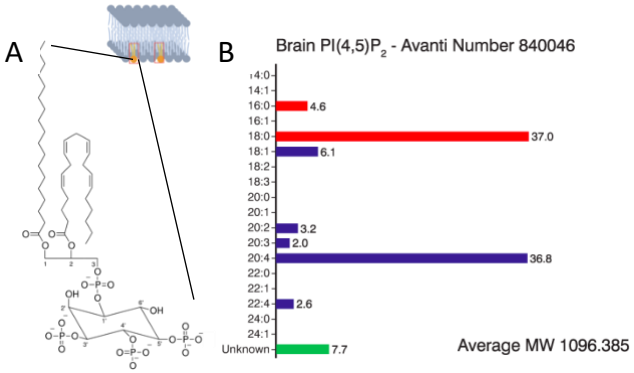

Figure 3.9 PIP2 has a unique structure that might boost the Cpx membrane binding. (A) One representative structure of PIP2 in the bPIP2 mixture. (B) The average acyl chain distribution of bPIP2. The acyl chain composition data is available from: https://avantilipids.com/product/840046.

range Coulombic interactions, bringing the proteins from afar into the proximity of the bilayer surface. This effect could be further augmented in neurons or neuroendocrine cells when PIP2 form clusters or microdomains at the vesicle docking/fusion sites (Aoyagi et al., 2005; van den Bogaart et al., 2011). Second, the large size of the headgroup of PIP2 might enhance the Cpx membrane binding by creating local positive curvatures on the vesicles or local curvature strain on the planar supported bilayers. Last but not the least, the polyunsaturated acyl chains of PIP2 (Figure 3.9 B) might destabilize the local lipid packing and favor the insertion of hydrophobic residues from the peptide.

3.4 The Membrane Affinity of Cpx and Binding to PIP2 Is Driven by Its C-terminal Domain

We know that Cpx binds the membrane via its both terminal domains (Seiler et al., 2009, Lai et al., 2016; Zdanowicz et al., 2017), and each domain of Cpx has been reported to have distinct functions in the regulation of neuronal exocytosis (Trimbuch and Rosenmund, 2016), but it is not clear which terminal domain(s) of Cpx contribute to the PIP2 sensitivity. To determine which domain(s) dictate(s) this novel PIP2 sensitivity, we have designed three Cpx mutants: Cpx without terminal domains (short Cpx, shCpx), N-terminal domain truncated (dNCpx), and C-terminal domain truncated (dCCpx), and the sequence diagrams of these mutants are represented in Figure 3.10 A. We labeled all these mutants, at E47 with Alexa546. By measuring the fluorescence intensity of each mutant together with the full length Cpx on the membrane bilayers containing 0, 1, 5 mol% PIP2 utilizing TIRF, we could determine the importance of each domain in showing PIP2 sensitivity with respect to Cpx-membrane binding (Figure 3.10 B).

In comparison with the full length Cpx, truncation of N-terminal domain has almost no effect on the membrane interaction, no matter how much PIP2 is present in the bilayer, suggesting that the N-terminal domain is not essential for sensing PIP2 or even membrane binding. However, the truncation of the amino acids at the C-terminal domain has a totally opposite effect: it almost abolishes the Cpx membrane interaction, especially with PO-PM0 and PO-PM1 bilayers. As dCCpx binding drops significantly no matter how much PIP2 is

in the bilayer, the binding intensity of dCCpx to PO-PM1 is almost the same as that of PO-PM0, implying that the C-terminal domain is not only essential for membrane binding, but also necessary to recognize PIP2 on the bilayers. The moderate binding of dCCpx to PO-PM5 might be electrostatic interaction between the negatively charged bilayer surface and the basic Cpx central helix domain. The membrane binding behavior of shCpx is very similar to the mutant dCCpx, again implying that the N-terminal domain does not really contribute much to the overall membrane affinity of Cpx.

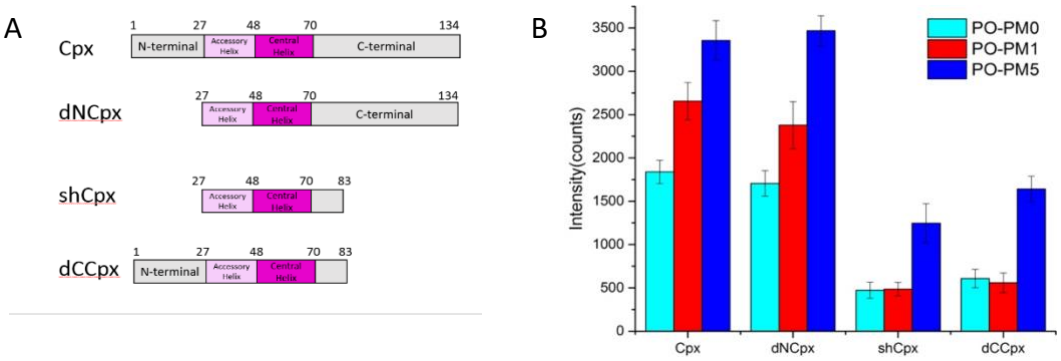

Figure 3.10 Cpx C-terminal domain confers its PIP2 sensitivity. (A) Sequence domain diagrams of full length Cpx, N-terminal domain truncated Cpx (dNCpx), both terminal domains truncated Cpx (shCpx), and C-terminal domain truncated Cpx (dCCpx). (B) Binding of 1 μM of the four Cpx constructs, each labeled with Alexa546 at E47, to the supported lipid bilayers containing 0, 1 and 5 mol% of bPIP2 using TIRF microscopy. The lipid composition was the same as in figure 3.8 C and D. Error bars represent the standard error of the mean of 4 to 10 independent bilayer preparations.

We found that reducing PIP2 levels in the bilayers reduces the membrane binding of either full length or N-terminal domain truncated Cpx and we know that it is only through the terminal domains that Cpx binds to the membranes. Such results suggest that the C-terminal domain of Cpx dominates its PIP2 sensitivity. It is known that proteins interact with PIP2 either through structured domains that contain positively charged regions such as C2 and PH domains, or through unstructured regions containing contiguous or non-contiguous basic charge clusters (Martin, 2015). Although it is not clear if Cpx C-terminal end binds to PIP2 via its four highly conserved lysine residues at position 98, 99 and 133, 134, but the identification of this PIP2 sensitive region in Cpx will enable direct

mutagenesis studies to assess in more detail about the mechanism of Cpx affinity to PIP2 in the future.

In neuronal exocytosis, multiple proteins are reported to bind to PIP2 and PIP2 binding enables PIP2 to regulate Ca^{2+}-triggered vesicle fusion by recruiting or activating these effector proteins (Martin, 2015). Such PIP2 effector proteins include synaptotagmin-1 (Syt), the major Ca^{2+}-sensor for synchronous release (Bai et al., 2004; Li et al., 2006; Kuo et al., 2011; Park et al., 2015; Pérez-Lara et al., 2016; Nyenhuis et al., 2019), α-synuclein implicated in the pathogenesis of Parkinson's diseases (Schechter et al., 2020), and Ca^{2+}-dependent activator protein for secretion (CAPS) (Grishanin et al., 2004). Among these effector proteins, Syt has been extensively investigated because it couples Ca^{2+}-influx precisely with evoked content release (Brose et al., 1992; Fernandez et al., 2001), but it is not clear yet how Cpx-membrane interaction will be influenced by Syt. Considering that both Cpx and Syt coexist with PIP2 in the presynaptic active zone, knowing the effect of Syt on the Cpx membrane interaction might help us understand the functional relationship between the two regulators in neurotransmission.

3.5 Cpx Competes with C2AB for Membrane Binding

3.5.1 C2AB Impairs the Cpx Interaction with PIP2 Containing Membranes

The membrane interactions of Cpx and Syt are both sensitive to curvature and PIP2. In addition to the Ca^{2+}-binding loops of both C2 domains, in the absence of Ca^{2+}, the C2B domain of Syt interacts with membranes via an electrostatic attraction between a lysine-rich polybasic face on the C2B concave surface and negatively multivalent PIP2 in the plasma membrane (Bai et al., 2004; Park et al., 2015). Moreover, it was reported that Syt prefers binding to more curved vesicles and electron microscopy images showed that overall membrane binding of Syt induces positive curvature and tubulates liposomes (Martens et al., 2007). These membrane binding features of Syt raise a question: could Cpx and Syt compete for membrane binding, given that the Cpx membrane interaction is PIP2-sensitive, highly curvature sensitive, and that Cpx even competes with itself for membrane binding?

To address this question, we chose planar supported lipid bilayer based TIRF microscopy. The very low lipid concentrations used in TIRF and the attachment of the bilayer to a solid support avoids problems that arise with lipid aggregation in a bulk assay

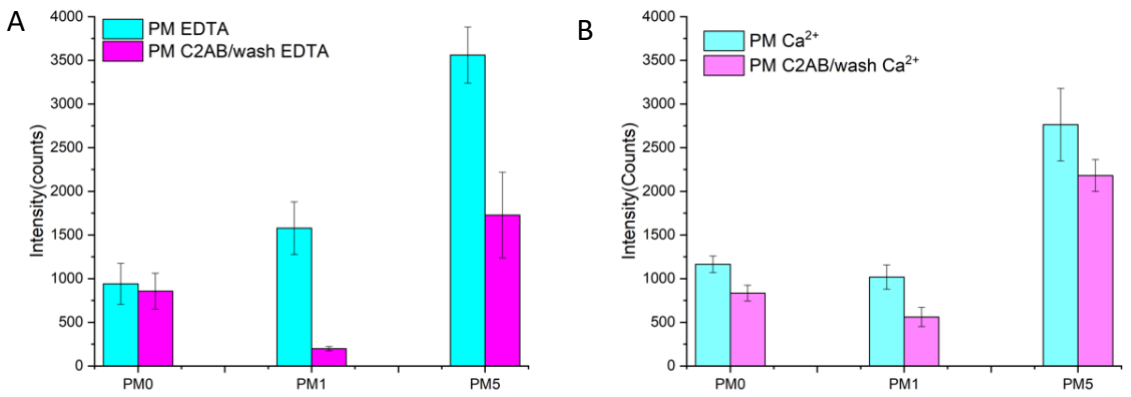

Figure 3.11 Cpx and C2AB compete for membrane binding only in the presence of bPIP2. The binding of $CpxE47A_{546}$ to planar supported lipid bilayers in EDTA (A) and Ca^{2+} (B) was measured using TIRF. The lipid bilayer, with the same composition as that was used in Figure 3.8 C and D, was either used directly after preparation (cyan) or incubated with 0.4 μM C2AB (magenta) for recording Cpx binding. Error bars represent standard error of the mean of 3~10 independent bilayer preparations.

upon Syt addition. We incubated the soluble fragment of Syt, C2AB, with the planar supported bilayers containing 0, 1 or 5 mol% PIP2. The specific C2AB concentration, 0.4 μM is chosen because fluorescence interference microscopy measurements demonstrated that 0.4 μM C2AB is sufficient to produce the same level of reconstituted fusion as wild-type dense core vesicles in Ca^{2+} (Kiessling et al., 2018). Then, Cpx binding to these bilayers was measured and compared to the binding with the corresponding bilayers that has not been treated with C2AB (Figure 3.11). For the bilayers without PIP2, incubation with C2AB produces almost no effect on the Cpx membrane binding to the PO-PM0 bilayers, and this is probably due to limited C2AB interaction with the bilayer without PIP2 in EDTA. Surprisingly, when 1 mol% PIP2 is introduced to the bilayer, incubation with C2AB reduces 88% of Cpx binding, implying that C2AB displaces Cpx from the membrane binding sites in the presence of PIP2. One reason C2AB undermines the Cpx membrane interaction is that the polybasic face of C2 domain might act to laterally sequester PIP2 as previously reported (Kuo, PhD thesis, 2010). Similarly, for PO-PM5

bilayers, incubation with C2AB decreases the binding by 48%, which is not as dramatical as the PO-PM1 bilayers. The percentage of Cpx binding decrease by C2AB is not proportional to the amount of PIP2 in the bilayer, and probably more C2AB is required to thoroughly 'shield' the increased molar percent of PIP2 in the bilayer. Since C2AB interacts with the membrane via different modes depending on the presence of Ca^{2+}(Kuo et al., 2009), we took measurements both in EDTA buffer (Figure 3.11 A) and Ca^{2+} buffer (Figure 3.11 B). In the Ca^{2+} buffer, the trend of PIP2-dependent competitive membrane binding between C2AB and Cpx persists, but the C2AB effect gets weaker for PM5

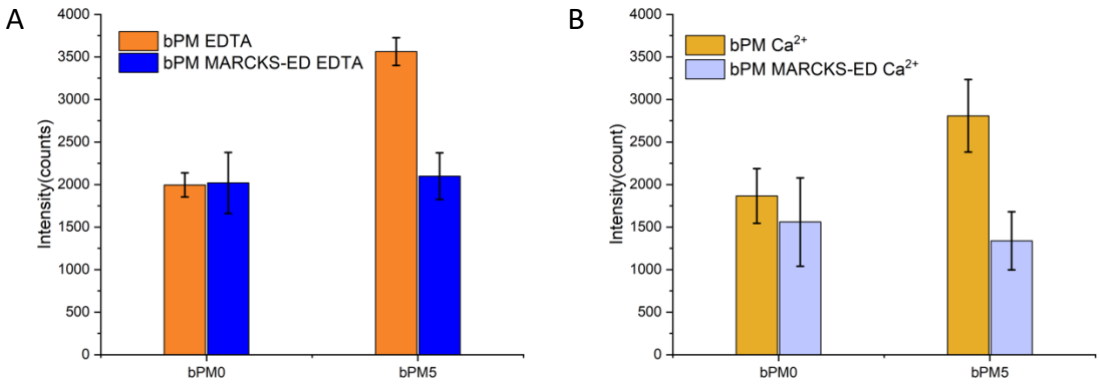

Figure 3.12 MARCKS-ED decreases Cpx binding to membranes containing PIP2. Shown here are binding intensities of $CpxE47A_{546}$ to planar supported bilayers bPM0 and bPM5 in EDTA (A) or Ca^{2+} (B) buffer. Orange (A) or yellow (B) bar represents the bilayer was used for binding directly after preparation. Blue (A) or sky-blue (B) bar represents the bilayer was incubated with 1 μM MARCKS-ED before it was used for binding. Error bars represent stand error from 3 to 5 independent bilayer preparations.

bilayers. The weaker C2AB effect might result from a different membrane binding mode of C2B in the Ca^{2+} buffer (Kuo et al., 2009).

Since Cpx does not interact with C2AB in solution (Xu et al., 2013), we hypothesize that the effect of C2AB on the Cpx membrane interaction is caused by lateral sequestration of PIP2 by C2AB. To test this hypothesis, we examined the effect of the Effector Domain of the Myristoylated Alanine Rich C-Kinase Substrate (MARCKS-ED) on the Cpx membrane interaction. MARCKS-ED, with a sequence of KKKKKRFSFKKSFKLSGFSFKKNKK, is a well-known peptide that interacts electrostatically as well as hydrophobically with acidic lipids, and particularly, each

MARCKS-ED molecule can laterally sequester 3 multivalent PIP2 (Rauch et al., 2002; Wang et al., 2002). Therefore, if incubation with MARCKS-ED decreases the Cpx membrane interaction, we would know that C2AB might inhibit the Cpx membrane interaction by sequestering PIP2 on the bilayer surface.

Taking planar supported bilayers without PIP2, PM0, as a control, we find that incubation with MARCKS-ED does not change the Cpx binding (orange and blue bars on the left side of Figure 3.12 A). Even though PIP2 is not required for the binding of MARCKS-ED to membranes containing physiological fractions of phosphatidylserine (Tanigchi and Manenti, 1993), this indicates that MARCKS-ED does not interfere with the Cpx membrane interaction in the absence PIP2. Next, we examined the effect of MARCKS-ED on Cpx binding to membrane bilayers containing 5 mol% PIP2 (orange and blue bars on the right side of Figure 3.12 A). Remarkably, incubation of PM5 bilayer with 1 μM MARCKS-ED caused Cpx binding dropped all the way down to the level comparable to the binding to PM0 bilayers. Similar MARCKS-ED effect has been observed in Ca^{2+} buffer (Figure 3.12 B). This PIP2-dependent MARCKS-ED effect reveals that laterally sequestration of PIP2 significantly decreases the Cpx membrane interaction. These data support our hypothesis that sequestration of PIP2 by the polybasic face on C2B domain accounts for the competitive membrane binding between C2AB and Cpx.

3.5.2 C2AB Impairs the Cpx Interaction with PIP2 Containing Bilayers Reconstituted with the Acceptor SNARE Complex

It is known that Cpx not only binds to the fully assembled SNARE complex, but also binds the acceptor SNARE (t-SNARE) complex, which consists of full length syntaxin (Syx-1a) and dodecylated SNAP25 (dSNAP25). Syx-1a and dSNAP25 on the plasma membrane, together with synaptobrevin on the vesicle membrane, play a central role in neuronal exocytosis as they drive the fusion between synaptic vesicle and plasma membrane via assembling into a four helical coiled-coil complex called the SNARE complex (Jahn R. and Fasshauer D., 2012; Südhof T. C., 2013; Han et al., 2017). Additionally, Cpx/t-SNARE complex binding enhances the Cpx membrane affinity, and membrane associated t-SNARE complex are more likely to interact with Cpx (Zdanowicz et al., 2017). Thus, we asked the

question if C2AB and Cpx still compete for membrane binding in a more physiological relevant condition: in the presence of the binary t-SNARE complex.

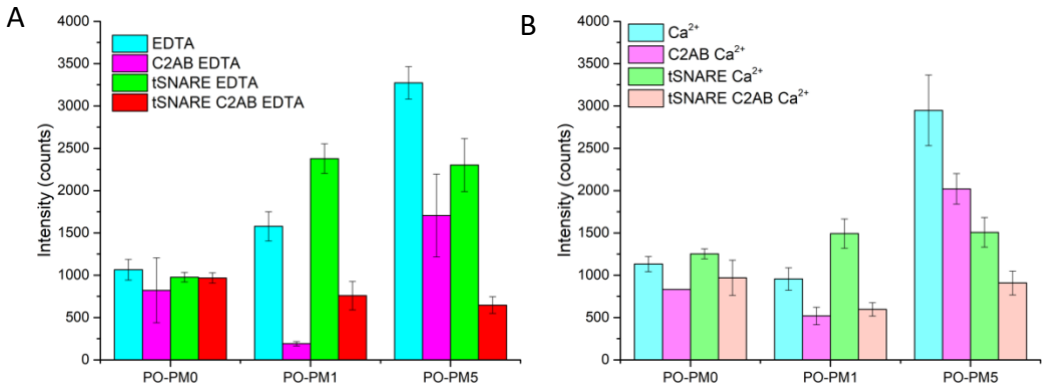

Figure 3.13. Effect of C2AB on Cpx membrane binding in the presence of Syx-1a/dSNAP25 complex. (A) Shown here are binding intensities of CpxE47A$_{546}$ to plain planar supported lipid bilayers (cyan bars), plain planar supported lipid bilayers that has been incubated with C2AB (magenta bars), bilayers reconstituted with Syx-1a and dSNAP25 (green bars), and bilayers reconstituted with Syx-1a and dSNAP25 that has been treated with C2AB (red bars) in EDTA buffer. (B) Shown here are binding intensities of CpxE47A$_{546}$ to plain planar supported lipid bilayers (light cyan bars), plain planar supported lipid bilayers that has been incubated with C2AB (light magenta bars), bilayers reconstituted with Syx-1a and dSNAP25 (light green bars), and bilayers reconstituted with Syx-1a and dSNAP25 that has been treated with C2AB (pink bars) in Ca^{2+} buffer. The percentage of PIP2 are as indicated in the x-axis as before. Error bars represent standard error from 5~10 independent bilayer preparations.

To determine the potential effect of C2AB on the Cpx membrane interaction in the presence of the t-SNARE complex, we repeated the experiments we did in Figure 3.11 but with planar supported lipid bilayers that has been reconstituted with t-SNARE complex. These experiments demonstrate that membrane associated t-SNARE complex has different effect on the competition between Cpx and C2AB depending on how much molar percent of PIP2 is in the bilayer. For PM0 bilayers without any PIP2, we didn't observe any effect of t-SNARE on the Cpx membrane binding (Figure 3.13 A, left, green bar) and incubation the t-SNARE complex containing bilayers with C2AB (Figure 3.13 A, left, red bar) did not decrease the Cpx binding neither (red bar). Again, this indicates that C2AB competes with the Cpx membrane binding only in the presence of PIP2, and the acceptor SNARE complex

reconstituted on the bilayer does not alter this trend. When 1 mol% PIP2 was added to the bilayers, comparing with PO-PM1 bilayers without t-SNARE complex, C2AB incubation decreases Cpx binding intensity by 68% (Figure 3.13A, middle, green and red bars). Although the decrease of Cpx binding intensity caused by C2AB incubation is not as strong as that observed on the PO-PM1 bilayers without the t-SNARE complex (88%), the effect of C2AB on the Cpx membrane binding is still dramatic. Interestingly, t-SNARE complex further boosts the Cpx membrane interaction by 50% when there is 1 mol% PIP2 in the bilayers (Figure 3.13A, middle, cyan and green bars). This stronger binding might be attributed to the high affinity of Cpx to the membrane associated t-SNARE complex as we observed before (Zdanowicz et al., 2017). For bilayers containing 5 mol% PIP2, the Cpx membrane binding is reduced by 72% when the t-SNARE reconstituted bilayer is pre-incubated with C2AB (Figure 3.13A, right group, green and red bars). The weaker Cpx membrane binding intensity compared with PO-PM5 bilayers without the t-SNARE complex reveals that the presence of the t-SNARE complex diminishes the Cpx membrane binding in the presence of 5 mol% PIP2. A possible explanation for this t-SNARE interference on the Cpx membrane binding is that the polybasic juxtamembrane linker of Syx-1a interacts and presumably consumes some of the PIP2 that was accessible by Cpx otherwise in the absence of the t-SNARE complex. There were researches showing that PIP2 binds electrostatically to the basic juxtamembrane domain (sequence 260~265: KARRKK) of Syx-1a, and this interaction induces mutual enrichment of PIP2 and Syx-1a at the vesicle docking and fusion sites (Murray and Tamm, 2009; van den Bogaart et al., 2011). This might also explain why Cpx binding is mitigated by about 30% when the t-SNARE complex is introduced to the bilayers containing 5 mol% PIP2 in the absence of C2AB (Figure 3.13A, right side, cyan and green bars). Similar pattern was observed in Ca^{2+} buffer (Figure 3.13 B).

Two conclusions could be drawn from these data. First, C2AB competes with Cpx for membrane binding as long as there is PIP2 in the membrane, and t-SNARE complex does not alter this trend. Second, t-SNARE complex could enhance as well as mitigate the Cpx membrane binding and the exact effect is depending on the molar percent of PIP2 in the bilayers. While it is unambiguous that both the membrane reconstituted acceptor SNARE complex and the accessible PIP2 in the bilayers modulate the Cpx membrane

affinity, additional measurements are needed to quantify the contribution from each factor respectively.

3.6 Cpx Colocalizes to the Dense Core Vesicle Docking Sites

One mechanism by which PIP2 regulates Ca^{2+}-triggered exocytosis is by recruiting PIP2-binding effector proteins to vesicle docking sites (Martin, 2015). While fluorescence imaging techniques showed that Syt interacts with PIP2 clusters organized by Syx-1a in artificial membranes (Honigmann et al., 2013), a recent study using CRISPRi-mediated gene knockout and 3D tomography approaches shows that PIP2/Syt interaction in mouse hippocampal synapses initiates synaptic vesicles docking (Chen et al., 2021). This prompts us to ask if Cpx could be recruited to the vesicle docking sites as well.

To this end, we employed TIRF microscopy to record Cpx binding to the t-SNARE reconstituted brain PM1 lipid bilayers in the presence of docked dense core vesicles (DCVs) purified from *Rattus norvegicus* PC12 cells. Our DCVs are functionally active in docking to and fusion with t-SNARE complex reconstituted planar supported bilayers. DCVs were labeled with Cy5 in order to clearly locate vesicle docking sites, and DCV docking in the presence of Cpx in EDTA buffer was improved by incubating the bilayers with 2 μM Cpx and 0.5 μM Munc18 before the addition of DCV (Kreutzberger et al., 2017).

Homogeneous Cpx membrane binding was observed across the whole field of bilayers before DCV addition (Figure 3.14 A, middle panel in the first column). Immediately after the perfusion of DCVs, DCV docking sites appeared and a few puncta of Cpx binding showed up exactly at the DCV docking sites as well (Figure 3.14 A, second column, arrow). As recording was kept for a few more minutes, more DCVs docked to the bilayers and Cpx intensity at the docking sites increased gradually (Figure 3.14 A, third and fourth columns). Further analysis of the fluorescence intensity traces of both Cpx and DCV at 14 docking sites show that, immediately after DCV docking, Cpx intensities increased gradually over a period of at least 3 minutes (Figure 3.14 B). In contrast, DCV intensities reached maximum instantly, but not gradually, and then slightly decreased as time increased (Figure 3.14 B), and the gradually decreasing DCV intensities might be

caused by fluorescence quenching. This indicates that Cpx recruitment occurs during the time period when DCV is docked at the site. It is highly possible that PIP2 might enhance the Cpx recruitment, considering that PIP2 might form microdomains at the DCV docking sites (Aoyagi et al., 2005; van den Bogaart et al., 2011). Since Cpx prefers binding to more curved membranes, it is also reasonable that Cpx recruitment to the DCV docking sites is

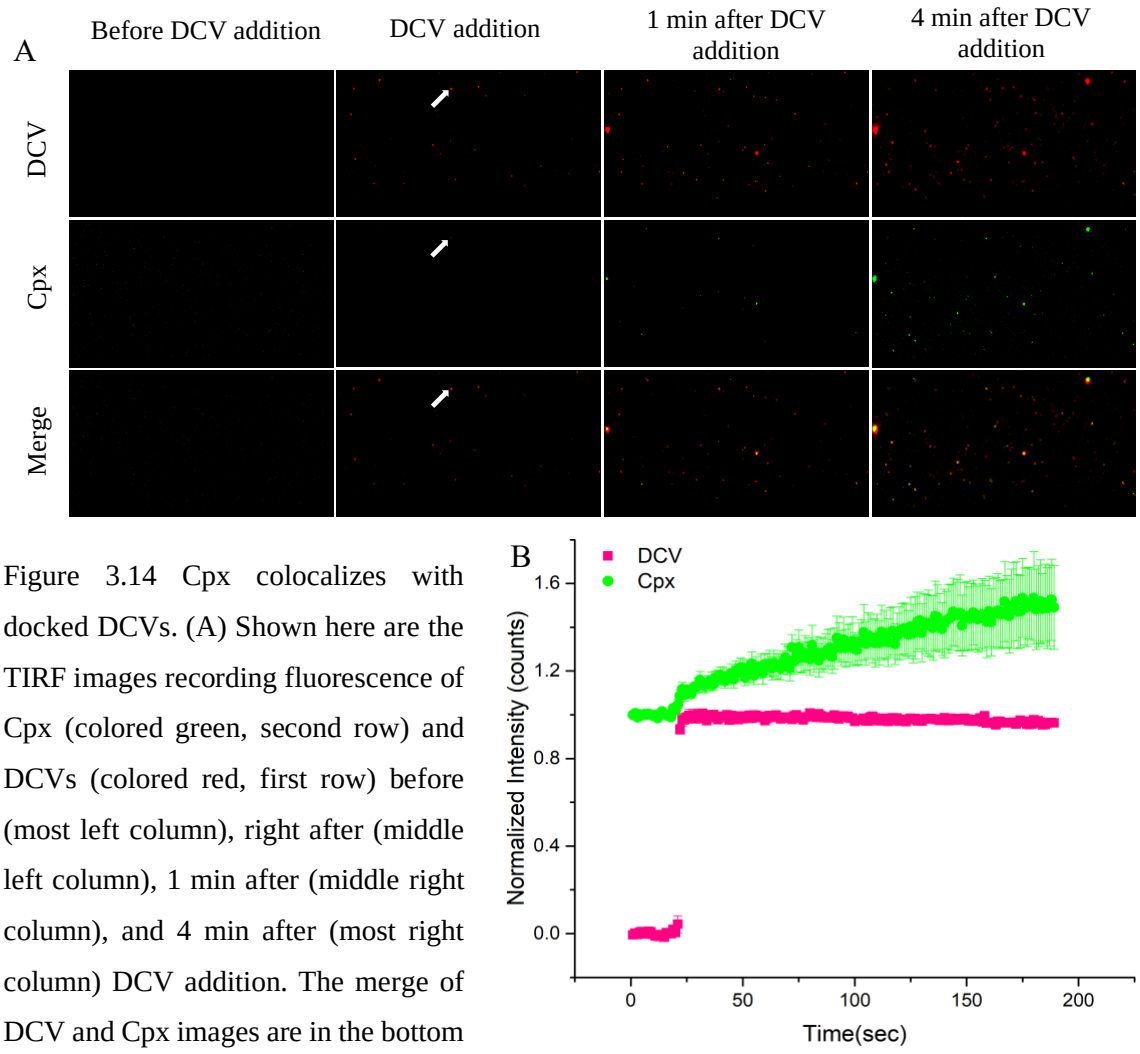

Figure 3.14 Cpx colocalizes with docked DCVs. (A) Shown here are the TIRF images recording fluorescence of Cpx (colored green, second row) and DCVs (colored red, first row) before (most left column), right after (middle left column), 1 min after (middle right column), and 4 min after (most right column) DCV addition. The merge of DCV and Cpx images are in the bottom row, showing that membrane binding at DCV docking sites was greatly enhanced. (B) Intensities of DCV fluorescence (magenta, normalized to initial binding intensities) and Cpx fluorescence (green, normalized to the Cpx intensity before DCV addition) from 15 different docking sites were averaged and plotted. DCVs were perfused at about 25 second.

partially contributed by interaction between Cpx and DCVs. Additional factors that recruit Cpx to the DCV docking sites might involve potential Cpx interaction with the trans-SNARE complex (Malsam et al., 2020), but further experiments are need before a

conclusion can be made. Recruiting Cpx to the DCV docking sites increases Cpx concentration locally at prospective vesicle fusion sites and this might function to magnify the effects of Cpx on membrane fusion, such as those due to modifying the membrane curvature.

Actually, single synaptic vesicle fusion assay indicates that PIP2 in the target bilayers reinforces the clamping function of Cpx in the absence of Ca^{2+}: the synaptic vesicle fusion probability decreases as more PIP2 is included in the lipid bilayer (personal communication with Dr. Alex Kreutzberger). This finding demonstrates the importance of PIP2 for the clamping function of Cpx.

4. DISCUSSION AND OUTLOOK

4.1 DISCUSSION

The complexin protein family is enriched in the synapse and are SNARE binding proteins that play indispensable roles in regulating neuronal exocytosis. In mice, genetic deletion of complexin-1/2 kills the newborn pups shortly after birth, loss of complexin-1 (Cpx) causes infertility due to impaired acrosomal exocytosis, and complexin-2 knockout damages the cognitive ability (Reim et al., 2001). Altered complexin expression levels in humans have been suggested to contribute to the symptoms of neurological disorders including Huntington's disease, depression, Parkinson's disease and Alzheimer's disease (Brose, 2008). Electrophysical recordings as well as lipid mixing assays reveal that complexin performs dual functions in neurotransmission: it synchronizes the evoked release as well as inhibits spontaneous release (Brose, 2008; Trimbuch and Rosenmund, 2016). Conventionally, Cpx consists of four domains: accessory helix, central helix, and two terminal unstructured domains flanking the helical domains. Each domain has distinct properties and thus might be involved in multiple mechanisms to regulate neuronal exocytosis. On the one hand, Cpx binds in an antiparallel manner to the SNARE complex with nanomolar affinity and with fast binding kinetics, and NMR, EPR, and X-ray crystallography data indicate that the central helix and the C-terminal side of the accessory helix are contributing to this stable interaction (Chen et al., 2002, Pabst et al., 2002;). On the other hand, the unstructured terminal domains of Cpx bind to the membranes via the amphipathic regions in a curvature sensitive manner (Snead et al., 2014; Lai et al., 2016; Zdanowicz et al., 2017). Much of early investigations of Cpx focused on the Cpx/SNARE interaction; however, more recent work has shown that the membrane interactions of the Cpx terminal domains is of critical functional importance (Seiler et al., 2009; Wragg et al., 2013). Despite the importance of the Cpx/membrane interaction, it has not been clear how the Cpx/membrane interaction regulates the synaptic vesicle fusion process. Part of the difficulty in identifying the role of the Cpx/membrane interaction in neuronal exocytosis is likely due to an insufficient characterization of the Cpx membrane interaction.

In this work, techniques to study the Cpx/membrane interaction included fluorescence anisotropy, EPR, and TIRF microscopy. We examined the effect of lipid composition, and factors including PIP2, C2AB, and SNAREs on the Cpx/membrane interactions. Using sonicated vesicles, titration results from fluorescence anisotropy indicate that Cpx prefers to bind bilayers consisting of more disordered acyl chains (Figure 3.3). This observation is in agreement with the curvature sensitive membrane binding pattern reported previously (Snead et al., 2014; Zdanowicz et al., 2017). Similar to the preference for more curved vesicles, more disordered acyl chains might enable an easier access of the hydrophobic residues of Cpx to the membrane acyl chain region.

Interestingly, in addition to sensing membrane curvature, Cpx must also modify membrane curvature. This is evidenced by three observations. First, titration experiments of Cpx/membrane binding made using EPR shows that truncation of N-terminal domain leads to stronger membrane binding of the C-terminal domain (Figure 4.5), implying that the two ends might compete with each other for limiting binding sites or space on the vesicle surface. Second, when 2, 20, 40, 80 μM Cpx was used in the titration, the Cpx membrane affinity is dramatically reduced (Figure 3.6 A and B), suggesting that membrane surfaces get saturated at relatively low concentrations of Cpx. Third, Cpx competes with itself for membrane binding in a protein:lipid ratio of 1:6000 (Figure 3.6 D). Such a low protein:lipid ration means the curvature strain brought by Cpx reduces further Cpx binding and acts over a long distance range covering an area of 4200 nm^2 or a length of 65 nm on the membrane interface. Amphipathic helices are known to sense membrane curvature and even participate in membrane remodeling (Drin and Antonny, 2009). When Cpx inserts its hydrophobic residues into the bilayers, Cpx binding might render the membrane more tightly packed, thus less likely to interact with another nearby Cpx molecule. The overall effect of Cpx binding on the membrane could be viewed as membrane gets less curved but more strained/stabilized when Cpx binds to the membrane. Synaptotagmin-1/Ca^{2+} was previously suggested to trigger and promote membrane fusion by inducing high local positive membrane curvature and thereby lowering the energy barrier for fusion upon Ca^{2+}-dependent membrane binding (Martens et al., 2007). In contrast to the positive curvature created by synaptotagmin-1/Ca^{2+}, strained/stabilized membrane surfaces that result from Cpx binding would require more energy to distort or destabilize. Recent progress in our

lab supports a model in which C2B binds in the curved membrane surfaces formed in the hemifusion state via its Ca^{2+}-binding loops, arginine apex and the polybasic face, and mutations in the arginine apex clearly affect the expansion of the fusion pore (Nyenhuis et al., 2021). This indicates that stimulating the synchronous release may involve controlling the energy of the fusion pore. Together, these results suggest a new model for Cpx inhibiting spontaneous release or vesicle fusion in the absence of Ca^{2+}: the Cpx membrane binding might delay the formation or expansion of the fusion pore until Ca^{2+} influx by introducing curvature strain into the membrane, and synaptotagmin-1/Ca^{2+} triggers membrane fusion via even stronger synaptotagmin-1/Ca^{2+} membrane interaction.

A second result observed here is that Cpx associates to the important plasma membrane component PIP2 and this finding is supported by four sets of experiments. First, titrations with SUVs using fluorescence anisotropy show that Cpx binds to the membranes with 1 mol% PIP2 with slightly higher affinity (Figure 3.2). Second, EPR titrations using 100 nm extruded vesicles indicate that Cpx binds with higher affinity to vesicles containing 2 mol% PIP2 regardless of the position of the spin label (Figure 3.7). Third, the PIP2-enhanced membrane interaction is further verified in TIRF measurements, as Cpx binding intensities increase when the planar supported bilayers contain more PIP2 (Figure 3.8). Fourth, once PIP2 in the bilayer is sequestered by peptide MARCKS-ED, the Cpx membrane binding drops to the same level with when it binds to bilayers without PIP2 (Figure 3.12). As a multi-functional lipid component, PIP2 has several binding partners, such as synaptotagmin-1, Munc13-1, CAPS, rabphilin, and α-synuclein, in the presynaptic active zone (Martin, 2015; Schechter et al., 2020). Yet, this is the first time that Cpx has been identified to associate to PIP2. PIP2 protein interaction mainly occurs electrostatically: negatively charged PIP2 binds clustered basic residues in unstructured loops such as MERCKS-ED, or basic regions in the structured modules such as C2 and PH domains. By comparing membrane binding affinity of Cpx mutants without either or both membrane binding domain(s), we further learned that Cpx C-terminal domain is responsible for its PIP2 sensitivity (Figure 3.10). There are two sites with contiguous lysines residues (residue 98, 99 and residue 133, 134) within Cpx C-terminal domain, and these sites might be involved in PIP2 binding. The observations that truncation of C-terminal domain makes Cpx much less sensitive to PIP2 and removal of C-terminal domain of Cpx disabled Cpx

to inhibit spontaneous fusion in *C. elegans* (Wragg et al., 2013) jointly imply that Cpx interaction with PIP2 is crucial for its inhibitory function.

One functional result of the Cpx/PIP2 association might be membrane targeting, and this hypothesis is supported by our observation that Cpx colocalizes to the dense core vesicle docking sites (Figure 3. 14). As a landmark for vesicle exocytosis, PIP2 was known to recruit functional PIP2-binding proteins (Martin, 2015) and in this recruiting process, proteins are brought to and enriched at the vesicle fusion sites so that they could fulfill their functions upon a Ca^{2+}-trigger. For example, microdomains formed by clustered syntaxin-1a and locally enriched PIP2 via electrostatic interaction were detected on PC12 membrane sheets as well as at the vesicle docking sites in PC12 cells (Aoyagi et al., 2005; van den Bogaart et al, 2011), and it was suggested that via synaptotagmin-1 interaction with PIP2, which is independent of Ca^{2+}, PIP2 clusters function to recruit vesicles to the syntaxin-1a/PIP2 clustered sites (Honigmann et al., 2013). For Cpx, one direct outcome of Cpx recruitment to the vesicle sites could be: locally enriched Cpx on the bilayer surface boosts the ability of Cpx to change the membrane curvature strain. Although it was previously reported that C-terminal domain of Cpx target Cpx to synaptic vesicles since Cpx prefers binding to more curved vesicle surfaces (Wragg et al., 2013), we show plasma membrane targeting here. Such an observation is reasonable if we consider that Cpx affinity to both the plasma membrane anchored t-SNARE complex (Zdanowicz et al., 2017) and plasma membrane component PIP2 are two of the factors that contribute to plasma membrane targeting.

Third, membrane bound Cpx could be displaced by the soluble fragment of synaptotagmin-1, C2AB, but only in the presence of PIP2 in the bilayer. Since Cpx and synaptotagmin-1 both modulate synaptic vesicle fusion at the presynaptic active zone, and both proteins not only prefer positively curved membrane surfaces but also bind PIP2 in the bilayers, we examined the potential interference of C2AB on the Cpx membrane interaction. As seen in Figures 3.11 and 3.13, Cpx binding to membranes without PIP2 remains unchanged when C2AB is added. However, C2AB incubation decreases the Cpx membrane binding dramatically when PIP2 was added to the lipid bilayers. Although the magnitude of Cpx intensity decrease upon C2AB incubation varies depending on the

specific molar percent of PIP2, C2AB continues to compete with Cpx for binding to PIP2 containing membranes when t-SNARE complex was reconstituted in the bilayer (Figure 3.13). Competitive membrane binding of Cpx and C2AB turns out to be PIP2-dependent but Ca^{2+}-independent, and this feature might result from the Ca^{2+}-independent interaction between PIP2 and the polybasic face of C2B (Kuo et al., 2009). Being Ca^{2+}-independent, C2AB effect on the Cpx membrane is more likely to play a role in spontaneous release before the Ca^{2+}-trigger. Considering that the Cpx membrane binding is highly sensitive to membrane curvature and curvature strain introduced by bound Cpx reduces further Cpx binding, synaptotagmin-1 might function to mediate plasma membrane curvature strain indirectly via affecting Cpx binding.

Together, our research shows that Cpx not only senses membrane curvature but also modulates membrane curvature. Moreover, for the first time, we demonstrate that Cpx binds to PIP2 via its C-terminal domain and PIP2 binding might contribute to targeting Cpx to the plasma membrane. We propose that Cpx might delay the formation or expansion of the fusion by introducing curvature strain into the membrane fusion intermediates, and such an inhibition can be released as soon as synaptotagmin/Ca^{2+} membrane interaction dominates the effect of protein binding on membrane surfaces.

4.2 Outlook

Our work significantly expanded current knowledge about Cpx/membrane interaction in three aspects: Cpx modifies membranes curvature; Cpx associates with PIP2; and Cpx gets recruited to the dense core vesicles docking sites. These progresses provide possibility to further understanding the regulatory mechanism of neuronal exocytosis by tackling the following types of problems:

First, in this thesis, we find that Cpx-1 not only senses membrane curvature, but also modifies it, but it remains unclear how changes in lipid composition will affect ability of Cpx-1 to modify the membrane curvature. It would be worth examining potential effects of certain lipid acyl chains or headgroups since this provides clues into the mechanism of the curvature-sensing and -modifying membrane binding mode, which would further

disclose the importance of the introduced curvature strain, once Cpx-1 binds the membrane, in regulating synaptic vesicle fusion.

Second, in the Cpx-1/PIP2 sensitivity experiments, we identified that the C-terminal domain mainly confers Cpx-1/PIP2 association and the potential residues involved might be two sites containing contiguous lysines at position 98, 99 and 133, 134. The lysines here could be mutated into noncharged resides such as alanine or glutamine and a similar binding assay using these Cpx-1 mutants would provide more detail about Cpx/PIP2 sensitivity. If a correlation could be established between the lysines and Cpx/PIP2 association, these mutants could be further utilized to probe any potential PIP2-dependent regulatory roles of Cpx-1, for example, the ability of Cpx to get recruited to the vesicle docking sites. These mutants could also be very useful in a single vesicle fusion assay to explore the potential effect of Cpx-1/PIP2 association on release probability and fusion pore dynamics.

Third, we observed recruitment of Cpx-1 to the docking sites of dense core vesicles, but it is not clear yet what are the contributing factors here. A highly possible player might be PIP2 and this hypothesis could be tested, in addition to the point mutation study mentioned in the previous point, by performing the Cpx-1 membrane binding assay with bilayers containing PIP2 or not. SNAP-25 could also recruit Cpx-1 given that it binds to Cpx-1 when reconstituted in the membrane bilayers (Zdanowicz et al., 2017). Moreover, syntaxin-1a might also be involved as it plays a vital role in the formation of PIP2 clusters at the vesicle docking sites (van den Bogaart et al., 2013). The effect of t-SNAREs on Cpx-1 recruitment could be examined similarly using bilayers reconstituted with either protein.

LIST OF REFERENCES

LIST OF REFERENCES

Ambrose E. J. (1956) A surface contact microscope for the study of cell movements. Nature. 178 (4543), 1194.

An S. J., Grabner C. P. and Zenisek D. (2010) Real-time visualization of complexin during single exocytic events. Nat. Neurosci. 13, 577-583.

Aoyagi K., Sugaya T., Umeda M., Yamamoto. S., Terakawa S. and Takahashi M. (2005) The activation of exocytotic sites by the formation of phosphatidylinositol 4,5-bisphosphate microdomains at syntaxin clusters. J. Biol. Chem. 280, 17346-17352.

Axelrod D. (1981) Cell-substrate contacts illuminated by total internal reflection fluorescence. J. Cell Biol. 89, 141-145.

Axelrod D., Thompson N. L. and Burghardt T. P. (1983) Total internal reflection fluorescent microscopy. J. Microsc. 129, 19-28.

Bai J., Tucker W. C. and Chapman E. R. (2004) PIP2 increases the speed of response of synaptotagmin and steers its membrane-penetration activity toward the plasma membrane. Nat. Struct. Mol. Biol. 11, 36-44.

Bartlett G. R. (1958) Phosphorus assay in column chromatography. J. Bio. Chem. 234(3), 466-468.

Berliner L. J., Grunwald J., Hankovszky H. O. and Hideg K. (1982) A novel reversible thiol-specific spin label: papain active site labeling and inhibition. Anal. Biochem. 119, 450-455.

Bradberry M. M., Bao H., Lou X. and Chapman E. R. (2019) Phosphatidylinositol 4,5-bisphosphate drives Ca^{2+}-independent membrane penetration by the tandem C2 domain proteins synaptotagmin-1 and Doc2β. J. Biol. Chem. 294(28), 10942-10953.

Brewer K. D. et al. (2015) Dynamic binding mode of a Synaptotagmin-1-SNARE complex in solution. Nat. Struct. Mol. Bio. 22(7), 555-564.

Brose N. (2008) For better or for worse: complexins regulate SNARE function and vesicle fusion. Traffic. 9, 1403-1413.

Brose N., Petrenko A. G., Südhof T. C. and Jahn R. (1992) Synaptotagmin: a calcium sensor on the synaptic vesicle surface. Science. 256, 1021-1025.

Chen X., Tomchick D. R., Kovrigin E., Araç D., Machius M., Südhof T. C. and Rizo J. (2002) Three-dimensional structure of the complexin/SNARE complex. Neuron. 33, 397-409.

Chen Y., et al. (2021) Synaptotagmin-1 interacts with PI(4,5)P2 to initiate synaptic vesicle docking in hippocampal neurons. Cell Rep. 34, 108842.

Chernomordik L. V. and Kozlov M. M. (2008) Mechanics of membrane fusion. Nat. Struct. Mol. Biol. 15, 675-683.

Cho R. W., Song Y. and Littleton J. T. (2010) Comparative analysis of Drosophila and mammalian complexins as fusion clamps and facilitators of neurotransmitter release. Mol. Cell. Neurosci. 45, 389-397.

Craig A. M. and Kang Y. (2007) Neurexin and neuroligin signaling in synapse development. Curr. Opin. Neurobiol. 17, 43-53.

Dawidowski D and Cafiso D. S. (2016) Munc18-1 and the syntaxin-1 N terminus regulate open-closed states in a t-SNARE complex. Structure. 24, 392-400.

De Craene J. O., Bertazzi D. L., Bär S. and Friant S. (2017) Phosphoinositides, major actors in membrane trafficking and lipid signaling pathways. Int. J. of Mol. Sci. 18(3), 634.

Domanska M. K., Kiessling V. and Tamm L. K. (2009) Single vesicle millisecond fusion kinetics reveals number of SNARE complexes optimal for fast SNARE-mediated membrane fusion. J. Biol. Chem. 284, 32158-32166.

Ellena J. F., Liang B., Wiktor M., Stein A., Cafiso D. S., Jahn R. and Tamm L. K. (2009) Dynamic structure of lipid-bound synaptobrevin suggests a nucleation-propagation mechanism for trans-SNARE complex formation. Proc. Natl. Acad. Sci. USA. 106, 20306-20311.

Falkenburger B. H., Jensen J. B., Dickson E. J., Suh B. C. and Hille B. (2010) Phosphoinositides: lipid regulators of membrane proteins. J. Physiol. 588.17, 3179-3185.

Fasshauer D., Sutton R. B., Brunger A. T. and Jahn R. (1998) Conserved structural features of the synaptic fusion complex: SNARE proteins reclassified as Q- and R-SNAREs. Proc. Natl. Acad. Sci. 95,15781-15786.

Fernandez I., Araç D., Ubach J., Gerber S. H., Shin O. H., Gao Y., Anderson R. G., Südhof T. C. and Rizo J. (2001) Three-dimensional structure of the synaptotagmin-1 C2B-domain: synaptotagmin-1 as a phospholipid binding machine. Neuron. 32, 1057-1069.

Fernández-Chacón R. Königstorfer A., Gerber S. H., García J., Matos M. F., Stevens C. F. Brose N., Rizo J., Rosenmund C. and Südhof T. C. (2001) Synaptotagmin I functions as a Ca^{2+}-regulator of release probability. Nature. 410, 41-49.

Geppert M., Goda Y., Hammer R. E., Li C., Rosahl T. W., Stevens C. F. and Südhof T. C. (1994) Synaptotagmin I: a major Ca^{2+} sensor for transmitter release at a central synapse. Cell 79, 717-727.

Gong J., Lai Y., Li X., Wang M., Leitz J., Hu Y., Zhang Y., Choi U. B., Cipriano D., Pfuetzner R. A., Südhof T. C., Yang X., Brunger A. T. and Diao J. (2016) C-terminal domain of mammalian complexin-1 localizes to highly curved membranes. Proc. Natl. Acad. Sci. 113(47), E7590-7599.

Grin G. and Antonny B. (2010) Amphipathic helices and membrane curvature. FEBS Lett. 584, 1840-1847.

Grishanin R. N., Kowalchyk J. A., Klenchin V. A., Ann K., Earles C. A., Chapman E. R., et al. (2004) CAPS acts at a prefusion step in dense-core vesicle exocytosis as a PIP2 binding protein. Neuron. 43, 551-62.

Han J., Pluhackova K. and Böckmann R. A. (2017) The multifaceted role of SNARE proteins in membrane fusion. Front. Physiol. 8, 5.

Han Y., Kaeser P., Südhof T. C. and Schneggenburger R. (2012) RIM determines Ca^{2+}-channel density and vesicle docking at the presynaptic active zone. Neuron. 69(2), 304-316.

Harayama T. and Riezman H. (2018) Understanding the diversity of membrane lipid composition. Nat. Rev. 19, 281-296.

Hay J. C., Fisette P. L., Jenkins G. H., Fukami K., Takenawa T., Anderson R. A. and Martin T.F. (1995) ATP-dependent inositide phosphorylation required for Ca(2+)-activated secretion. Nature. 374, 173-177.

Hemminga M. A. and Berliner L. J. (2007) ESR Spectroscopy in Membrane Biophysics. ISBN: 978-0-387-25066-3. Springer. Page 21.

Hendrickson H. S. (1969) Physical properties and interactions of phosphoinositides. Ann. N. Y. Acad. Sci. 165, 668-676.

Herrick D. Z., Kuo W., Huang H., Schwieters C. D., Ellena J. F. and Cafiso D. S. (2009) Solution and membrane-bound conformations of the tandem C2A and C2B domains of synaptotagmin 1: evidence for bilayer bridging. J. Mol. Biol. 390(5), 913-923.

Heuser J. E. and Reese T. S. (1981) Structure changes after transmitter release at the frog neuromuscular junction. J. Cell Bio. 88, 564-580.

Honigmann A., et al. (2013) Phosphatidylinositol 4,5-bisphosphate clusters act as molecular beacons for vesicle recruitment. Nat. Struct. Mol. Biol. 20(6), 679-686.

Hubbell W. L., Cafiso D. S. and Altenbach C. (2000) Identifying conformational changes with site-directed spin labeling. Nat. Struct. Bio. 7, 735-739.

Huntwork S. and Littleton J. T. (2007) A complexin fusion clamp regulates spontaneous neurotransmitter release and synaptic growth. Nat. Neurosci. 10, 1235-1237.

Ingólfsson H. I., Carpenter T. S., Bhatia H., Bremer P. T., Marrink S. J. and Lightstone F. C. (2017) Computational lipidomics of the neuronal plasma membrane. Biophys. J. 113, 2271-2280.

Ishizuka T., Saisu H., Odani S., Abe T. (1995) Synaphin: a protein associated with the docking/fusion complex in presynaptic terminals. Biochem Biophys Res. Commun. 213, 1107-1114.

Ishizuka T., Saisu H., Suzuki T., Kirino Y., Abe T. (1997) Molecular cloning of synaphins/complexins, cytosolic proteins involved in transmitter release, in the electric organ of an electric ray (Narke japonica). Neurosci. Lett. 232,107-110.

Jahn R. and Fasshauer D. (2012) Molecular machines governing exocytosis of synaptic vesicles. Nature 490, 201-207.

Jahn R. and Scheller R. H. (2006) SNAREs-engines for membrane fusion. Nat. Rev. Mol. Cell Biol. 7(9), 631-643.

Jahn R., Lang T. and Südhof T. C. (2003) Membrane fusion. Cell. 112, 519-533.

Janmey P. A., Iida K., Yin H. L. and Stossel T. P. (1987) Polyphosphoinositide micelles and polyphosphoinositide-containing vesicles dissociate endogenous gelsolin-actin complexes and promote actin assembly from the fast-growing end of actin filaments blocked by gelsolin. J. Biol. Chem. 262, 12228-12236.

Jeschke. (2012) DEER distance measurements on proteins. Annu. Rev. Phys. Chem. 63, 419-446.

Jontes J. D. (2018) The cadherin superfamily in neural circuit assembly. Cold Spring Harb. Pespect. Biol. 10(7), a029306.

Jurkiewicz P., Cwiklik L., Vojtíšková A., Jungwirth P. and Hof M. (2011) Structure, dynamic, and hydration of POPC/POPS bilayers suspended in NaCl, KCl, and CsCl solutions. Biochim. Biophys. Acta. 1818, 609-616.

Kaeser P. S., Deng L., Wang Y., Dulubova I., Liu X., Rizo J. and Südhof T. C. (2011) RIM proteins tether Ca^{2+}-channels to presynaptic active zones via a direct PDZ-domain interaction. Cell. 144(2), 282-295.

Kalb E., Engel J. and Tamm L. K. (1990) Bind of proteins to specific target sites in membranes measured by total internal reflection fluorescence microscopy. Biochemistry. 29, 1607-1613.

Kalb E., Frey S. and Tamm L . K. (1992) Formation of supported planar bilayers by fusion of vesicles to supported phospholipid monolayers. Biochim. Biophys. Acta. 1103, 307-316.

Katz B. (1969) The Release of Neural Transmitter Substances. Liverpool University Press, Liverpool.

Kiessling V., Kreutzberger A. J. B., Liang B., Nyenhuis S. B., Seelheim P., Castle J. D., Cafiso D. S. and Tamm L. K. (2018) A molecular mechanism for calcium-mediated synaptotagmin-triggered exocytosis. Nat. Struct. Mol. Bio. 25, 911-917.

Kiessling V., Liang B. and Tamm L. K. (2015) Reconstituting SNARE-mediated membrane fusion at the single liposome level. Methods. Cell Biol. 128, 339-363.

Kiessling V., Liang B., Kreutzberger A. J. B. and Tamm L. K. (2017) Planar supported membranes with mobile SNARE proteins and quantitative fluorescence microscopy assays to study synaptic vesicle fusion. Front. Mol. Neurosci. 10, 72.

Kiessling V., Yang S. T. and Tamm L. K. (2015) Supported lipid bilayers as models for studying membrane domains. Curr. Top. Membr. 75, 1-23.

Kozlov M. M. and Markin V. S. (1983) Possible mechanism of membrane fusion. Biofizika 28, 255-261.

Kreutzberger A. J. B., Kiessling V. and Tamm L. K. (2015) High cholesterol obviates a prolonged hemifusion in fast SNARE-mediated membrane fusion. Biophys. J. 109, 319-329.

Kreutzberger A. J. B., Kiessling V., Liang B., Seelheim P., Jakhanwal S., Jahn R., CastleJ. D. and Tamm L. K. (2017) Reconstitution of calcium-mediated exocytosis of dense-core vesicles. Sci. Adv. 3, e1603208.

Kreutzberger A. J. B., Kiessling V., Liang B., Yang S. T., Castle J. D. and Tamm L. K. (2017) Asymmetric phosphatidylethanolamine distribution controls fusion pore lifetime and probability. Biophys. J. 113(9), 1912-1915.

Krishnakumar S. S.,Li F., Coleman J., Schauder C. M., Kümmel D., Pincet F., Rothman J. E. and Reinisch K. M. (2015) Re-visiting the *trans* insertion model for complexin clamping. eLife. 4, e04463.

Kümmel D., Krishnakumar S. S., Radoff D. T., Li F., Giraudo C. G., Pincet F., Rothman J. E. and Reinisch K. M. (2011) Complexin cross-links prefusion SNAREs into a zigzag array. Nat. Struct. Mol. Biol. 18, 927-933.

Kuo W. (2010) Electrostatic interaction of synaptotagmin I with PIP2 containing membranes. University of Virginia. Chapter 3.

Kuo W., Herrick D. Z. and Cafiso D. S. (2011) Phosphoinositol 4,5-bisphosphate alters synaptotagmin 1 membrane docking and drives opposing bilayers closer together. Biochemistry 50, 2633-2641.

Kuo W., Herrick D. Z., Ellena J. and Cafiso D. S. (2009) The calcium-dependent and calcium-independent membrane binding of synaptotagmin 1: two modes of C2B binding. J. Mol. Biol. 387, 284-294.

Lai A. L., Huang H., Herrick D. Z. Epp N. and Cafiso D. S. (2011) Synaptotagmin 1 and SNAREs form a complex that is structurally heterogeneous. J. Mol. Biol. 405(3), 696-706.

Lai Y., Choi U. B., Zhang Y., Zhao M., Pfuetzner R. A., Wang A. L., Diao J. and Brunger A. T. (2016) N-terminal domain of complex independently activates calcium-triggered fusion. Proc. Natl. Acad. Sci. USA. 113(32), E4698-E4707.

Lakowicz J. R. (2006) Principles of fluorescence spectroscopy. Baltimore, Springer Science Business Media, LLC, P. 353.

Lapinski M. M., Castro-Forero A., Greiner A. J., Ofoli R. Y. and Blanchard G. J. (2007) Comparison of liposomes formed by sonication and extrusion: rotational and translational diffusion of an embedded chromophore. Langmuir. 23(23), 11677-11683.

Lasic D. D. (1988) The mechanism of vesicle formation. Biochem. J. 256, 1-11.

Lauwers E., Goodchild R. and Verstreken P. (2016) Membrane lipids in presynaptic function and diseases. Neuron 90, 11-25.

Lewis B. A. and Engelman D. M. (1983) Lipid bilayer thickness varies linearly with acyl chain length in fluid phosphatidylcholine vesicles. J. Mol. Biol. 166, 211-217.

Li L., Shin O. H., Rhee J. S., Araç D., Rah J. C., Rizo J., Südhof T. and Rosenmund C. (2006) Phosphatidylinositol phosphates as co-activators of Ca^{2+} binding to C2 domains of synaptotagmin 1. J. Biol. Chem. 281(23), 15845-15852.

Liang B., Kiessling V. and Tamm L. K. (2013) Prefusion structure of syntaxin-1a suggests pathway for folding into neuronal trans-SNARE complex fusion intermediate. Proc. Natl. Acad. Sci. USA. 110, 19384-19389.

Lin C.-C., Seikowski J., Pérez-Lara A., Jahn R., Höbartner C. and Walla P. J. (2014) Control of membrane gaps by synaptotagmin-Ca^{2+} measured with a novel membrane distance ruler. Nat. Commun. 5, 5859.

Lin M. Y., Rohan J . G., Cai H., Reim K., Ko C. P. and Chou R. H. (2013) Complexin facilitates exocytosis and synchronizes vesicle release in two secretory model systems. J. Physiol. 591, 2463-2473.

Link E., Edelmann L., Chou J. H., Binz T., Yamasaki S., Eisel U. Baumert M., Südhof T. C. and Jahn R. (1992). Tetanus toxin action: inhibition of neurotransmitter release linked to synaptobrevin proteolysis. Biochem. Biophys. Res. Commun.189(2), 1017-1023.

Lira R. B., Robinson T., Dimova R. and Riske K. A. (2019) Highly efficient protein-free membrane fusion: a giant vesicle study. Biophys. J. 116, 79-91.

Littleton J. T., Stern M., Schulze K., Perin M. and Bellen H. J. (1993) Mutational analysis of Drosophila synaptotagmin demonstrates its essential role in Ca^{2+}-activated neurotransmitter release. Cell 74(6), 1125-1134.

Lodish H., Berk A., Kaiser C. A., Krieger M., Bretscher A., Ploegh H., Amon A. and Martin K. C. (2016) Molecular Cell Biology. 8th edition. W. H. Freeman and Company. Page 272.

López-Murcia F. J., Reim K., Jahn O., Taschenberger H. and Brose N. (2019) Acute complexin knockout abates spontaneous and evoked transmitter release. Cell Rep. 26, 2521-2530.

Luo L. (2020) Principles of neurobiology. 2nd edition. Taylor & Francis Group, LLC. Page 29 and 77.

Ma C., Su L., Seven A. B., Xu Y. and Rizo J. (2013) Reconstitution of the vital functions of Munc18 and Munc13 in neurotransmitter release. Science. 339, 421-425.

Malsam et a., (2020) Complexin suppresses spontaneous exocytosis by capturing the membrane-proximal regions of VAMP2 and SNAP25. Cell Rep. 32, 107926.

Martens S., Kozlov M. M. and McMahon H. T. (2007) How synaptotagmin promotes membrane fusion. Science. 316, 1205-1208.

Martin J. A., Hu Z., Fenz K. M., Fernandez J. and Dittman J. S. (2011) Complexin has opposite effects on two modes of synaptic vesicle fusion. Curr. Biol. 21, 97-105.

Martin T. F. J. (2012) Role of PI(4,5)P2 in vesicle exocytosis and membrane fusion. Subcell. Biochem. 59, 111-130.

Martin T. F. J. (2015) PI(4,5)P_2-binding effector proteins for vesicle exocytosis. Biochim. Biophys. Acta. 1851, 785-793.

Mchaourab H. S., Lietzow M. A., Hideg K. and Hubbell W. L. (1996) Motion of spin-labeled side chains in T4 lysosome. Correlation with protein structure and dynamics. Biochemistry. 35, 7692-7704.

McMahon H. T. and Boucrot E. (2015) Membrane curvature at a glance. J. Cell. Sci. 128, 1065-1070.

McMahon H. T., Kozlov M. M. and Martens S. (2010) Membrane curvature in synaptic vesicle fusion and beyond. Cell. 140, 601-605.

McMahon H. T., Missler M., Li C., Südhof T. C. (1995) Complexins: cytosolic proteins that regulate SNAP receptor function. Cell. 83, 111-119.

Meher G. and Chakraborty H. (2019) Membrane composition modulates fusion by altering membrane properties and fusion peptide structure. J. Membr. Biol. 252, 261-272.

Mohrmann R., Dhara M. and Bruns D. (2015) Complexins: small but capable. Cell Mol. Life Sci. 72, 4221-4235.

Müller C. P., Reichel M., Mühle C., Rhein C., Gulbins E. and Kornhuber J. (2015) Brain membrane lipids in major depression and anxiety disorders. Biochim. Biophys. Acta. 1851, 1052-1065.

Murray D. H. and Tamm L. K. (2009) Clustering of syntaxin-1A in model membranes is modulated by phosphatidylinositol 4,5-bisphosphate and cholesterol. Biochemistry. 48, 4617-4625.

Nyenhuis S. B., Karadndikar N., Kiessling V., Kreutzberger A., Thapa A., Liang B., Tamm L. K. and Cafiso D. S. (2021) Conserved arginine residues in synaptotagmin 1 regulate fusion pore expansion through membrane contact. Nat. Commun. 12, 761.

Nyenhuis S. B., Thapa A. and Cafiso D. S. (2019) Phosphatidylinositol 4,5 bisphosphate controls the *cis* and *trans* interactions of synaptotagmin 1. Biophys. J. 117, 247-257.

Pabst S., Margittai M., Vainius D., Langen R., Jahn R. and Fasshauer D. (2002) Rapid and selective binding to the synaptic SNARE complex suggests a modulatory role of complexins in neuroexocytosis. J. Biol. Chem. 277(10), 7838-7848.

Park Y. and Ryu J. K. (2018) Models of synaptotagmin-1 to trigger Ca^{2+}-dependent vesicle fusion. FEBS Lett. 592, 3480-3492.

Park Y., et al. (2015) Synaptotagmin-1 binds to PIP2-containing membrane but not to SNAREs at physiological ionic strength. Nat. Struct. Mol. Biol. 22, 815-823.

Patil Y. P. and Jadhav S. (2014) Novel methods for liposome preparation. Chem. Phys. Lipids. 177, 8-18.

Pérez-Lara Á., Thapa A., Nyenhuis S. B., Nyenhuis D. A., Halder P., Tietzel M., Tittmann K., Cafiso D. S. and Jahn R. (2016) PtdInsP2 and PtdSer cooperate to trap synaptotagmin-1 to the plasma membrane in the presence of calcium. eLife. 5, e15886.

Pobbati A. V., Stein A. and Fasshauer (2006) N- to C-terminal SNARE complex assembly promote rapid membrane fusion. Science. 313, 673-676.

Pokorny A., Birkbeck T. H. and Almeida P. F. (2002) Mechanism and kinetics of δ-lysin interaction with phospholipid vesicles. Biochem. J. 41, 11044-11056.

Puchkov D. and Haucke V. (2013) Greasing the synaptic vesicle cycle by membrane lipids. Trends Cell. Biol. 23, 493-503.

Quade B., et al. (2019) Membrane bridging by Munc13-1 is crucial for neurotransmitter release. eLife. 8, e42806.

Rauch M. E., Ferguson C. G., Prestwich G. D and Cafiso D. S. (2002) Myristoylated alanine-rich C kinase substrate (MARCKS) sequesters spin-labeled phosphatidylinositol-4,5-bisphosphate in lipid bilayers. J. Biol. Chem. 277, 14068-14076.

Reim K., Mansour M., Varoqueaux F., McMahon H. T., Südhof T. C., Brose N. and Rosenmund C. (2001) Complexins regulate a late step in Ca^{2+}-dependent neurotransmitter release. Cell. 104, 71-81.

Reim K., Wegmeyer H., Brandstatter J. H., Xue M., Rosenmund C., Dresbach T., Hofmann K. and Brose N. (2005) Structurally and functionally unique complexins at retinal ribbon synapses. J. Cell. Biol. 169, 669-680.

Rizo J and Südhof T. C. (2012) The membrane fusion enigma SNAREs, Sec1/Munc18 proteins, and their accomplices-guilty as charged? Annu. Rev. Cell Dev. Biol. 28, 279-308.

Rosenmund C. and Stevens C. F. (1996) Definition of the readily releasable pool of vesicles at hippocampal synapses. Neuron. 16, 1197-1207.

Sabatini B. L. and Regehr W. G. (1996) Timing of neurotransmission at fast synapses in the mammalian brain. Nature 384, 170-172.

Schechter M., Atias M., Elhadi S. A., Davidi D., Gitler D. and Sharon R. (2020) α-Synuclein facilitates endocytosis by elevating the steady-state levels of phosphatidylinositol 4,5-bisphosphate. J. Biol. Chem. 295(52), 18076-18090.

Schiavo G., Benfenati F., Poulain B., Rossetto O., Polverino de Laureto P., DasGupta B. R. and Montecucco C. (1992). Tetanus and botulinum-B neurotoxins block neurotransmitter release by proteolytic cleavage of synaptobrevin. Nature. 359(6398), 832-835.

Seiler F., Malsam J., Krause J. M. and Söllner T. H. (2009) A role of complexin-lipid interactions in membrane fusion. FEBS Lett. 583(14), 2343-2348.

Shin O. H., Xu J., Rizo J. and Südhof T. C. (2009) Differential but convergent functions of Ca^{2+}-binding to synaptotagmin-1 C2 domains mediate neurotransmitter release. Proc. Natl. Acad. Sci. USA. 106(38), 16469-16474.

Singer S. J. and Nicolson G. L. (1972) The fluid mosaic model of the structure of cell membranes. Science. 175, 720-731.

Snead D., Wragg R. T., Dittman J. S. and Eliezer D. (2014) Membrane curvature sensing by the C-terminal domain of complexin. Nat. Commun. 5, 4955.

Söllner T., Whiteheart S. W., Brunner M., Erdjument-Bromage H., Geromanos S., Tempst P. and Rothman J. E. (1993) SNAP receptors implicated in vesicle targeting and fusion. Nature. 362, 318-324.

Stone T. J., Buckman T., Nordio P. L. and McConnell H. M. (1965) Spin-labeled biomolecules. Proc. Natl. Acad. Sci. USA. 54(4), 1010-1017.

Südhof T. C. (2004) The synaptic vesicle cycle. Annu. Rev. Neurosci. 27, 509-547.

Südhof T. C. (2013) Neurotransmitter release: the last millisecond in the life of a synaptic vesicle. Neuron. 80,675-690.

Südhof T. C. (2014) The molecular machinery of neurotransmitter release (Nobel Lecture). Angew. Chem. Int. Ed. 53, 12696-12717.

Tamm L. K., Crane J. and Kiessling V. (2003) Membrane fusion: a structural perspective on the interplay of lipids and protein. Curr. Opin. Struct. Biol. 13, 453-466.

Tang J, Maximov A., Shin O. H., Dai H., Rizo J. and Südhof T. C. (2006) Switch controls fast synaptic vesicle exocytosis. Cell. 126, 1175-1187.

Taniguchi H. and Manenti S. (1993) Interaction of myristoylated alanine-rich protein kinase C substrate (MARCKS) with membrane phospholipid. J. Biol. Chem. 268, 9960-9963.

Trimbuch T. and Rosenmund C. (2016) Should I stop or should I go? The role of complexin in neurotransmitter release. Nat. Rev. Neurosci. 17, 118-125.

Trimbuch T., Xu J., Flaherty D., Tomchick D. R., Rizo J. and Rosenmund C. (2014) Re-examining how complexin inhibits neurotransmitter release. eLife 3, e02391.

van den Bogaart et al., (2013) Membrane protein sequestering by ionic protein-lipid interactions. Nature. 479, 552-555.

Vicogne J., Vollenweider D., Smith J. R., Huang P., Frohman M. A. and Pessin J. E. (2006) Asymmetric phospholipid distribution drives in vitro reconstituted SNARE-dependent membrane fusion. Proc. Natl. Acad. Sci. USA 103, 14761-14766.

Victor K. G. and Cafiso D. S. (2001) Location and dynamics of basic peptide at the membrane interface: electron paramagnetic resonance spectroscopy of tetramethyl-piperidine-N-Oxyl-4-amino-4carboxylic acid-labeled peptides. Biophys. J. 81, 2241-2250.

Voleti R., Jaczynska K. and Rizo J. (2020) Ca^{2+}-dependent release of synaptotagmin-1 from the SNARE complex on phosphatidylinositol 4,5-bisphosphate-containing membranes. eLife. 9, e57154.

Wagner M. L. and Tamm L. K. (2000) Tethered polymer-supported planar lipid bilayers for reconstitution of integral membrane proteins: silane-polyethyleneglycol-lipid as a cusion and covalent linker. Biophys. J. 79, 1400-1414.

Wagner M.L. and Tamm L.K. (2001) Reconstituted syntaxin-1a/SNAP-25 interacts with negatively charged lipids as measured by lateral diffusion by lateral diffusion in planar supported bilayers. Biophys. J. 81, 266-275.

Walter A. M., Groffen A. J., Sorensen J. B. and Verhage M. (2011) Multiple Ca^{2+}-sensors in secretion: teammates, competitors or autocrats? Trends Neurosci. 34, 487-497.

Wan C., Kiessling V., Cafiso D. S. and Tamm L. K. (2011) Partitioning of synaptotagmin I C2 domains between liquid-ordered and liquid-disordered leaflet lipid phases. Biochemistry. 50, 2478-2485.

Wang J., Gambhir A., Hangyás-Mihályné G., Murray D., Golebiewska U. and McLaughlin S. (2002) Lateral sequestration of phosphatidylinositol 4,5-bisphosphate by the basic effector domain of myristoylated alanine-rich C kinase substrate is due to nonspecific electrostatic interaction. J. Biol. Chem. 227(37), 34401-34412.

Wang S., Li Y., Gong J., Ye S., Yang X., Zhang R. and Ma C. (2019) Munc18 and Munc13 serve as a functional template to orchestrate neuronal SNARE complex assembly. Nat. Commun. 10, 69.

Waugh M. G. (2015) PIPs in neurological diseases. Biochim. Biophys. Acta. 1851, 1066-1082.

Weber T., Zemelman B. V., McNew J. A., Westermann B., Gmachl M., Parlati F., Söllner T. H. and Rothman J. E. (1998) SNAREpins: minimal machinery for membrane fusion. Cell. 92, 759-772.

Wen P. J., Osborne S. L. and Meunier F. A. (2011) Dynamic control of neuroexocytosis by phosphoinositides in health and disease. Prog. Lipids. Res. 50(1), 52-61.

Weninger K., Bowen M. E., Choi U. B., Chu S. and Brunger A. T. (2008) Accessory proteins stabilize the acceptor complex for synaptobrevin, the 1:1 syntaxin/SNAP-25 complex. Structure.16, 308-320.

Wragg R. T., Snead D., Dong Y., Ramlall T. F., Menon I., Bai J., Eliezer D. and Dittman J. S. (2013) Synaptic vesicles position complexin to block spontaneous fusion. Neuron. 77(2), 323-334.

Xu J., Brewer K., Perez-Castillejos R. and Rizo J. (2013) Subtle interplay between synaptotagmin and complexin binding to the SNARE complex. J. Mol. Biol. 425, 3461-3475.

Xue M. et al. (2007) Distinct domains of complexin I differentially regulate neurotransmitter release. Nat. Struct. Mol. Biol. 14, 949-958.

Xue M., Craig T. K., Xu J., Chao H. T., Rizo J. and Rosenmund C. (2010) Binding of the complexin N terminus to the SNARE complex potentiates synaptic-vesicle fusogenicity. Nat. Struct. Mol. Biol. 17, 568-575.

Xue M., Lin Y. Q., Pan H., Reim K., Deng H., Bellen H. J. and Rosenmund C. (2009) Tilting the balance between facilitatory and inhibitory functions of mammalian and Drosophila Complexins orchestrates synaptic vesicle exocytosis. Neuron. 64, 367-380.

Xue M., Stradomska A., Chen H., Brose N., Zhang W., Rosenmund C. and Reim K (2008) Complexins facilitate neurotransmitter release at excitatory and inhibitory synapses in mammalian central nervous system. Proc. Natl. Acad. Sci. USA. 105(22), 7875-7880.

Yang H. J., Sugiura Y., Ikegami K., Konishi Y. and Setou M. (2012) Axonal gradient of arachidonic acid-containing phosphatidylcholine and its dependence on actin dynamics. J. Biol. Chem. 287, 5290-5300.

Yang L. and Huang H. W. (2002) Observation of a membrane fusion intermediate structure. Science. 297, 1877-1879.

Yang S. T., Kreutzberger A. J., Lee J., Kiessling V. and Tamm L. K. (2016) The role of cholesterol in membrane fusion. Chem. Phys. Lipids. 199, 136-143.

Yoon T. Y., Okumus B., Zhang F., Shin Y. K. and Ha T. (2006) Multiple intermediates in SNARE-induced membrane fusion. Proc. Natl. Acad. Sci. USA. 103, 19731-19736.

Zavoisky E. (1944) Paramagnetic absorption in perpendicular and parallel fields for salts, solutions and metals. (PhD thesis)

Zdanowicz R., Kreutzberger A., Liang B., Kiessling V., Tamm L. K. and Cafiso D. S. (2017) Complexin binding to membranes and acceptor t-SNAREs explains its clamping effect on fusion. Biophys. J. 113, 1-16.

Zhao W. D., Edaeni H., Wonchul S., Wen P. J., Krystofiak E. S., Villarreal S. A., Chiang H. C., Kachar B. and Wu L. G. (2016) Hemi-fused structure mediates and controls fusion and fission in live cells. Nature. 534, 548-552.

Zhou Q., et al. (2015) Architecture of the synaptotagmin-SNARE machinery for neuronal exocytosis. Nature 525,62-67.

Zhou Q., Zhou P., Wang A. L., Wu D., Zhao M., Südhof T. C. and Brunger A. T. (2017) The primed SNARE-complexin-synaptotagmin complex for neuronal exocytosis. Nature. 548 420-425.